Worcester Polytechnic Institute
Digital WPI

Doctoral Dissertations (All Dissertations, All Years) | Electronic Theses and Dissertations

2017-01-11

Application of Phase Change Materials to Improve the Thermal Performance of Buildings and Pavements

Naser Pourakbar Sharifi
Worcester Polytechnic Institute

Follow this and additional works at: https://digitalcommons.wpi.edu/etd-dissertations

Repository Citation
Pourakbar Sharifi, N. (2017). *Application of Phase Change Materials to Improve the Thermal Performance of Buildings and Pavements.* Retrieved from https://digitalcommons.wpi.edu/etd-dissertations/22

This dissertation is brought to you for free and open access by Digital WPI. It has been accepted for inclusion in Doctoral Dissertations (All Dissertations, All Years) by an authorized administrator of Digital WPI. For more information, please contact wpi-etd@wpi.edu.

Application of Phase Change Materials to Improve the Thermal Performance of Buildings and Pavements

by

Naser Pourakbar Sharifi

A Dissertation

Submitted to the faculty

of the

WORCESTER POLYTECHNIC INSTITUTE

In partial fulfillment of the requirements for the

Degree of Doctoral of Philosophy

in

Structural Engineering

in the Civil and Environmental Engineering Department

May 2016

APPROVED:

Dr. Aaron R. Sakulich, Advisor _____

Doctoral Committee:

Professor Tahar El-Korchi _____

Dr. Leonard D. Albano _____

Dr. Nima Rahbar _____

ABSTRACT

In recent decades, much research has investigated the efficiency of Phase Change Materials (PCMs) in improving the thermal performance of buildings and pavements. In buildings, increasing the thermal inertia of structural elements by incorporating PCMs decreases the energy required to keep the inside temperature in the comfort range. In concrete pavements, using PCMs decreases the number of freeze/thaw cycles experienced by the pavement and thus increases service life. However, PCMs cannot be added to cementitious binders directly, because they interfere with the hydration reactions between cement and water that produce strength-bearing phases. Therefore different carriers have been proposed to indirectly incorporate PCMs in cementitious materials.

Lightweight Aggregate (LWA) is one of the materials that has been proposed as PCM carrier agent. However, it was not studied in depth before. Various experiments were conducted to investigate the problems associated with incorporating LWA presoaked in PCM in cementitious media. The results show that a portion of PCM leaks out of the LWA's structure and subsequently affects different chemical, physical, and mechanical properties of the binder. In addition, the applicability of Rice Husk Ash (RHA), a common material never before used to encapsulate PCM, as a PCM carrier agent was investigated. The results show that RHA can absorb and contain liquids in its porous structure; and regarding its compatibility with the cementitious media, it can be used as PCM carrier.

Different computational simulations using Typical Meteorological Year data were conducted to evaluate the efficiency of PCMs in improving the thermal performance of buildings. Utilizing PCM-incorporated gypsum boards was shown to be a promising strategy to achieve the governmental plans of "Zero Net Energy" buildings. The results show that using a PCM with a melting point near the occupant comfort zone delays and reduces the inside peak temperature, increases the duration of time during which the inside temperature stays in the comfort zone, and decreases the cost and energy required by HVAC system to keep the inside temperature in this range. However, PCMs' efficiency is completely dependent on the input temperature profile.

Key Words: Phase Change Materials, Temperature Changes in Buildings, Occupant Comfort, Service Life of Pavements, Lightweight Aggregate, Rice Husk Ash

DEDICATION

To my family …

I couldn’t have done this without you,

Thanks for all of your support along the way.

ACKNOWLEDGMENT

Firstly, I would like to express my sincere gratitude to my advisor, Aaron Sakulich for the continuous support of my Ph.D. studies and related research, for his patience, motivation, and immense knowledge. His guidance helped me in all the time of research and writing of this thesis. Besides my advisor, I would like to thank the rest of my thesis committee, Tahar El-Korchi, Leonard Albano, and Nima Rahbar, who have generously given their time and expertise to better my work. I thank them for their contribution and their good-natured support. I would like to thank Rajib Mallick, the graduate coordinator of the Civil and Environmental Engineering (CEE) Department at Worcester Polytechnic Institute (WPI), for his guidance and support during my studies at WPI. I am also grateful to Terri Camesano, the dean of graduate studies at WPI, for funding the last few credits of my program.

My sincere thanks and appreciation goes to my fellow lab mates and great friends, Hajar Jafferji, Sina Askarinejad, and Faezeh Shalchi for all their help and support. Thank you to the graduate students in the CEE Department at WPI, Gregory Freeman, Joseph Szafarowicz, and Gert Guldentops for helping me throughout my research. Also, thanks to the undergraduate students Madison Blanchard, Billal Taourit, Savannah Reynolds, and Ahsan Adel Nizam Shaik who joined our research group from different departments and helped me advance my research.

I must acknowledge the lab managers of the CEE Department, Mr. Donald Pellegrino and Mr. Russell Lang, as well as the CEE staff, Mrs. Marylou Horanzy, Mrs. Agata Lajoie, and Mrs. Cynthia Bergeron for being always supportive to me. I also would like to thank Dr. Boquan Li, Professor Germano Iannacchione, Mr. Siamak Najafi, as well as the technicians in the Gateway Laboratories at WPI who helped me conduct my experiments and simulations. Thanks to the Graduate Student Government at WPI for their financial support for me to attend different conferences. Finally I thank the Northeast Solite Corporation for providing the lightweight aggregate.

TABLE OF CONTENTS

LIST OF TABLES

LIST OF FIGURES

NOMENCLATURE

OPC	Ordinary Portland Cement
PCM	Phase Change Material
LWA	Lightweight Aggregate
RHA	Rice Husk Ash
T	Temperature (°C, K, °F, and R)
Q	Heat flow (W and BTU/h)
q	Heat flow per unit area (W/m^2 and $BTU/h \cdot ft^2$)
h	Heat transfer coefficient ($W/m^2 \cdot K$ and $BTU/h \cdot ft^2 \cdot R$)
λ	Thermal conductivity ($W/m \cdot K$ and $BTU/h \cdot ft \cdot R$)
Cp	Specific heat at constant pressure ($J/g \cdot K$ and $BTU/lb \cdot R$)
L	Latent heat of fusion (J/g and BTU/lb)
ρ	Density of the solid material (kg/m^3 and lb/ft^3)
σ	Stefan-Boltzmann constant ($W/m^2 \cdot K^4$ and $BTU/h \cdot ft^2 \cdot R^4$)
ε	Surface emissivity
Θ	Volume fraction of PCM in mortar
β	Volume fraction of PCM in phase one
ϕ	Time Lag
f	Decrement Factor
EEF	Energy Efficiency Factor
CEF	Cost Efficiency Factor

CHAPTER ONE
INTRODUCTION

Energy consumption all around the world has been increasing significantly during the last two decades [1, 2]. Between only 1998 and 2009, the total energy consumption of the entire world increased by more than 30% [3]. This energy is mostly gained from fossil fuels. The excessive combustion of fossil fuels puts exorbitant amounts of CO_2 into the atmosphere. High levels of CO_2 mean that heat from the earth is retained in the atmosphere, thus intensifying the greenhouse effect and global warming [4].

A big portion of the generated energy is consumed in residential and commercial buildings. In the European Union, up to 40% of all energy was used by buildings in 2012 [4]. In the United States in 2015, roughly the same percentage of the total energy consumption was due to residential and commercial buildings [5]. Also, the energy consumption of Chinese buildings has doubled between 1998 and 2009 [6]. Therefore, decreasing the energy consumption of buildings has been the topic of many governmental plans and building codes [7].

For instance, in the United States, the state of California follows strategies to achieve Zero-Net-Energy (ZNE) residential buildings by 2020, and ZNE commercial buildings by 2030 [8]. Also, Washington State Building Code Council has developed energy codes to achieve a 70% reduction

in building energy use by 2030 compared to 2006 levels [9]. Improving the energy efficiency in existing buildings, as well as new buildings, was recognized as one of the main strategies to reduce energy consumption and reach ZNE buildings.

The share of space heating and cooling in the buildings' total energy consumption in the world was reported to be 34% in 2010 [10]. This share was more than 35% in the U.S. [11]. These statistics show that reducing the energy required for the air conditioning of buildings is one of the key elements to achieve the aforesaid goals. Thus, significant research has been done during the last two decades to improve energy efficiency of buildings [12, 13]. Different methods, such as utilizing polystyrene insulation boards [14], and lightweight insulating concretes [15], have been introduced to reduce the energy lost through the walls, floors, and roofs of buildings. These methods also address changes in the interior temperatures of buildings and suggest different methods for keeping that temperature in the comfort range and reducing HVAC energy consumption [16, 17]. Implementing these strategies not only improves occupant comfort, but also reduces the electricity demand and the associated emission of gasses such as CO_2 [18].

The other topic that has attracted the attention of governments is the maintenance costs of infrastructure such as roads and bridges. In 2011, the U.S. federal government and state departments of transportation spent over $100 billion on maintaining and improving core highways, roads, and bridges [19, 20]. Despite this, the American Society of Civil Engineers gave a grade of D to American roads in 2013, and reported that an estimated $100 billion is needed annually to maintain the current roadway conditions, while an additional $79 billion annually is needed to improve the quality of the roadways [21].

Cracking due to extreme temperatures, i.e., both very low and very high temperatures, is one of the main failure mechanisms in pavements [22, 23]. Cyclic changes in temperature can also cause

fatigue failure in pavements after a period of time [24]. In addition, freeze/thaw cycles can cause cracks in concrete pavements due to the solidification and expansion of pore solution [22, 25]. Thus, decreasing the thermal vulnerability has been recognized as one of the key strategies to increase the service life of pavements and reduce the costs of maintenance [26].

The incorporation of Phase Change Materials (PCMs) in construction and pavement materials has been proposed as one promising method to address both of the mentioned concerns [26, 27]. PCMs are substances with relatively high latent heats of fusion. When the ambient temperature rises above its melting point, a given PCM absorbs heat and turns to the liquid phase while remaining at an almost constant temperature. When the ambient temperature falls below the melting point, the PCM begins to release heat and solidify, again remaining at an almost constant temperature [28]. A large number of PCMs with different melting points, from roughly -33 °C to 800 °C (-27 °F to 1472 °F), and different latent heats of fusion, are industrially available [29].

PCMs divide into three main categories: organic, inorganic, and eutectic. Organic PCMs are further divided in paraffin and non-paraffin groups. Paraffin waxes consist of a mixture of mostly straight chains of *n-alkanes* CH_3-(CH_2)-CH_3. Non-paraffin PCMs have highly varied properties [30]. Fatty acids, with the general formula of CH_3-$(CH_2)_{2n}$-COOH, are considered to be one of the important types of PCMs in this category. Organic PCMs can melt and freeze repeatedly without phase segregation or degradation in their latent heat of fusion, and are mostly stable under normal conditions, chemically inert, predictable, relatively cheap, and show little volume change on phase transition [31]. However, they have low thermal conductivity and relatively low latent heat of fusion [32].

Inorganic PCMs are further classified as salt hydrates and metallics. Salt hydrates have relatively high latent heat of fusion, relatively high thermal conductivity, and small volume changes on phase

transition [33]. However, the main problem associated with them is their structural degradation under cyclic phase transitions. Metallics include low melting point metals and metal eutectics. They have low heat of fusion per unit weight, high heat of fusion per unit volume, high thermal conductivity, and low specific heat [30].

Finally, a eutectic PCM is a composition of two or more components, where each of them melts and freezes congruently [34]. Eutectics nearly always melt and freeze without segregation, especially on melting where both of the components liquefy simultaneously. However, there is a low chance of separation between the two components during freezing.

Using PCMs in buildings prevents rapid changes in the inside temperature and saves energy by reducing heating/cooling demands [35]. Laboratory tests prove using PCM in construction materials increases the heat storage capacity and decreases thermal conductivity [36-38]. Utilizing a PCM-impregnated boards over the existing walls was reported to keep the inside temperature 6 °C (10.8 °F) cooler during the days and 4 °C (7.2 °F) warmer during the nights [39].

Another laboratory test showed that using PCM panels in a building can reduce interior peak temperatures by 2.46 °C (4.43 °F) during the summertime [40]. The results of a study shows that encapsulating PCMs within the surfaces of walls, ceilings, and floors enhances the energy storage of buildings to capture and reserve solar energy [41, 42]. PCMs can also be used in air conditioning systems in buildings. The results of a small scale experimental study showed that up to 90% of a daily cooling load could be stored each night in a system in which a 30 mm (1.18”) thick packed bed of granular PCM [43].

In addition to laboratory studies, many numerical and computational studies can be found in the literature, indicating that PCMs can improve the thermal performance of buildings [44-46]. The

results of a study on a passive house duplex located in the U.S. state of Oregon showed that using PCM in a building can reduce the annual overheated hours, the total hours in a year that the inside temperature is above the occupant comfort level of 26 °C (78.8 °F), by 50% [47]. Another simulation showed that by utilizing a layer of PCM, the temperature fluctuation of the floors was considerably decreased and the ability of the floor to provide the necessary warmth during the cold part of the day was increased [48].

PCMs can also be used as an additive to increase the service life of concrete pavements [49]. Cyclic changes in temperature in cold and humid climates increase the number of freeze/thaw cycles experienced by the pavement, finally leading to failure [22, 25]. Using PCMs in pavements increases the thermal inertia of the media and reduces the potential of thermally induced deterioration, and thus, increases the service life of the pavement [26, 50, 51].

However, PCMs cannot be directly added to concrete as a liquid, because as a chemical component, they interfere with the hydration reactions occurring in the cementitious media [52]. Hydration reactions are a series of chemical reactions between cement and water that yield calcium silicate hydrates (C-S-H), the primary strength bearing phase in concrete. Anything that interferes with the hydration reaction diminishes the mechanical properties of the concrete. Therefore various carrier agents, such as high density polyethylene balls and rectangular steel pipes, have been introduced to indirectly incorporate PCMs into the cementitious materials [53, 54],

This dissertation contains two main parts: laboratory experiments and computational simulations. The first part aims to evaluate the applicability of Lightweight Aggregate (LWA) to be used as a PCM carrier agent in cementitious materials. Even though it was previously suggested as a carrier [55], more investigations need to be conducted to study the problems associated with using LWA as a PCM carrier, such as the potential leakage of PCM out of the LWA and its effects on

different properties of the media, in depth. Also, the ability of Rice Husk Ash (RHA), a common material never before used to encapsulate PCM, as an alternative carrier agent is investigated. Various experiments are conducted to study the effects of incorporating RHA presoaked in PCM on different properties of the mortar.

In the second part, COMSOL® Multiphysics software[1] is used to study the application of PCMs in buildings and pavements. Although the efficiency of PCMs to decrease the energy usage in buildings and to increase the service life of pavements has been evaluated by different studies, few studies have investigated the changes in temperature of a structural or pavement element under specific, realistic temperature profiles. Therefore various models are developed to simulate temperature changes in PCM-impregnated concrete walls, as well as PCM-impregnated concrete pavements, under the real temperature profiles of different locations and for different periods of time.

The efficiency of utilizing PCM-impregnated gypsum boards to improve the thermal performance of buildings was also investigated. This strategy can be used to achieve the desired thermal performance by the governmental plans and building codes for the buildings that already exist. Since the amount of PCM used could be varied in a given system until the optimum conditions are reached, i.e., until the desired energy efficiency and cost efficiency levels are attained, the models contained different percentages of PCMs.

Four different criteria, including the decrease in the inside peak temperature, the delay in the occurrence of this peak, increase in the duration of being in the comfort zone, and reduction in the

[1] This software is identified and explained in this study in order to specify the simulations and modeling procedures adequately. However, such identification is neither intended to imply recommendation or endorsement, nor is it intended to imply that this software is necessarily the best available for the purpose.

energy required by the HVAC system to keep the inside temperature in this range, are considered to evaluate the efficiency of PCM to improve the thermal performance of buildings.

CHAAPTER TWO
MATERIALS

Different materials such as aggregates, cement, Phase Change Materials (PCMs), etc., were used to conduct various experiments. These materials are widely available, however, most of them were provided from local resources. The materials were safely and attentively kept in a separate and marked cabinet in the laboratory that was used solely for material storage. The Material Safety Data Sheets (MSDS) of the chemicals were kept in the same cabinet. The used materials are identified here in order to specify the experimental procedure adequately. However, such identifications are neither intended to imply recommendation or endorsement, nor is it intended to imply that the materials or equipment identified are necessarily the best available for the purpose.

2.1 Aggregates

2.1.1 Sand

Ordinary sand with a specific gravity of 2.61 from local sources was used. Sieve analysis was performed according to ASTM C136 to determine the size distribution of the aggregates. Sand particles larger than the sieve #4 and finer than sieve #100 were removed. This modified aggregate

size distribution was used for all mixes (Figure 2.1). The smooth graph shows that the aggregate was well distributed between all the particle sizes.

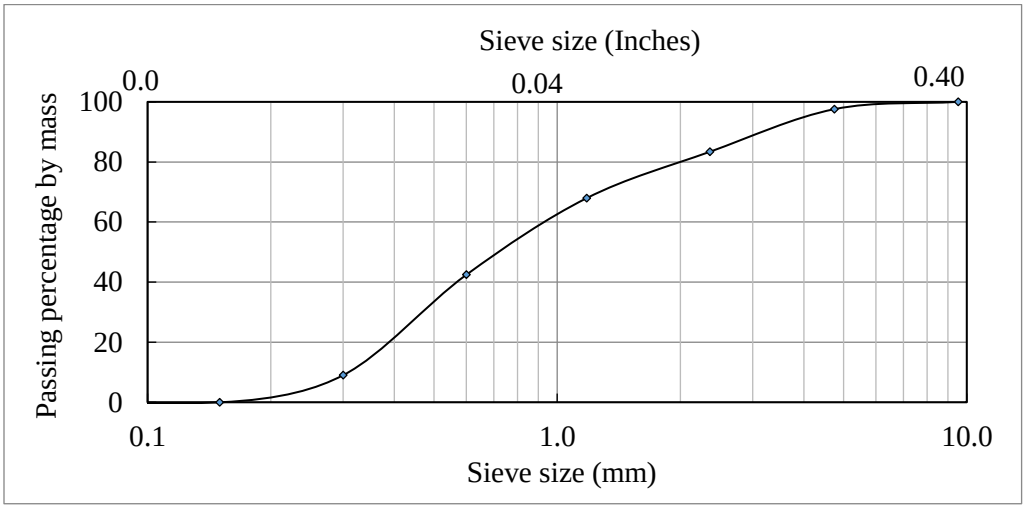

Figure 2.1. Sieve size distribution for the sand

2.1.2 Lightweight Aggregate (LWA)

LWA is a porous aggregate that can absorb liquids by capillary action, which enables its use as a carrier for different liquids in cementitious media. The LWA used was expanded shale (Northeast Solite Corporation) with a specific gravity of 1.5. When LWA was used in mixes, it replaced sand on a volumetric basis; as such, the aggregate size distributions were the same in specimens with and without LWA. This means that the size distributions of sand, LWA, and mixtures thereof follow the distribution described in Section 2.1.1.

2.1.2.1 Scanning Electron Microscopy of LWA

Scanning Electron Microscopy (SEM) was used to study the porous structure of LWA. To create specimens for SEM, a small piece of the sample was placed in a plastic mold which was then filled with resin. After solidification, the sample was removed and a series of six sandpapers

(#120, #240, #600, 1µm, 0.3µm, 0.05µm) were used to polish the surface of the specimen. The surface was then sputter coated with a thin layer of gold. The porous structure of LWA is shown in Figure 2.2.

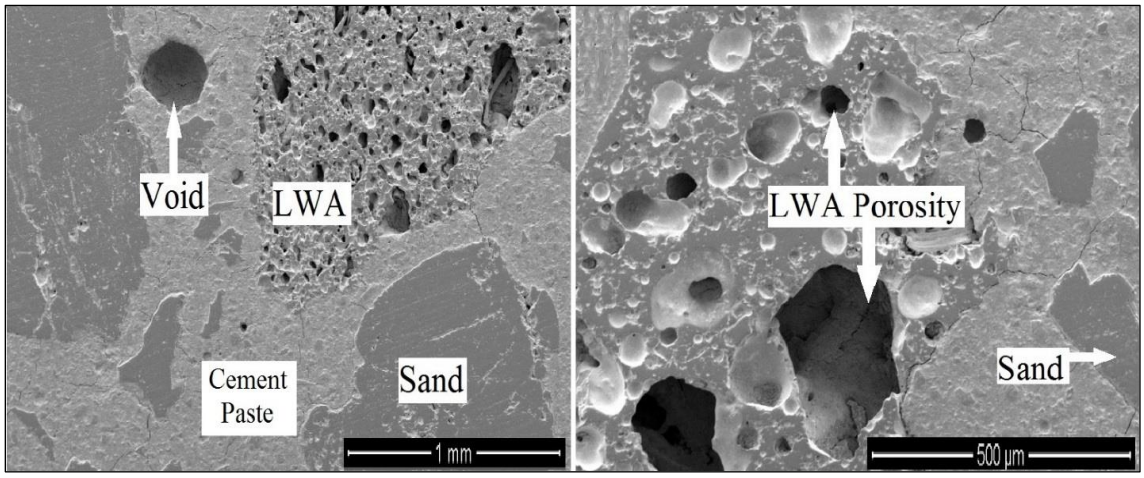

Figure 2.2. SEM of the porous structure of LWA

2.1.2.2 Absorption Test for LWA

The water absorption capacity of the LWA was reported by the manufacturer to be equal to 17.5 wt. %. However, absorption tests were carried out to determine the amount of PCM that can be absorbed by LWA. The LWA was placed in mesh containers and soaked in PCM6 for 24 h. (The utilized PCMs are described below.) Afterwards, the mesh containers were kept in an oven at a constant temperature of 40 °C (104 °F) for one week.

The weight change of the LWA was recorded daily. The test was done separately for each sieve size of aggregate (#8, #16, #30, #50, and #100) as well as for the mix following the size distribution described in Section 2.1.1. Although the finer particles seemed to absorb more PCM, this was actually due to the higher surface area per unit volume of the fine particles which caused PCM to simply adhere to the surface of the LWA particles (Figure 2.3, overleaf).

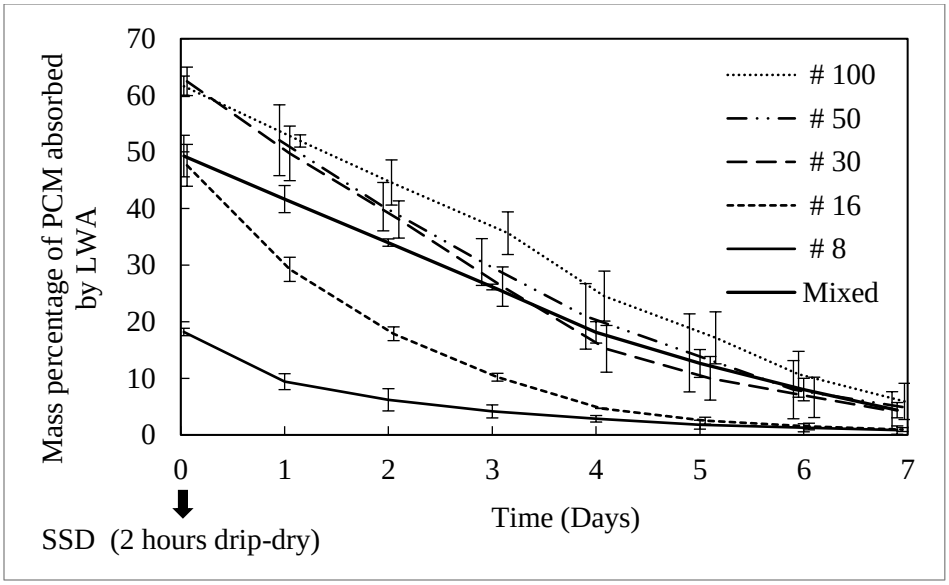

Figure 2.3. Apparent PCM absorbed by LWA

A second test was carried out in this manner, but with sand in place of the LWA. Because sand is not porous and cannot absorb liquid, any increase in the weight of sand after soaking in the PCM is the result of PCM adhering to the surface. To estimate the net amount of PCM absorbed by the LWA, the amount 'absorbed' by sand was subtracted from the total amount absorbed by the LWA (Figure 2.4, overleaf). By this estimation, the capacity of LWA to absorb PCM is roughly 30 wt.% , which is larger than the amount of water that the LWA can absorb as reported by the manufacturer. This difference could be the result of different testing methods for measuring the absorption capacity of LWA, or the different chemical and physical properties of PCM and water, such as specific gravity and adhesion force between the PCM and the LWA.

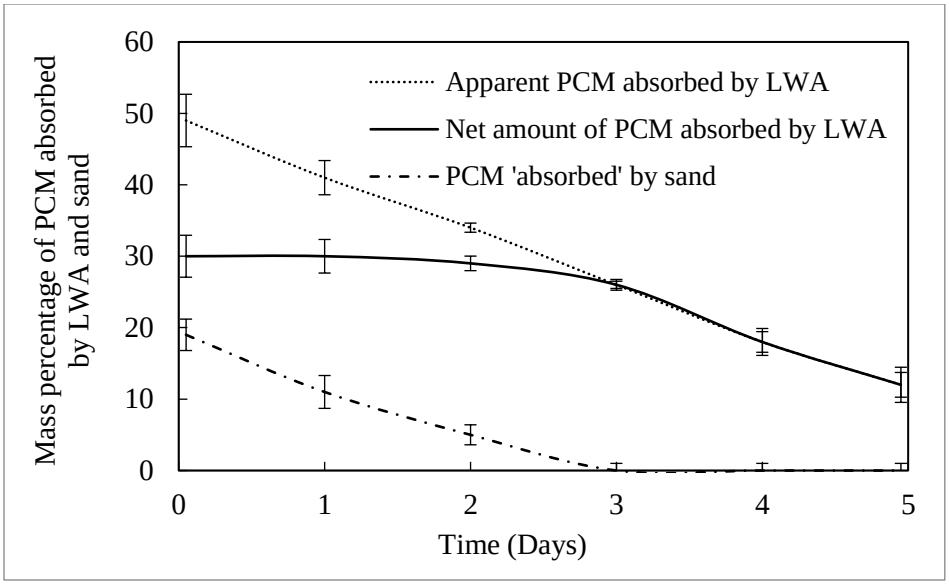

Figure 2.4. PCM ‘absorbed’ by sand and the net amount of PCM absorbed by LWA

2.2 Cement

Type I Ordinary Portland Cement (OPC) conforming to ASTM standard C150 / C150M, with a specific gravity of 3.15, was used. Hydrating cement undergoes a series of chemical reactions between cement and water that yields calcium silicate hydrates (C-S-H), the primary strength bearing phase in concrete.

2.2.1 Chemical Shrinkage of cement

Cement hydration products occupy less physical volume than the reactants; thus, the cement paste undergoes a shrinkage known as chemical shrinkage that results in the formation of internal pores. The volume of this porosity is one of the important characteristics of a cement, therefore chemical shrinkage tests were conducted. To measure the chemical shrinkage of the cement paste, ASTM standard C1608-07 was followed. Five ampoules were partially filled with cement paste with a water/cement ratio of 0.4 by mass. Then the ampoules were completely filled with water and

covered by a cap with a capillary tube. To prevent evaporation, a drop of oil was added to the capillary tube after the water. The samples were kept in a water bath at 25 °C (77 °F), and the drop in the height of the water in the graded capillary tube was recorded over the first 115 h.

The chemical shrinkage per unit mass of cement at time 't' was computed as:

$$CS(t) = \frac{h(t) - h(60min)}{M_{Cement}} \quad (1)$$

in which CS(t) is the chemical shrinkage at time t (mL/g cement); h(t) is the water level in capillary tube at time t (mL); h_{60min} is the water level in capillary tube at time 60 min; and M_{Cement} is the mass of the cement (g). The final chemical shrinkage of the paste was calculated to be equal to 0.042 mL/g (1.162 in^3/lb) (Figure 2.5), which is similar to the values of 0.046 mL/g (1.273 in^3/lb) and 0.039 mL/g (1.080 in^3/lb) determined by Merzuki and Pang, respectively, [56, 57]. The result of this test was not directly used to make a conclusion, rather, it was mainly done to measure one of the important characteristics of the utilized cement that was required for conducting other experiments.

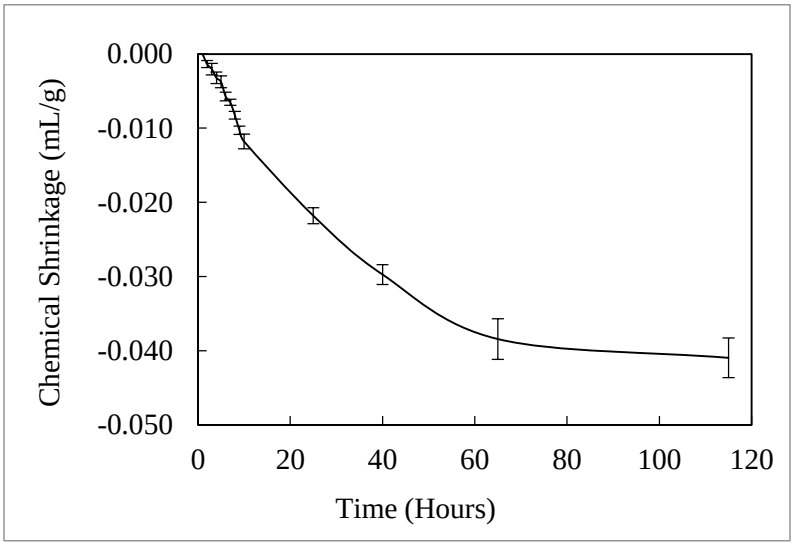

Figure 2.5. Chemical Shrinkage of the cement

2.3 Rice Husk Ash (RHA)

Rice Husk Ash (RHA) was used as another carrier for the PCM. To produce RHA, rice husk was burned in an electric furnace at two different temperatures 300 °C (572 °F) and at 650 °C (1202 °F), separately. The burning duration was 6 h for each case. The ash burned at 300 °C (572 °F) was black in color and had a weight loss of 52%; the one burned at 650 °C (1202 °F) was white in color and had a weight loss of 81% (Figure 2.6).

Figure 2.6. a) RHA burned at 300 °C (572 °F). b) RHA burned at 650 °C (1202 °F)

2.3.1 Scanning Electron Microscopy of RHA

The porous structure of the ash burned at 650 °C (1202 °F) was studied using electron microscopy. For sample preparation, small particles of powder were stacked on a specimen stub with double-sided conductive tape. Compressed air was used to remove particles that were not tightly adhered to the tape. The images appeared to show that RHA powder had two sides with different level of porosities (Figure 2.7).

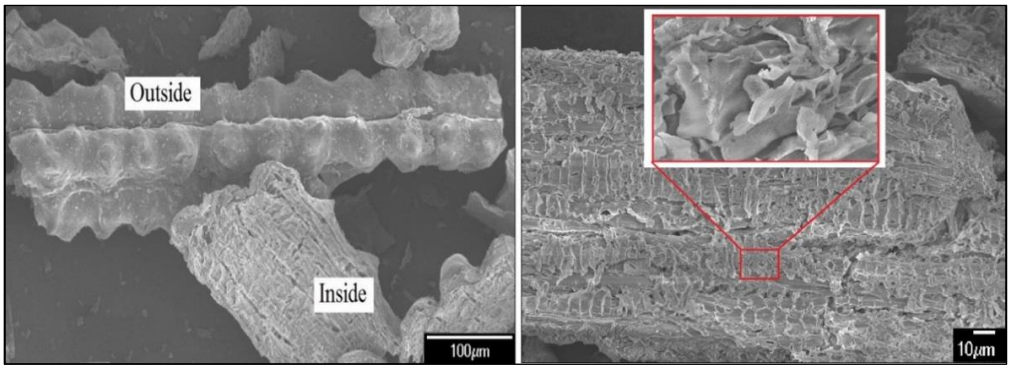

Figure 2.7. SEM imaging of Rice Husk Ash burned at 650 °C (1202 °F)

2.3.2 X-Ray Diffraction and Fourier Transform Infrared spectroscopy of RHA

XRD and FTIR tests were conducted on the RHA powders to study their crystal structure and chemical composition. The test procedures for the tests are described in Section 3.1.7 and Section 3.1.8, respectively. The results of the XRD test show that the ash burned at 300 °C (572 °F) had a completely amorphous structure and there is not any peak hump in that (Figure 2.8). The ash burned at 650 °C (1202 °F) had also mostly an amorphous structure, however, there is an amorphous hump, related to silica, created at to 23°-2Θ that matches with the results presented in [58, 59]. Yu *et al.* also reported that RHA contains about 90 wt.% of silica [60].

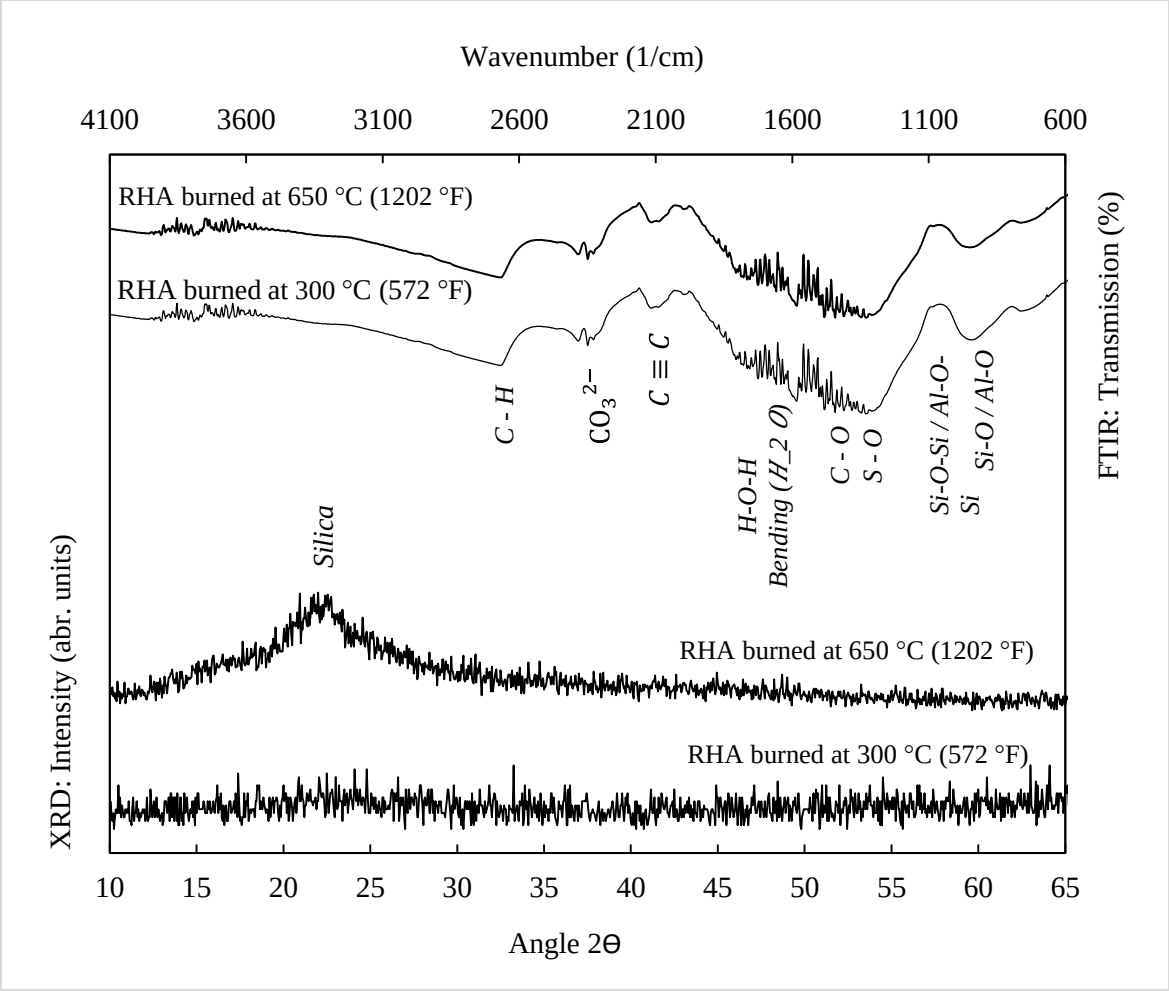

Figure 2.8. XRD diffractograms and FTIR spectra of RHA

The results presented in another study show that for a RHA burned at a higher temperature, in addition to the hump at 23°-2Θ that is related to silica, there is a smaller hump at 27°-2Θ that is attributed to quartz [61]. These results suggest that burning rice husk at a low temperatures, close to 300 °C (572 °F), does not yield a material with crystal structure, but using higher temperatures results a more crystallite structure.

FTIR spectra of both ashes shows a broad peak around 2700 cm^{-1} indicating C-H, a broad hump centered around 2100 cm^{-1} that could indicate C≡C, a hump around 1700 cm^{-1} indicating bending vibrations in water, a hump around 1300 cm^{-1} indicating S-O, and a hump centered around 900 cm^{-1} indicating Si-O and/or Al-O stretching vibrations (Figure 2.8). These results suggest that using different temperatures does not significantly change the chemical composition of RHA.

2.4 Phase Change Materials (PCMs)

Three different types of PCM with melting points of -10 °C, 6 °C, and 28°C (14 °F, 42.8 °F, and 82.4 °F, respectively) were used. These PCMs are referred to as PCM-10, PCM6, and PCM28, respectively. All of the PCMs were a paraffin blend with specific gravities less than one (about 0.8), and thermal conductivity of about 0.18 W/m·K (0.104 BTU/hr·ft·°F) in the liquid phase and 0.24 W/m·K (0.139 BTU/hr·ft·°F) in the solid phase. Based on the MSDS of the PCMs, they are all stable under normal conditions of handling and storage, inflammable under 400 °C (752 °F), have slight water solubility, and have a mild wax odor.

2.4.1 Differential Scanning Calorimetry of PCMs

Differential Scanning Calorimetry (DSC) was conducted to measure the specific heat and heat of fusion of the PCMs. In this technique, heat flow through a small amount of PCM sample, about 20 g (0.7 oz.), was compared to a reference. A temperature rate of 1°C/min (1.8 °F/min) over a range of 30 °C (54 °F) was used for each PCM sample. When the PCM undergoes phase transition, a different amount of heat will be required to maintain the sample and the reference at the same temperature. During melting, the PCM absorbed heat, which increased heat flow and caused an upward peak in the heat flow as a function of time. During solidification, the PCM released the absorbed heat and decreased the needed heat flow, causing a downward peak in the graph (Figure 2.9). The differences among the magnitudes of three peaks of the graphs are because of the differences among the latent heats of fusion of the PCMs.

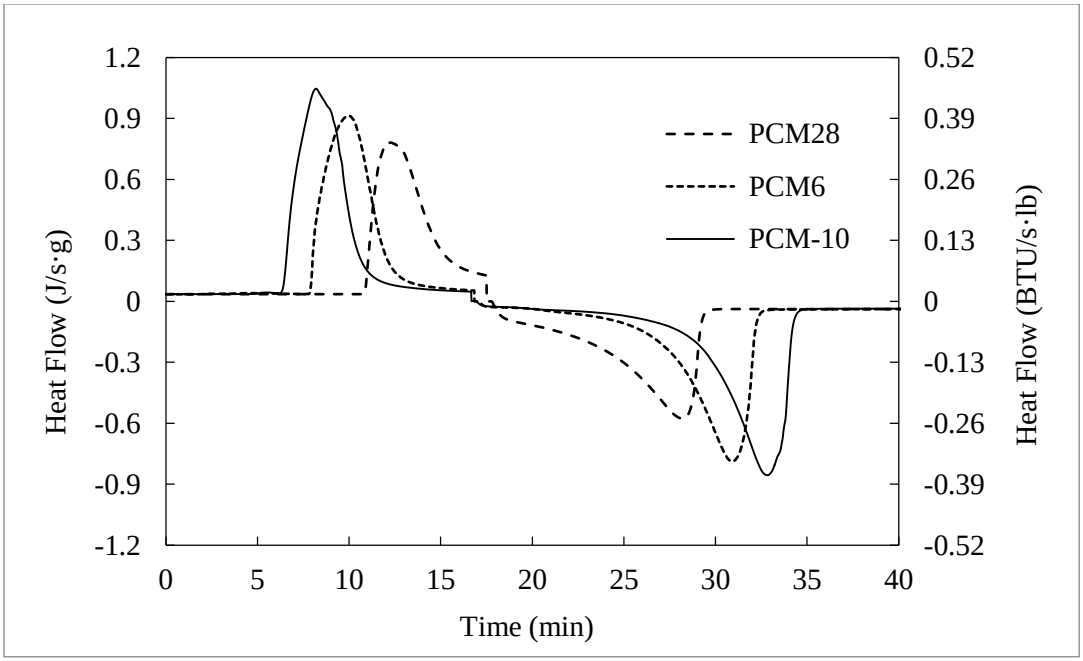

Figure 2.9. Heat flow per unit mass of PCM vs. time, as determined by DSC

Both melting and solidification of the PCMs took place in a range of 6 °C (10.8 °F) (Figure 2.10). For all of the samples, solidification started at the temperature that was reported as the phase change temperature by the manufacturer; whereas melting started at a temperature roughly 10 °C (18 °F) lower than the reported temperature. The difference between calculated melting and solidifying temperatures may be because of experimental conditions, such as the amount of the material that is used for the test, pressure, cooling and heating rate, the presence of impurities, etc. [62].

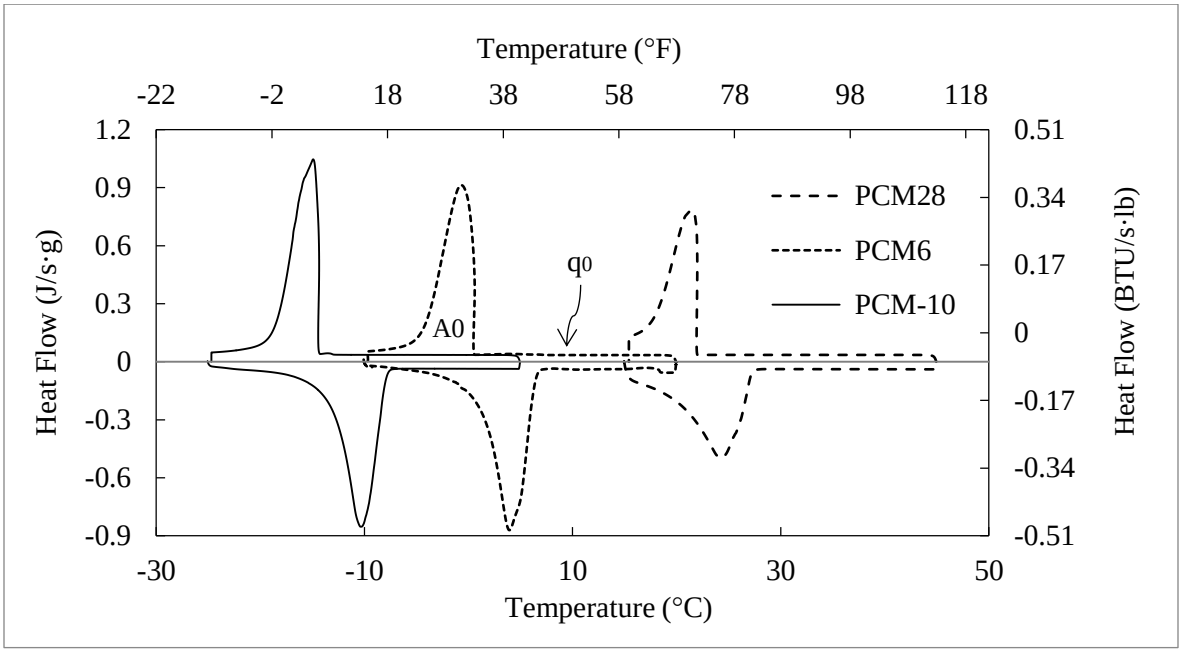

Figure 2.10. Heat flow per unit mass of PCM vs. temperature, as determined by DSC, where q_0 is the heat flow in steady state condition per unit mass of the PCM, and A_0 is the area under the peak of heat flow per unit mass of the PCM

The specific and latent heats of PCMs can be measured by using the heat flow vs. temperature graph. The specific heat of a PCM is equal to heat flow in steady state condition per unit mass of the PCM (q_0) divided by the temperature change rate (dT/dt). The latent heat of the PCM can be calculated by dividing the area under the peak of heat flow (A_0) by the temperature change rate:

$$L = \frac{\int_{T_1}^{T_2} q.dT}{(dT/dt)} \quad (2)$$

where L is the latent heat per unit mass of the PCM (J/g); q is the heat flow per unit mass of the PCM (J/s·g); T_1 is the temperature that phase change starts (°C); T_2 is the temperature that phase change ends (°C); and dT/dt is temperature change rate (°C/s).

The properties of the PCMs reported by the company as well as determined here by DSC are provided in Table 2.1. These results are consistent with the results reported in other studies. Duti *et al.* reported the specific heat and latent heat of fusion of the organic PCMs to be equal to 2 J/g·K (0.48 BTU/lb·°F) and 190 J/g (83 BTU/lb), respectively [45]. Zhou *et al.* reported the specific heat of paraffin PCMs to be in the range of 2.1 J/g·K (0.502 BTU/lb·°F) and 2.16 J/g·K (0.516 BTU/lb·°F); and the latent heat of fusion of this type of PCMs to be in the range of 152 J/g (65 BTU/lb) to 244 J/g (104.9 BTU/lb) [63].

Table 2.1. Properties of PCM-10, PCM6, and PCM28

PCM	Phase Change Temperature (From Manufacturer)	Measured temperature of initiation of phase change		Specific Heat (Measured)	Heat of Fusion	
		Solidifying	Melting		From Manufacturer	Measured
PCM-10	-9.5 ºC (15 °F)	-10 °C (14 °F)	-15 °C (5 °F)	2.10 J/g·K (0.50 BTU/lb·°F)	175 J/g (75 BTU/lb)	192 J/g (83 BTU/lb)
PCM6	6 ºC (43 ºF)	6 °C (43 °F)	0 °C (32 °F)	2.08 J/g·K (0.50 BTU/lb·°F)	160 J/g (69 BTU/lb)	178 J/g (77 BTU/lb)
PCM28	28 ºC (82 ºF)	27 °C (81 °F)	22 °C (72 °F)	2.11 J/g·K (0.50 BTU/lb·°F)	150 J/g (64 BTU/lb)	161 J/g (69 BTU/lb)

All of the PCMs have almost the same specific heat, but they have different latent heats of fusion, with PCM-10 having the highest and PCM28 the lowest, causing the time between the melting and solidifying of PCM-10 and PCM28 to be the longest and shortest, respectively. It should be mentioned that the calculated latent heat during melting of PCM is equal to the calculated latent heat during solidification, with less than the 1.5% error that is attributed to the instrument's accuracy. This confirms that all of the energy that is stored by the PCM during melting is released during solidification.

2.5 Other materials

WD-40, which is a lubrication oil, was used to cover the surface of some of the equipment such as the compressive strength molds, total shrinkage molds, and Vicat Needle setup to make it easier to demold the samples and also to protect the equipment against corrosion. Foamular® 250 Rigid Foam Insulation with the R-value of 10 was used to insulate the calorimetry apparatus. Also, to ensure good contact between different pieces of the calorimetry setup, a highly conductive thermal transfer medium, thermal gap filler pad, was used. Drinking water at room temperature was used for mixing the mortars.

CHAPTER THREE
LABORATORY EXPERIMENTS

A series of various laboratory experiments were conducted to study the effects of incorporating LWA, RHA, and PCM on the different chemical, physical, and mechanical properties of the mortars. The ASTM standard for each experiment was followed. In this chapter, at first the methodology of each experiment is explained, and then the results of the experiments are presented and compared with the results of other studies.

3.1 Methodology

3.1.1 Mix Proportioning

Four sets of mixes, with twelve total mixes, were prepared. Set one, includes Mix 1, set two includes Mix 2, set three includes Mixes 3 and 4, and set four includes Mixes 5 to 7. For Mix 1, the control mix, only sand, cement, and water were used. For Mix 2, PCM was directly added to the mortar without using any carrier. In Mixes 3 and 4, LWA was used as the carrier. For these mixes, two different factors may affect the properties of the mortar: the carrier, which has a different composition and is mechanically weaker than sand, and the incorporation of the PCM, which may interfere with hydration reactions. In order to distinguish between the effects of

incorporating the PCM and the carrier, two mixes were prepared: Mix 3W in which LWA was presoaked in water, and Mix 3P in which LWA was presoaked in PCM. The mass of added water was 17.5 wt.% of LWA, the water absorbance capacity reported by the manufacturer. An equal volume of PCM (13.3 wt.% of LWA, due to the lower specific gravity) was used in Mix 3P.

LWA presoaked in water provides internal curing for the mortar since it has the ability to absorb and keep the water inside its porous structure. When the mix water is consumed during hydration reactions, the LWA releases its absorbed water into the media due to the induced osmotic pressure; this eliminates or reduces the meniscus forces in the internal porosity and decreases the autogenous strain [64]. A comparison between internal curing and external curing is provided in Figure 3.1. In contrast with external curing, internal curing provides a uniform water supply for the entire media.

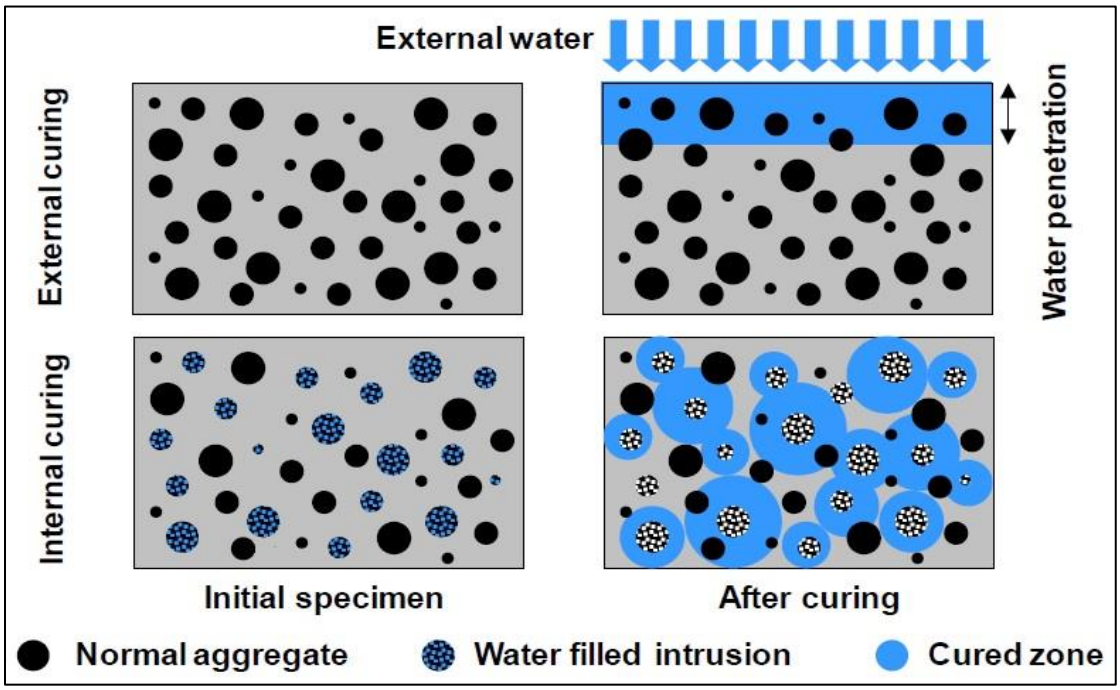

Figure 3.1. Illustration of the difference between external and internal curing. The water-filled inclusions should be distributed uniformly and spaced close enough to provide coverage for the entire paste system [64]

The mass of incorporated LWA was calculated using the equation commonly used to determine mix proportions for systems in which water-soaked LWA is used to provide 'internal curing' [65]:

$$M_{LWA} = \frac{C_f \times CS \times \alpha_{max}}{S \times \phi_{LWA,max}} \quad (3)$$

where M_{LWA} is the mass of dry LWA per unit volume of mortar (kg/m^3), C_f is the cement factor of the mortar (kg/m^3), CS is the chemical shrinkage of the cement (g of water/g of cement), α_{max} is the maximum expected degree of hydration of cement, S is the saturation degree of LWA, and $\phi_{LWA,\ max}$ is the water absorption capacity of lightweight aggregate (kg water/kg dry LWA). For all mixes, C_f was 585 kg/m^3 (36.5 lb/ft^3), CS was calculated by the chemical shrinkage test (following ASTM method C1608-07), α_{max} and S were assumed to be equal to 1.0 and 0.95, respectively, and $\phi_{LWA,\ max}$ was reported by the manufacturer to be 0.175 kg/kg (0.175 lb/lb). For Mixes 4W and 4P, the absorption capacity of LWA was assumed to be equal to 30 wt.%, as calculated in Section 2.1.2.2. Therefore, the amount of water added to LWA for Mix 4W was 30% of the mass of LWA, and the same volume of PCM6 was added to LWA for Mix 4P.

For Mixes 5 to 7, RHA was used as the PCM carrier agent. For these mixes, RHA replaced 10 wt.% of the cement. RHA has been widely used in concrete to replace cement [66-68], but it has not been used as a carrier agent to indirectly incorporate liquids into the mix. Therefore, the capacity of RHA to absorb liquids was not known, and thus, three different quantities of water and PCM were used to presoak the RHA. For Mix 5W, the mass of added water was equal to 80% of the RHA mass; for Mix 6W, the mass of added water was equal to 40% of the RHA mass; and for Mix 7W, the mass of added water was equal to 20% of the RHA mass. The same volumes of PCM were added to Mix 5P, Mix 6P, and Mix 7P, respectively. For all mixes, a water/cement ratio of 0.4 by mass and an aggregate/mortar ratio of 0.55 by volume were used. The air content of all mixes

(necessary for the mix proportioning) was measured to be equal to 3 vol.% of the mortar (see Section 3.1.2). The mix proportioning of all mixes is provided in Table 3.1.

Table 3.1. Mix Proportioning for 1000 cm^3 (61 in^3) of mortar, grams (lb)

Mix #	Sand	LWA	RHA	Cement	Water	Presoaked Water	Presoaked PCM
1	1435.5 (3.16)	-	-	585.3 (1.29)	234.1 (0.52)	-	-
2	1435.5 (3.16)	-	-	585.3 (1.29)	234.1 (0.52)	-	21.1 (0.046)
3W	1160.6 (2.56)	158.1 (0.35)	-	585.3 (1.29)	234.1 (0.52)	27.7 (0.061)	-
3P	1160.6 (2.56)	158.1 (0.35)	-	585.3 (1.29)	234.1 (0.52)	-	21.1 (0.046)
4W	1160.6 (2.56)	158.1 (0.35)	-	585.3 (1.29)	234.1 (0.52)	47.4 (0.105)	-
4P	1160.6 (2.56)	158.1 (0.35)	-	585.3 (1.29)	234.1 (0.52)	-	36.0 (0.080)
5W	1435.5 (3.16)	-	58.5 (0.129)	526.8 (1.16)	210.7 (0.46)	46.8 (0.103)	-
5P	1435.5 (3.16)	-	58.5 (0.129)	526.8 (1.16)	210.7 (0.46)	-	35.6 (0.078)
6W	1435.5 (3.16)	-	58.5 (0.129)	526.8 (1.16)	210.7 (0.46)	23.4 (0.052)	-
6P	1435.5 (3.16)	-	58.5 (0.129)	526.8 (1.16)	210.7 (0.46)	-	17.8 (0.039)
7W	1435.5 (3.16)	-	58.5 (0.129)	526.8 (1.16)	210.7 (0.46)	11.7 (0.026)	-
7P	1435.5 (3.16)	-	58.5 (0.129)	526.8 (1.16)	210.7 (0.46)	-	8.9 (0.020)

3.1.2 Air Content

The air content of the mixes was measured using the procedure outlined in ASTM C185. Incorporating pre-wet LWA or RHA did not have a significant effect on the air content of the mixes. For all of the mixes, the air content was measured to be about 3 vol.% of the mortar.

3.1.3 Shrinkage

3.1.3.1 Autogenous Shrinkage

According to ASTM method C1698-09, autogenous shrinkage is "the bulk strain of a sealed specimen of a cementitious mixture, not subjected to external forces and under constant temperature, measured from the time of final setting until a specified age." Chemical shrinkage produces voids in the cementitious binder of a mortar. If these voids are partially filled with water, inward meniscus forces will be generated that cause the matrix to undergo autogenous shrinkage. However, if the pores are kept filled, autogenous shrinkage does not take place.

In order to record the autogenous shrinkage of the cement paste for each mixture, five samples of each mix were produced using flexible corrugated tubes. The samples were placed in zipped plastic bags and kept in a moist curing room for 28 days. The length of each sample was recorded at the final setting time and at intervals during the first 28 days to calculate L(t):

$$L(t) = L_{ref} + R(t) - 2 \times L_{plug} \quad (4)$$

in which L_{ref} is the length of the reference bar (mm); R(t) is the length reading of the mortar at each time (mm); and L_{plug} is the average length of the end plugs (mm). Using the length reading at any time period, the autogenous strain was calculated using:

$$Autogenous\ Strain = \frac{R(t) - R(t_{sf})}{L(t_{sf})} \times 10^6 \frac{\mu m}{m} \quad (5)$$

in which R(t) is the length reading of the mortar at each time (mm), and $R(t_{sf})$ is the length reading of the mortar at the final setting time (mm).

Autogenous shrinkage causes macroscopic volume changes in the media that can lead to early-age cracking [69, 70]. However, it can be eliminated by internal curing, where the water supplied by internal reservoirs keeps the pores fully saturated [69, 71-74]. Neutron radiography has been used to evaluate the water distribution around a pre-wetted LWA particle in a 6 mm × 13 mm (0.236" × 0.512") cement mortar [75]. This study showed pre-wetted LWA provided a water supply for the mortar (Figure 3.2). The cement paste appears in the light gray, the dry LWA appears in the darker inclusion on the top part of cross-section, and the pre-wetted LWA is on the bottom and cannot be easily distinguished in the first images after mixing. With the progress of hydration (moving left to right across the top and bottom rows), water is released from the LWA to the cement paste. Locations in which the neutron signal increased correspond with water being absorbed from the paste and are shown in red, while the locations where the neutron signal decreased correspond with the release of water to the paste and are shown in blue. Water released from the LWA traveled at least 3 mm (0.118") from the LWA into the cement paste in the first day; suggesting that the internal curing process is fast and that the water is distributed homogeneously from the LWA to at least 3 mm (0.118") into the hydrating paste.

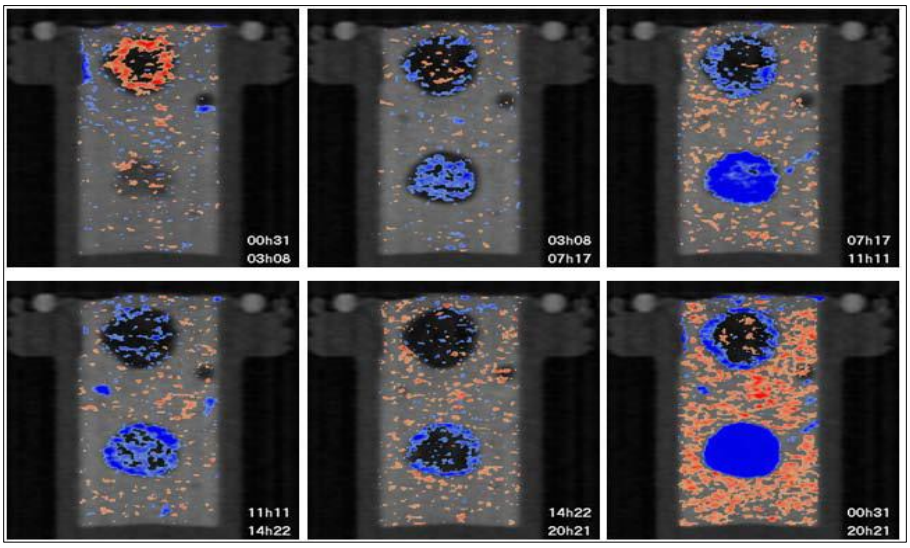

Figure 3.2. Internal curing. The two indicated times in the lower right corner of each frame correspond to the times that were subtracted to create the shown image [75]

3.1.3.2 Total Shrinkage

Total shrinkage tests were conducted based on ASTM method C596-07. Six samples from each mix were prepared using 25.4 mm × 25.4 mm × 292.1 mm (1” × 1” × 11.5”) prism molds. The molded samples were kept in zipped plastic bags in a curing room for 24 h. Once demolded, samples were submerged in water to cure for 48 h, and then were taken out and kept at room conditions for 25 more days. Measurements were taken on the day of demolding and periodically for the first 28 days.

3.1.4 Calorimetry

The hydration reactions between cement and water are exothermic. Some of the factors that affect the kinetics of these reactions are cement composition, fineness of cement, curing conditions, water to cement (w/c) ratio, and the presence of admixtures and additives [76]. The utilized cement, the curing conditions, and w/c ratio were kept constant over the course of all of the experimental procedures; therefore, when the LWA or RHA presoaked in PCM was used in the mortar, any reduction in the generated heat was attributed to the interference of the PCM with the hydration reaction. Similarly, when the carriers presoaked in water were incorporated in the mortar, any reduction in the generated heat was attributed to the changes in the water content of the mix. Two types of calorimetry experiments were conducted to evaluate the effect of incorporating LWA and RHA presoaked in PCM and water into the mortar on the hydration reaction between cement and water.

3.1.4.1 Semi-adiabatic Calorimetry

Semi-adiabatic calorimetry tests were conducted in which 101.6 mm × 203.2 mm (4” × 8”) cylinders were filled with mortar and insulated on all the sides. A K-type thermocouple was embedded in the center of the cylinder and the temperature was recorded for three days by a data acquisition apparatus connected to a computer. A thermocouple was also used to record the ambient air temperature over the course of the experiment (Figure 3.3).

This test was conducted on all of the mixes to study the effect of incorporating LWA and RHA presoaked in PCM and water. The PCM that was used in Mix 3P, Mix 4P, Mix 5P, Mix 6P, and Mix 7P was PCM6. In these tests, the percentage of utilized PCM in the carrier was different. However, in order to study the effect of incorporating different types of PCMs on the hydration reaction, another set of experiments needed to be conducted. To do that, Mix 4P was presoaked in PCM-10 and PCM28, and the results were compared to the results obtained from PCM6.

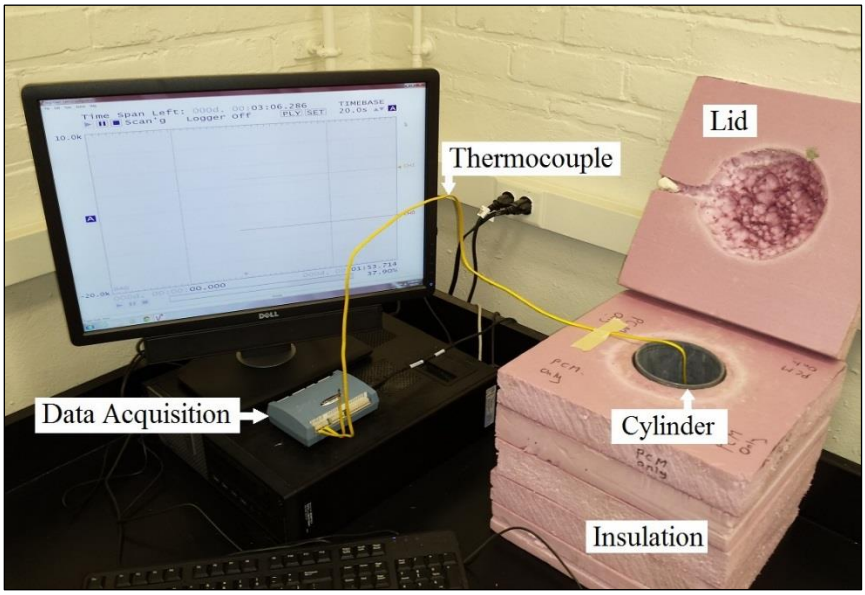

Figure 3.3. Semi-adiabatic calorimetry set-up

3.1.4.2 Isothermal Calorimetry

Isothermal calorimetry was also used for each mix to study hydration effects. For each mix, two ampoules were partially filled with the mortar sample, capped, and the caps were crimped in order to be sealed. The operation temperature of the machine was 25 ºC (77 ºF), and initial and final baselines were acquired over a period of 30 minutes. In order to provide an indication of variability, two specimens from the same mix were tested in neighboring calorimeter cells.

For all samples, reference ampoules contained 10 g (0.35 oz.) of cement powder. The specific heat of each sample was equal to the specific heat of the reference. To calculate the equivalent sample mass, the specific heat of sand and LWA, cement, water, and PCM were taken as 0.76 J/g°C (0.182 Btu/lb°F), 0.75 J/g°C (0.179 Btu/lb°F), 4.18 J/g°C (0.998 Btu/lb°F), and 2.08 J/g°C (0.497 Btu/lb°F), respectively. The results were normalized per unit mass of cement in the sample. Similar to semi-adiabatic calorimetry, this test was also repeated for Mix 4P presoaked in PCM-10 and PCM28, and the results were compared to the results obtained from PCM6.

3.1.5 Setting Time

In order to evaluate the effect of PCM incorporation on mortar setting time, ASTM C191 (the Vicat needle method) was used to measure the initial and final setting time of the mixes. The penetration of the needle was recorded every 15 min and after allowing the needle to settle for 30 s. By definition, the initial setting time is the time when 25 mm (0.98”) of penetration is obtained, and the final setting time is when the needle does not sink visibly into the paste.

Since hydration reaction yields stiff phases such as C-S-H in the matrix, anything that interferes with this reaction delays the creation of stiff products and delays the setting times. For this experiment, all three type of PCMs, PCM6, PCM-10, and PCM28, were used to examine the effect

of different types of PCMs, with different chemical structures, on the setting time of the mortar. Thus, this experiment was conducted on Mix 1, Mix 2, Mix 3P, and Mix 4P.

3.1.6 Compressive Strength

The compressive strength of a mortar or concrete is an important characteristic. Therefore, if any new material or additive was incorporated in a mortar or concrete, compressive strength tests need to be conducted to assure that the functionally is not drastically diminished. The compressive strength of a mortar increases over time as the hydration reaction progresses and rigid phases such as C-S-H are created. However, this test is mostly conducted on samples at ages of less than four weeks after mixing, because the main part of the hydration reactions takes place before this age. ASTM method C109 / C109M was followed for the compressive strength test. After mixing, mortar was placed in 50.8 mm (2") cube stainless steel molds for 24 h, and after demolding, the cubes were kept in a curing room. Keeping the samples in the curing room prevents the water that exists in the mix from evaporating and helps the hydration reactions to properly take place. For each mix, three specimens were tested at ages of 3, 7, and 28 days. Since the loading rate directly affects the compressive strength, it was kept constant for all of the mixes and was chosen to be equal to 13.8 MPa/min (2,000 psi/min). The PCM used in Mix 2, Mix 3P, Mix 4P, Mix 5P, Mix 6P and Mix 7P was PCM6.

3.1.7 X-Ray Diffraction (XRD)

XRD tests were conducted on the samples that contained LWA, RHA, and PCM to examine if incorporation of these materials affects the crystal structure of the mortars. After 28 days of curing, a specimen of Mix 1, Mix 4P, and Mix 5P was grounded to very fine powder (mesh #200) to prepare samples for XRD experiments. Mix 4P and Mix 5P were selected because they had the highest amount of PCM in them. For the XRD tests, about 0.5 g (0.018 oz.) of the powder was placed in the sample holder and was packed down tightly by spatula to prepare a relatively flat surface. A range of the angle 2θ from 10° to 65° with an interval of 0.05° was used. XRD tests were also conducted on RHA samples by grinding them to very fine powders. The same angle range was used for the RHA powders.

3.1.8 Fourier Transform Infrared Spectroscopy (FTIR)

FTIR tests were conducted on the samples that contained LWA, RHA, and PCM to examine if incorporation of these materials affects the chemical composition of the mortars. Similar to XRD, a specimen of Mix 1, Mix 4P, and Mix 5P was grounded to very fine powder (mesh #200) after 28 days of curing to prepare samples for FTIR experiments. The sample size for the FTIR test was about 5 mg (0.00018 oz.). All the samples were studied in the range of the wavenumber (λ) from 600 cm^{-1} to 4100 cm^{-1} and an interval of 2 cm^{-1}. To eliminate the error introduced by the machine and/or by the ambient condition, the test was at first conducted when no sample was placed in the machine, and the results from this background run were subtracted from the actual test results. FTIR tests were also conducted on RHA samples by grinding them to very fine powders. The same wavenumber range was used for the RHA powders.

3.1.9 Guarded Longitudinal Comparative Calorimetry (GLCC)

To evaluate the effect of different PCMs on the thermal properties of mortar, the guarded longitudinal calorimetry technique was used. A programmable cold plate was used to produce a temperature gradient (and thus heat flow) through a sample stack. This stack was composed of a cube sample placed in between two Pyroceram 9606 meter bars of known thermal conductivity. Thermal transfer media was used to ensure good contact between the cold plate and lower meter bar, as well as between the sample and the meter bars. K-type thermocouples were used to record the temperature at the thermal transfer media (Figure 3.4-a). Insulation, Foamular® 250, was placed around the sample stack to eliminate axial heat loss and ensure unidirectional heat flow. The insulation was surrounded with aluminum plates in contact with the cold plate to neutralize the temperature gradient through the insulation, and the entire stack was covered with a final layer of insulation (Figure 3.4-b).

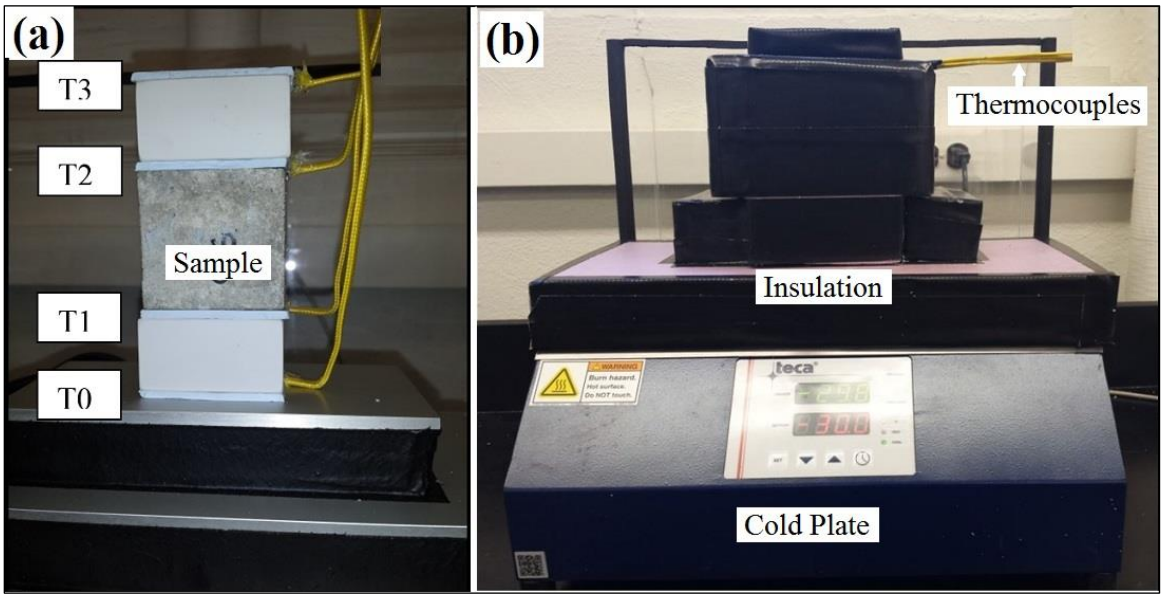

Figure 3.4 a) The meter bar/sample/meter bar stack. Sample between two meter bars, with thermocouples embedded in thermal transfer media. b) Final arrangement of the longitudinal calorimeter, showing cold plate and insulation

ASTM standard methods D5470-12 and E1225-09 describe procedures for determining the thermal properties of solid materials by means of the guarded-comparative-longitudinal heat flow technique. Due to the different melting temperature of the PCMs investigated, two different temperature profiles were used; the first one for the samples that contain PCM6 and PCM-10, and the second one for the samples that contain PCM28 (Figure 3.5).

In both cases, the cold plate was cooled at a rate of 2 °C/h (3.6 °F/h) over 50 h. At the target temperatures of -25 °C and -10 °C (-13 °F and 14 °F), respectively, the temperature was kept constant for 4 h to allow the sample to reach equilibrium. Then, the temperature was increased to the initial temperature at a rate of 4 °C/h (7.2 °F/h) within 12 h 30 min. It should be noted that this was an arbitrarily selected temperature profile intended to display general behavior, and other temperatures and conditions could be applied during this test.

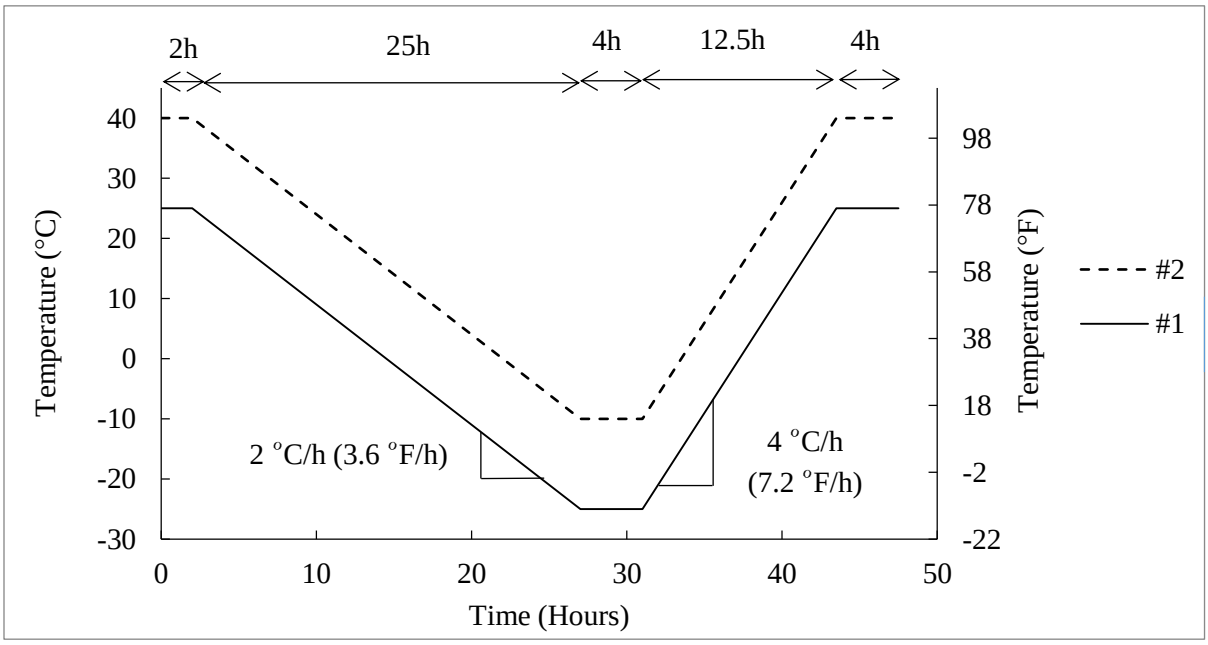

Figure 3.5. The two temperature profiles applied to the samples as the thermal load. Profile #1 for samples presoaked in PCM6 and PCM-10, and Profile #2 for sample presoaked in PCM28

The 50.8 mm (2”) cube mortar samples were placed between two Pyroceram 9606 meter bars of known thermal conductivity. The thermal conductivity of this material is a function of temperature and can be calculated by [77]:

$$\lambda_{PC} = -0.0061(T) + 4.2013 \qquad (-50\,°C < T < 40\,°C) \tag{6}$$

where λ_{PC} is the thermal conductivity of the Pyroceram (W/m·K) and T is the temperature (°C). More information about Pyroceram 9606 can be found in [78].

To record the temperature at different points of the meter bar/sample/meter bar stack, an array of four thermocouples with an accuracy of 0.1 °C (0.18 °F) was used. By knowing the thermal conductivity of the meter bars and using the temperature recorded at different points, heat flow through the samples was calculated. By definition, heat flow is the rate of energy passing through a sample due to a temperature gradient. The needed equations to calculate these two parameters are provided in ASTM E1225-09, D5470-12, and C1045-07. It should be mentioned that these equations are proposed for steady state conditions, while the current experimental program was performed in a quasi-steady state condition. Therefore cooling and heating rates were assigned to be relatively low to reach almost steady state conditions. The heat flow per unit area for the bottom and top Pyroceram meter bars can be calculated by:

$$q_B = \lambda_{PC} \times \frac{T_1 - T_0}{d_{PC}} \tag{7}$$

$$q_T = \lambda_{PC} \times \frac{T_3 - T_2}{d_{PC}}$$

where T_0, T_1, T_2, and T_3, are the temperatures at the bottom of the lower meter bar, at the top of the lower meter bar, at the bottom of the upper meter bar, and at the top of the upper meter bar,

respectively (°C); q_B and q_T are the heat flow per unit area through the lower and upper meter bars, respectively (J/s.m^2); and d_{PC} is the thickness of the meter bars (m).

Using the heat flow per unit area through the top and bottom meter bars, the heat flow through the sample can be calculated by:

$$q_{Sample} = \frac{q_T + q_B}{2}$$
$$Q_{Sample} = q_{Sample}.A \quad (8)$$

where q_{sample} is the average heat flow per unit area through the sample (J/s·m^2); Qsample is the average heat flow (J/s) through mortar sample, and A is the cross-sectional area of the sample (m^2). Heat flow vs. average temperature of the samples under the two temperature profiles was also graphed. The average temperature of the sample was calculated as:

$$T_{avg} = \frac{T_1 + T_2}{2} \quad (9)$$

Farnam *et al.* used this calorimetry set up and graphed heat flow as a function of average temperature to evaluate the effect of deicing salt on the freeze/thaw damage of mortars [79].

3.2 Results and Discussion

3.2.1 Shrinkage

3.2.1.1 Autogenous Shrinkage

Autogenous Shrinkage test was conducted to examine if LWA and RHA, as the carriers for water and PCM, release a portion of the presoaked liquids out of their porous structure. If the voids in the bulk cement paste are empty of water, inward meniscus forces will be generated that cause the matrix to undergo autogenous shrinkage. However, if the pores are kept filled, autogenous shrinkage will be reduced. Therefore, the reduction in the autogenous shrinkage in the mixes in which presoaked LWA or RHA is incorporated shows that the presoaked liquid has leaked out of the carrier.

For Mix 1 (the control), the hydration reactions consume much of the pore solution, inducing menisci and leading to autogenous shrinkage that increased over time (Figure 3.6-a, overleaf). At day seven, the autogenous shrinkage was -154 µm/m, and it reached -435 µm/m after four weeks. Autogenous shrinkage for the first week of a mortar with w/c ratio of 0.35 wt.% was reported to be equal to -178 µm/m by Zhutovsky *et al.* [80]. Tazawa *et al.* argued that the autogenous shrinkage of a mortar is affected by w/c ratio, and it increases with decreases in the w/c ratio. Their research showed that the autogenous shrinkage of a mortar at the age of 28 days is equal to -520 µm/m, -1220 µm/m, -1490 µm/m, and -4240 µm/m for w/c ratio to 40 wt.%, 30 wt.%, 23 wt.%, and 17 wt.%, respectively [81].

For Mix 3W, pre-wetted LWA provided internal curing for the mortar; thus not only was the autogenous shrinkage completely mitigated, but there was a slight expansion in the specimen's length (Figure 3.6-a). Lura *et al.* have attributed such expansion to the water provided by the LWA providing the cement paste with a saturated curing condition, lowering the surface

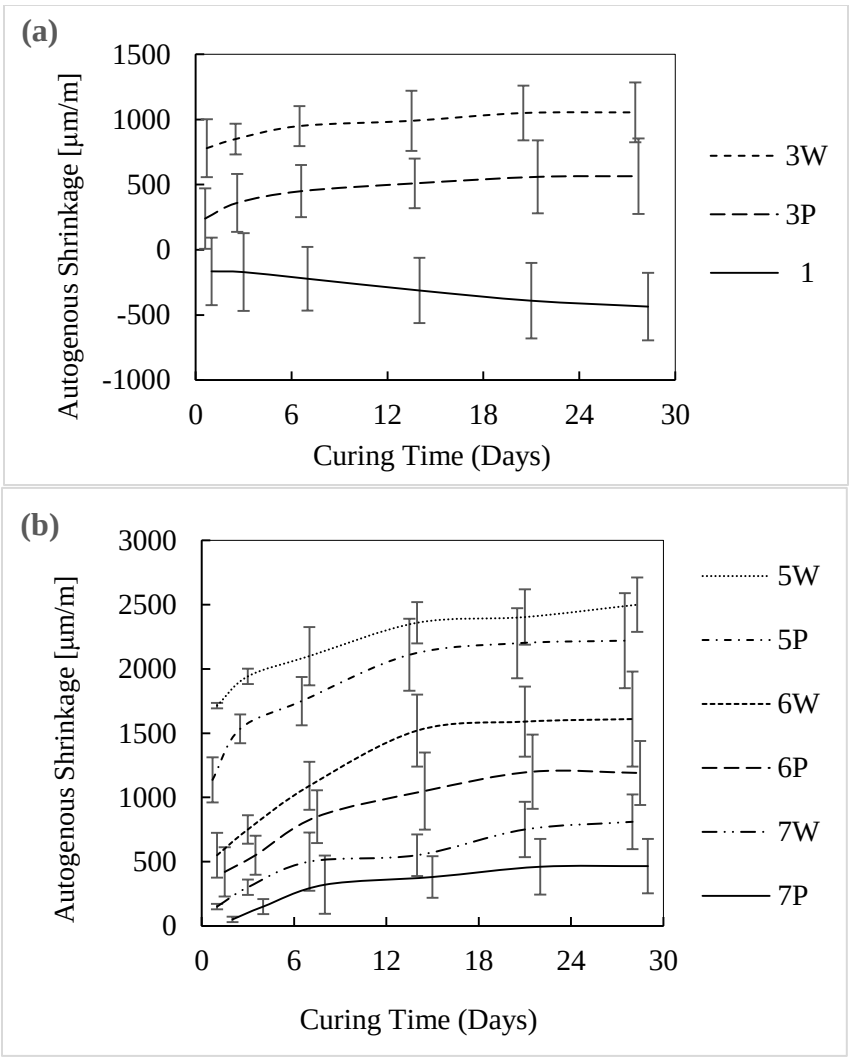

Figure 3.6. Autogenous Shrinkage. a) Mixes with LWA as the carrier. b) Mixes with RHA as the carrier

tension between the cement gel particles, and therefore no capillary pressure develops to oppose the expansion of the solid phase [82]. Bentur *et al.* also showed that incorporation of LWA in the Saturated Surface Dry (SSD) condition not only eliminates the autogenous shrinkage, but also causes expansion in concrete, however, LWA in air dry condition cannot provide internal curing for concrete [71].

Similarly, Mix 3P (containing LWA presoaked in PCM6), underwent autogenous expansion (Figure 3.6-a). Since the volume of PCM in which the LWA was soaked was equal to the volume

of LWA porosity, this result suggests that a portion of PCM has been released by LWA to the media or that some PCM from the surface of the LWA entered the mix. This shows that LWA cannot completely keep the PCM inside its porous structure, and a portion of PCM leaks out of the LWA over the course of hydration reaction. Thus, LWA cannot perfectly perform as a PCM carrier; however, in view of its compatibility with the cementitious media and low cost, it can be considered as an efficient PCM carrier. It should be mentioned that no study was found discussing the leakage of PCM out of LWA.

The same pattern was observed for the mixes with RHA presoaked in water or PCM6 (Figure 3.6-b). For all of these mixes, autogenous expansion occurred, implying that a portion of water and PCM had stuck on the surface of RHA, or leaked out of the RHA pores, and thus entered the bulk cement paste. The expansion level for Mix 7W, where the water/RHA was 20 wt.%, was close to the results of Mix 3W, where LWA was used as the carrier. The water absorption capacity of LWA was reported to be equal to 17.5 wt.%. This suggests that the capacity of RHA to absorb water is closer to 20 wt.%.

The two forces that are involved in the water leakage out of RHA pores are the adhesion force between the RHA surface water molecules, and the osmose force from the bulk cement paste. Kovler *et al.* discussed that leakage of water out of the RHA particles depends on the suction force from the cement paste [83]. At early ages, the water content of the cement paste is still high, thus only water in the big pores of the RHA particles will be released. However, when the hydration reaction proceeds, it consumes the water in the paste and reduces the water content of the paste. Therefore the difference in relative humidity between the cement paste and RHA pores increases, which leads to the increase of osmotic forces. This causes the cement paste to suck the water out

of the finer pores of RHA [84]. However, the much finer pores, i.e. smaller than 4 nm in diameter, in RHA particles remain water-filled for a very long period of time [85].

It should be mentioned that in addition to LWA, other materials such as saturated superabsorbent polymer particles were suggested to be used as a water supply to provide extra water for hydration reaction [86]; however, RHA presoaked in water was not previously used for internal curing purposes.

Water/RHA was not selected to be less than 20 wt.%, because even with this percentage, the mix had a very low workability, and it was difficult to cast in molds. RHA has a high specific surface area (50 – 100 m^2/g (244 – 488 kip^2/lb) [58]), thus RHA particles that are in partially saturated or saturated surface dry condition may absorb mix water and lower the workability of the mortar. In the case that a lower percentage of water is used, additives like superplasticizers could be used to reach the desirable workability.

3.2.1.2 Total Shrinkage

In the total shrinkage mechanism, all three shrinkage mechanisms, chemical, autogenous, and drying, take place simultaneously. Chemical shrinkage takes place because the hydration reactions occur and the chemical products occupy less space than the reactants; autogenous shrinkage takes place because the pores are created in the bulk cement paste and the inward meniscus forces are generated; and since the specimens are kept at room condition and the water in the paste evaporates, the water content of the paste is reduced and thus the volume of the mortar shrinks.

For Mix 1, since no external curing and/or internal curing was provided and also the hydration reactions took place over time causing a decrease in the water content, the shrinkage increased (Figure 3.7). Since the ASTM C596-07 standard recommends that the shrinkage values should not

be prefixed with a minus sign, the absolute value of the results are presented. The rate of the shrinkage was higher in the first 14 days because the main part of the reaction and water evaporation take place during the first two weeks after mixing.

Persson argued that increasing the w/c ratio not only does not eliminate the total shrinkage, but also increases it [87]. The total shrinkage of Mix 1, with w/c ratio of 0.4 was measured to be equal to 0.061%. The total shrinkage of a mix with w/c ratio of 0.35 was reported to be equal to 0.052% that is less because of its lower water content [87]. However, Hansen argued that the relative ambient humidity affects the total shrinkage because it affects the rate of water evaporation from the mix. An increase in relative humidity decreases the total shrinkage because it decreases the water loss of the mix [88].

For Mix 3W, where a portion of the sand was replaced by LWA, total shrinkage increased. It is established in some studies that the lower restraint provided by LWA can lead to increased total

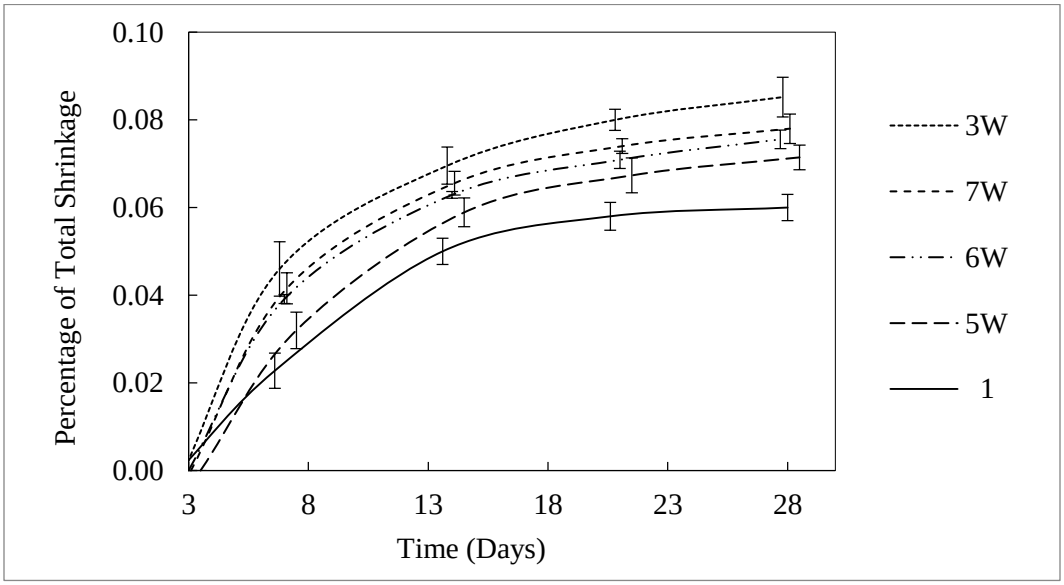

Figure 3.7. Total Shrinkage for mixes in which the carrier was presoaked in water

shrinkage compared with mixtures containing only sand [89]. This also shows that additional water provided by LWA may not be effective in reducing the total shrinkage of the mortar, because the extra water may evaporate over time. Qian *et al.* also showed that even by incorporating superplasticizer, the total shrinkage of mortar or concrete cannot be eliminated [90].

The same trend can be observed for the mixes to which RHA presoaked in water was added (Figure 3.7). A portion of cement was replaced by RHA in these mixes and therefore less C-S-H, the primary binding phase in cementitious binders, was produced during the hydration reactions. It is possible that the lower strength of RHA compared to the strong phase of C-S-H provided less restraint against shrinkage and therefore the total shrinkage increased. Considering the standard deviations of Mixes 5W, 6W, and 7W, it can be concluded that, since extra water in the media will evaporate over time, presoaking RHA in more water does not make a difference in the level of total shrinkage in the long term. For the mixes in which the carrier was presoaked in PCM the results had the same trend; incorporating LWA and RHA in the mix increased the total shrinkage and the amount of presoaked PCM did not make a meaningful difference in the results.

3.2.2 Calorimetry

3.2.2.1 Semi-adiabatic Calorimetry

The semi-adiabatic calorimetry test was conducted to examine if water or PCM leaks out of LWA and/or RHA and interferes in the hydration reactions. Incorporation of LWA and RHA presoaked in PCM and water decreased the magnitude, and delayed the onset of, the peak temperature for all the mixes (Figure 3.8, overleaf). For Mix 1, the control, the peak temperature reached 58.2 °C (136.8 °F) and occurred at 13 h 30 min; however, for Mix 2, where the PCM

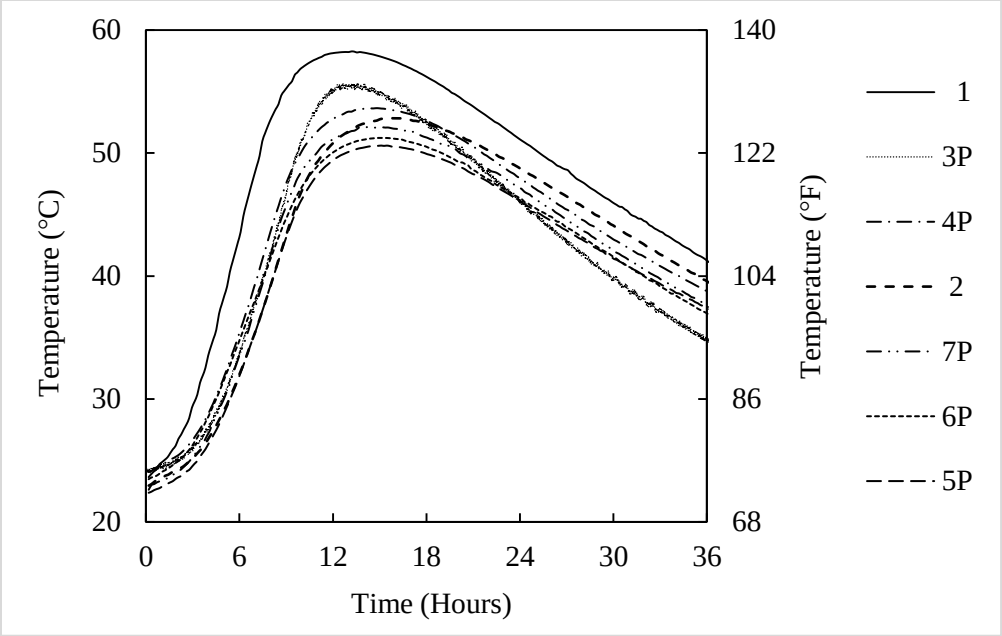

Figure 3.8. Semi-adiabatic Calorimetry for mixes with carrier presoaked in PCM6

was directly added to the mix, the peak temperature was 52.9 °C (127.2 °F) and took place at 15 h 50 min. This means that incorporating PCM in the cementitious media without using a carrier can decrease the heat released by the hydration reaction by about 10% and delay reaching the peak temperature by about 17%. The PCM that exists in the matrix could act as a retardant by coating cement particles, hampering the transport of water into those particles, and thus, reducing the rate and degree of hydration [26].

The results of semi-adiabatic calorimetry of Eddhahak *et al.* showed that incorporating of 1 vol.%, 3 vol.%, and 5 vol.% PCM in a mortar reduces the peak temperature by 9%, 12%, and 15%, respectively and delays reaching to that by 15%, 18%, and 22%, respectively [52]. Bentz *et al.* also argued that incorporating PCMs directly in mixture reduces the peak temperature by 8 °C (14.4 °C), and delays that by more than one hour [49].

For mix 3P, where the amount of pre-soaked PCM was equal to the LWA absorption capacity reported by the manufacturer (17.5 wt.%), the peak temperature reached 55.7 °C (132.3 °F) and was delayed by 30 min. This shows that using LWA as the PCM carrier can prevent PCM from interfering with the hydration reaction. However the small reduction in the peak temperature and the short retardation is attributed to the effects of the PCM that was stuck on the surface of LWA particles and/or had leaked out the LWA pores (Figure 3.8). Bentz and Turpin showed that if LWA is used as PCM carrier and the amount of presoaked PCM was equal to the capacity of LWA, there will be a very small reduction and delay in reaching to the peak temperature [49].

For mix 4P, where the amount of LWA pre-soaked in PCM was equal to the LWA absorption capacity measured by the absorption test described in Section 2.1.2.2 (30 wt.%), the reduction in peak temperature and the delay in that was about the same with Mix 2, where no carrier was used. This suggests that since the capacity of LWA to absorb PCM was overestimated by the absorption test, and a large portion of the presoaked PCM leaked into the bulk cement paste (Figure 3.8).

The same phenomenon was observed in mixes where RHA was the carrier and contained 20 wt.% of PCM (Mix 7P). However, a larger decrease in peak temperature and a longer delay were observed when more PCM was used in Mix 6P with 40 wt.% and Mix 5P with 80 wt.% of PCM incorporated in RHA, respectively. This suggests that a portion of PCM leaked out of the RHA and that, similar to the LWA, RHA cannot completely contain PCM inside its porous structure. It should be added that in general, the mixes with RHA had a lower peak temperature compared to the mixes with LWA as a carrier because of the lower cement content in those mixes (Figure 3.8).

Similar results were obtained when LWA and RHA were presoaked in water (Figure 3.9). For Mix 3W, where the pre-soaked water in the LWA was 17.5 wt.%, there was about 3% reduction in the peak temperature. Since a portion of water leaks out of the carrier, incorporating LWA and

RHA presoaked in water increases water content of the mix. Water has a larger heat capacity than cement, sand, or LWA; a mix will therefore reach a reduced peak temperature as the water absorbs energy. Also, for a fixed volume, larger w/c means less cement per unit volume, and thus less heat generation. These results match with other studies where it is shown that incorporating LWA presoaked in water into the cementitious materials lowers the peak temperature and delays that, because of the larger heat capacity of water [91].

For Mix 4W, where the amount of pre-soaked water is more than the LWA's capacity, the decrease and delay in peak temperature is more. Also, for mixes with RHA as the carrier, Mixes 5W, 6W, and 7W, the peak temperature is decreased and delayed which shows that the w/c ratio had been increased; this suggests that the pre-soaked water has leaked out of the RHA (Figure 3.9).

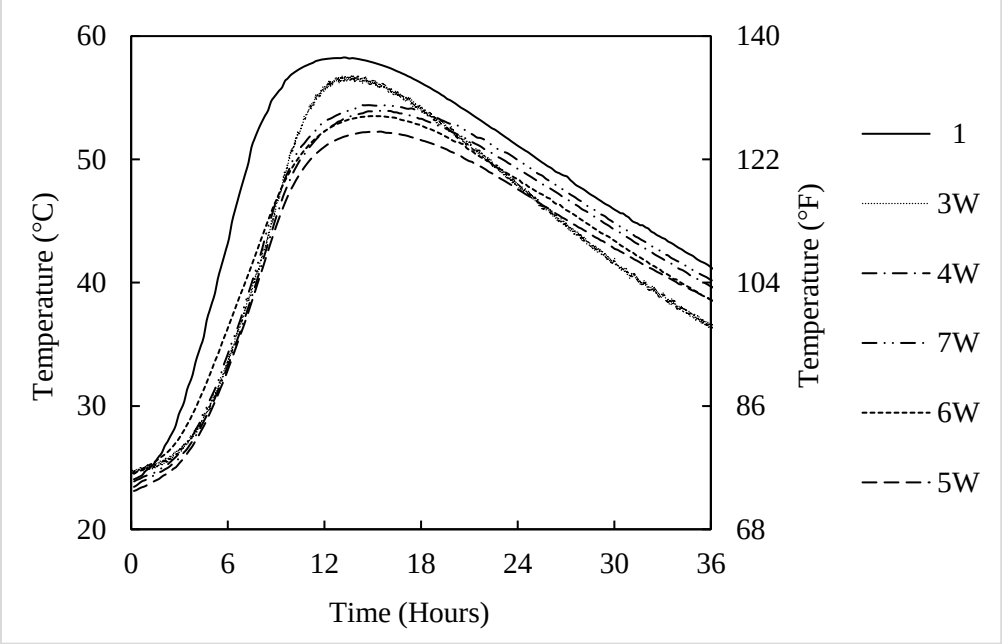

Figure 3.9. Semi-adiabatic Calorimetry for mixes with carrier presoaked in water

The effect of the type of incorporated PCM was studied by incorporating LWA presoaked in PCM6, PCM-10, and PCM28 (Figure 3.10). In Mix 4P, the amount of PCM exceeds the LWA capacity, therefore a relatively large amount of PCM enters the bulk cement paste and the effect of that on the hydration reaction would be visible. All of the PCMs are paraffin waxes that are made of hydrocarbon chains; however, the difference in their chemical composition made a slight difference in their effect on the hydration reaction. The effect of PCM6 and PCM28 look almost the same, however, PCM-10 seems to have a smaller effect on the hydration reaction (Figure 3.10). Another study also showed that the effect of PCM on the hydration reaction was dependent on the PCM type [26].

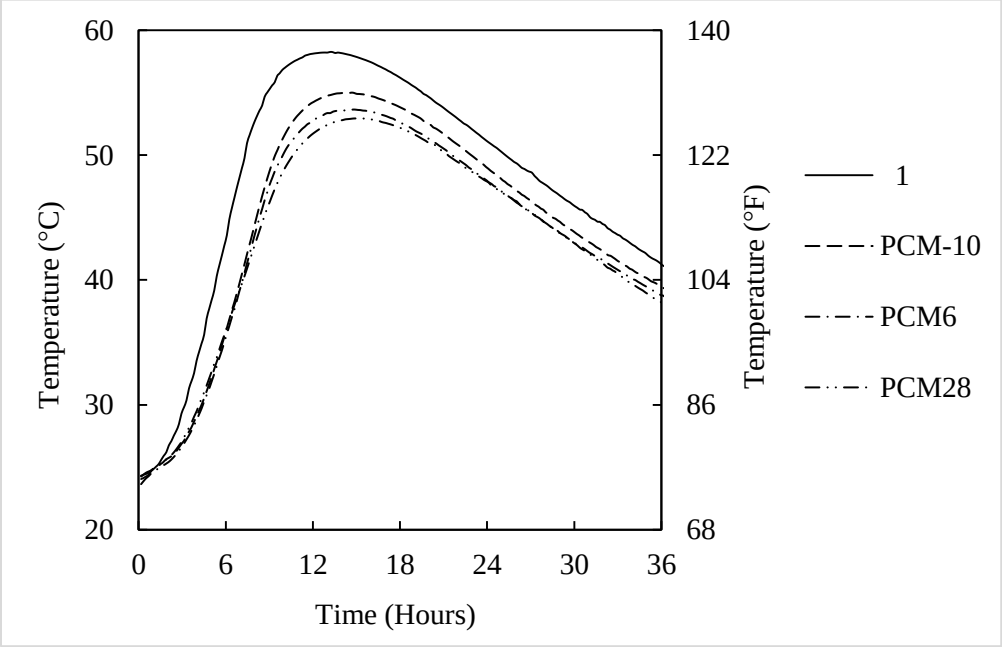

Figure 3.10. Semi-adiabatic calorimetry test to study the effect of PCM type on the hydration reaction. Mix 4P with incorporated LWA presoaked in PCM6, PCM-10, and PCM28

3.2.2.2 Isothermal Calorimetry

Isothermal calorimetry tests were conducted on all the mixes to better understand the effect of incorporating LWA and RHA presoaked in PCM and water on the hydration reaction between cement and water. This test is more precise than semi-adiabatic calorimetry. For Mix 1, the control, the heat flow reached to 0.0047 W/(g of cement) after 4 h 15 min (Figure 3.11). This primary peak is the result of the hydration of Alite (tricalcium silicate, with the oxide notation of $3CaO.SiO_2$). The hydration of Alite is described as [76]:

$$2Ca_3SiO_5 + 6H_2O \rightarrow 3CaO \cdot 2SiO_2 \cdot 3H_2O + 3Ca(OH)_2 \qquad (10)$$

This is a fast reaction that releases a large amount of heat over a short period of time and controls the set time and the initial strength of the mortar.

There is a secondary peak with the magnitude of 0.0041 W/(g of cement) at the age of 6 h 50 min. This peak is the result of the creation of Belite phase (dicalcium silicate, with the oxide notation of $2CaO.SiO_2$). The hydration of Belite can be described as [76]:

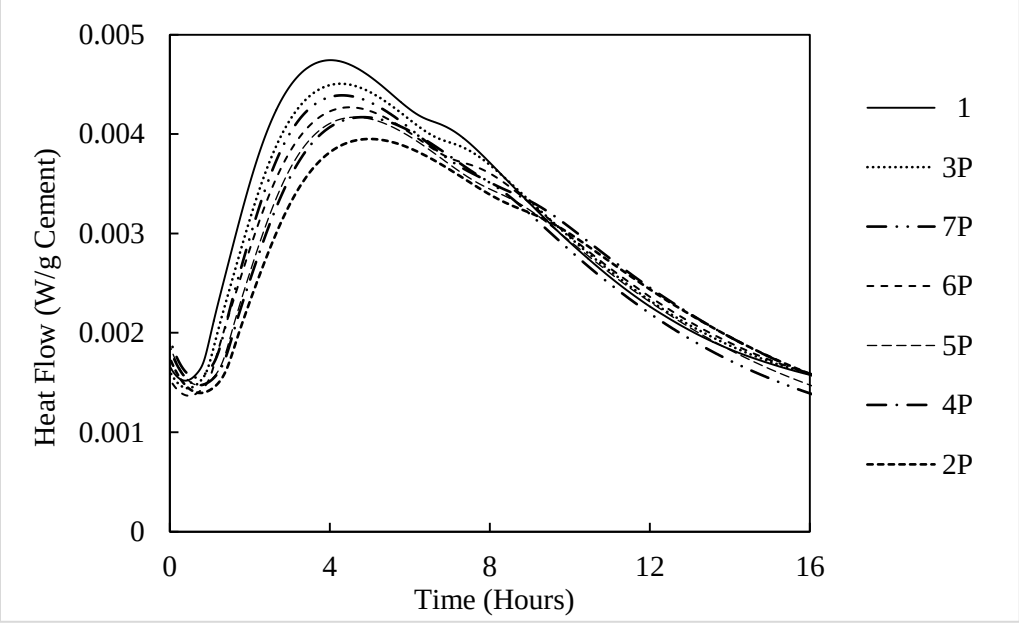

Figure 3.11. Isothermal calorimetry for mixes with carrier presoaked in PCM6

$$2Ca_2SiO_4 + 4H_2O \rightarrow 3CaO \cdot 2SiO_2 \cdot 3H_2O + Ca(OH)_2 \quad (11)$$

This is a slow reaction that releases a relatively small amount of heat at a longer time and adds strength to the mortar over long time periods. Alite and Belite account for more than 70 wt.% of Ordinary Portland Cement-based clinker, and thus their hydration of them forms the major properties of a cementitious system [76]. Therefore, there is not a visible third peak corresponding to the hydration of other phases in the isothermal calorimetry graphs. It should be mentioned that since a 45-minute equilibrium period was used when setting up the experiment during which data were not recorded, the peaks corresponding to the hydration of phases such as Aluminate (tricalcium aluminate with the oxide notation of $3CaO.Al_2O_3$) and/or Ferrite (tetracalcium aluminoferrite with the oxide notation of $4CaO.Al_2O_3.Fe_2O_3$) also are not visible.

For Mix 2, where PCM was directly added to the mortar, the primary peak had a magnitude of 0.0040 W/(g of cement) and took place after 5 h 5 min. The secondary peak had a magnitude of 0.0032 W/(g of cement) and took place after 9 h 10 min. This means that the primary peak was decreased by 17% and was delayed by 20%, and the secondary peak was decreased by 21% and was delayed by 32%. These decreases and delays in the peak are attributed to the interference of the PCM with the hydration reactions. The results also suggest that the hydration of Belite is somewhat more affected by this interference than Alite (Figure 3.11).

For Mix 3P, where the amount of pre-soaked PCM was equal to the LWA absorption capacity reported by the manufacturer (17.5 wt.%), the primary peak had a magnitude of 0.0044 W/(g of cement) and took place after 4 h 20 min. The secondary peak had a magnitude of 0.0037 W/(g of cement) and took place after 7 h 20 min. This means that the primary peak was decreased by only 7% and was delayed by 4%, and the secondary peak was decreased by 10% and was delayed by 7% (Figure 3.11). These results match with another research where the peak and

magnitude of the heat flow was reduced and delayed by 16% and 12%, respectively, where LWA presoaked in PCM was incorporated in the mix [26]. This reduction and delay was attributed to the effect of PCM to encourage the production of reaction products that produce less heat.

For Mix 4P, where the amount of presoaked PCM into the LWA was equal to the LWA absorption capacity measured by the absorption test described in Section 2.1.2.2 (30 wt.%), the primary peak had a magnitude of 0.0041 W/(g of cement) and took place after 4 h 45 min. The secondary peak had a magnitude of 0.0034 W/(g of cement) and took place after 8 h 10 min. This means that the primary peak was decreased by more than 15% and was delayed by 15%, and the secondary peak was decreased by 17% and was delayed by 19% (Figure 3.11).

Similar to the semi-adiabatic results, comparison of the results for Mix 3P and 4P suggest that the absorption capacity of LWA was overestimated by the absorption test, and when LWA is presoaked in extra PCM, LWA cannot effectively hold all of the PCM inside its porous structure. However, if the amount of pre-soaked PCM in the LWA is equal to the absorption capacity of the LWA, LWA can effectively hold the PCM inside its porous structure and prevent it from interfering with the hydration reaction. But even in this case, LWA releases a small portion of PCM to the bulk cement paste.

Similar results can be obtained when RHA is used as the PCM carrier (Figure 3.11). For Mix 7P with 20 wt.% of PCM pre-soaked in RHA, the decrease and delay in the heat flow peak is almost the same as for Mix 3P. Unlike the semi-adiabatic calorimetry, the results of this test were normalized with the mass of cement available in the mix, thus the peak heat flows of the mixes with RHA as the carrier were not affected by the lower cement content in the mix. This suggests that the absorption capacity of RHA is about 20 wt.%. However, a more accurate experiment is required to better estimate the RHA absorption capacity. For Mix 6P and 5P with 40 wt.%

and 80 wt.% of PCM pre-soaked in RHA, respectively, a bigger decrease and longer delay in both primary and secondary heat flow peaks were observed (Figure 3.11).

Similar results were obtained when LWA and RHA were presoaked in water (Figure 3.12). By incorporating LWA presoaked in water in the mortar, Mix 3W, there is a small reduction in the peak heat flow and a retarding effect. LWA releases water to the mix which increases the w/c of the mortar. Water has a larger heat capacity than other components in the mix, and thus the heat capacity of the mortar that has pre-wet LWA increases. This reduces the peak of the heat flow [91]. For Mix 4W, where more water is presoaked in LWA, the reduction in the peak of heat flow and its delay are more (Figure 3.12).

These results are in contrast with the results presented by Pane *et al.* [92]. Their results showed that the peak of heat flow was diminished and slightly delayed for mixtures with lower water content. They argued that since the since the space available for the growth of hydration products is smaller, the hydration is diminished and retarded for the systems with lower water content.

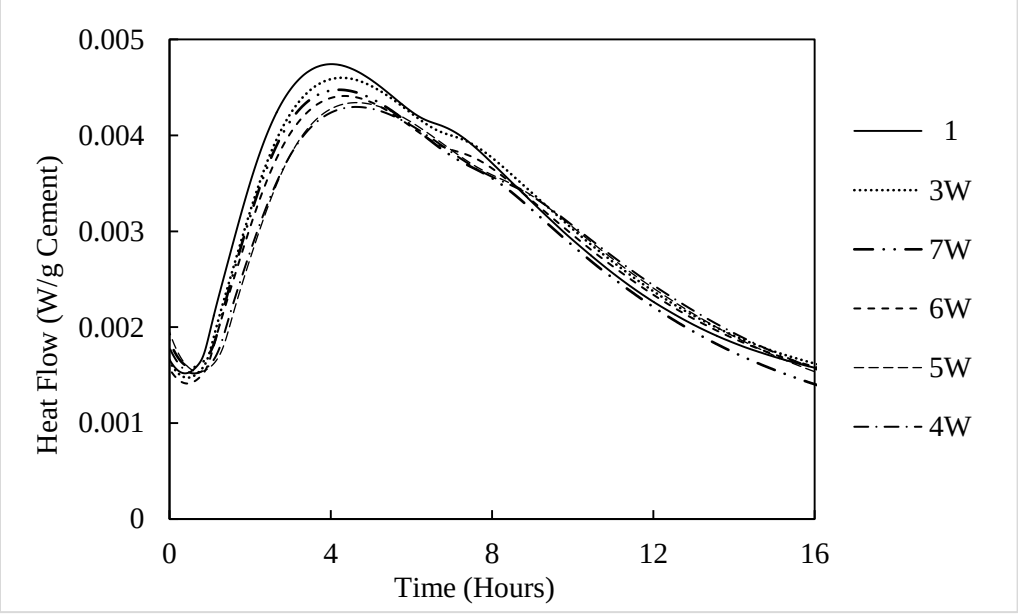

Figure 3.12. Isothermal calorimetry for mixes with carrier presoaked in water

Incorporating RHA presoaked in water, Mix 5W, 6W, and 7W, yields similar results: the more water in the mix, the smaller the peak in the heat flow. This again suggests that the carriers release a portion of the presoaked water to the bulk cement paste and/or the water that was stuck to the surface of the carrier particles enters the bulk. Unlike semi-adiabatic calorimetry, the results of this test were normalized with the mass of cement available in the mix, thus the peak heat flows of the mixes with RHA as the carrier were not affected by the lower cement content in the mix (Figure 3.12).

The effect of the PCM type of the hydration reaction was studies by presoaking LWA in PCM6, PCM-10, and PCM28 (Figure 3.13). Similar to semi-adiabatic calorimetry, the results of this test also show that the effect of PCM6 and PCM28 are quite similar, but the effect of PCM-10 is slightly less, which is attributed to the different chemical composition of each PCM. These results match with those of another study where the effect of PCM on the hydration reaction was reported to be dependent on the PCM type [26].

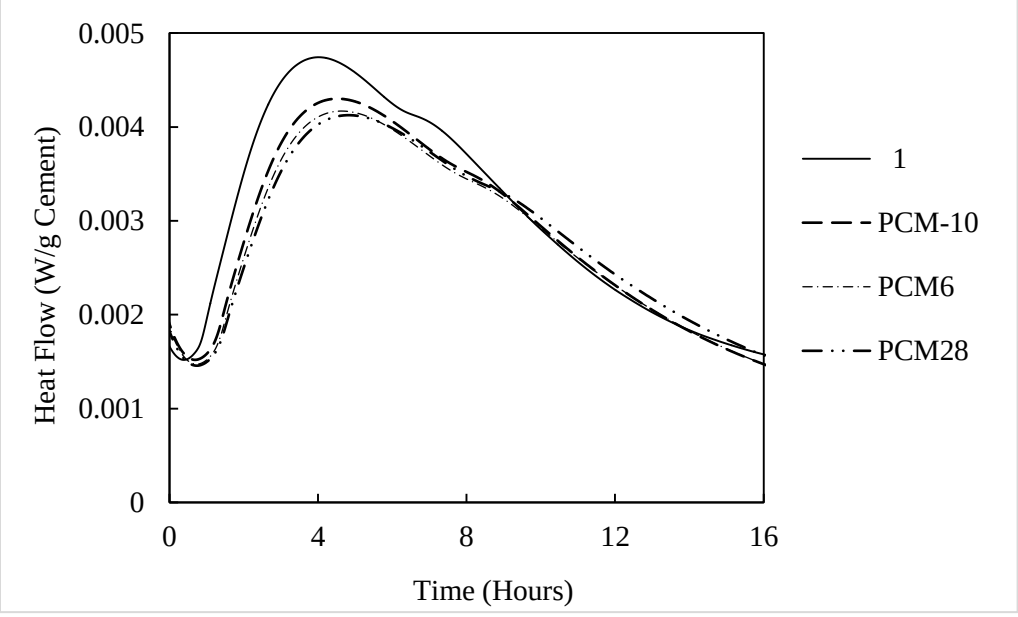

Figure 3.13. Isothermal calorimetry test to study the effect of PCM type on the hydration reaction. Mix 4P with incorporated LWA presoaked in PCM6, PCM-10, and PCM28

3.2.3 Setting Time

For Mix 1, the control, the initial and final setting times were equal to 120 min and 180 min, respectively. In the case that PCM6 was used, when it was directly added to the mix, Mix 2, the initial setting time was delayed 25% and the final setting time was delayed by 41%. The existence of a large amount of a PCM in the mix drastically affected the hydration reaction and retarded the rate of nucleation and growth of hydrates. Therefore the formation of stiff phases was delayed and it took a longer time until the mortar was stiff enough to prevent the needle's penetration (Table 3.2).

For Mix 3P, and in the case of PCM6, the LWA kept PCM inside its porous structures and prevented it from interfering with the hydration reaction. Therefore, the delays in the initial and final setting times were only 12.5% and 16.7%. These small delays are attributed to the effect of the PCM that was stuck to the surface of LWA aggregates and/or the portion on PCM that was leaked out of LWA. When the amount of presoaked PCM was more than the LWA absorption capacity, Mix 4P and in the case of PCM6, the delay in both of the setting times were close to the case that no LWA was used (Table 3.2).

Table 3.2. Setting Time (min)

Mix #	PCM6		PCM-10		PCM28	
	Initial	Final	Initial	Final	Initial	Final
1	120	180	120	180	120	180
2	150	255	150	240	75	135
3P	135	210	120	180	90	150
4P	150	240	135	225	75	135

Similar results were obtained in the case that PCM-10 was used. However, the effect of PCM-10 was relatively lower than the effect of PCM6. The difference is attributed to difference in the chemical properties of the two PCMs. These results match with the results of the calorimetry tests (Table 3.2). Uchikawa *et al.* and Lv *et al.* also reported that the setting time of cement paste would be delayed by adding organic admixtures and PCMs, respectively, since they act as retarders [93, 94]. However, Kim *et al.* argued that incorporation of PCM in the mixture decreases the initial and final setting time because it works as an accelerator and expedites the hydration reaction of cement [95].

In the case of PCM28, the initial and final setting times were decreased for all the mixes. PCM28 is solid at room temperature and had to be kept in the oven at a temperature of 40 °C (104 °F) before mixing with the LWA. Mixing was done at room temperature which was below the melting point of PCM28. Therefore, right after molding the mortar, PCM28 started to solidify and cause the aggregate particles to stick together. This created a stiffer mortar in a shorter time and decreased the apparent setting time. Comparing the results of setting times for Mixes 2, 3P, and 4P, and for the cases that PCM28 is utilized, shows that a larger amount of PCM utilized in the mix causes a more pronounced effect on the initial and final setting times. The biggest effect was observed from Mix 2, in which no carrier was used, where the initial and final setting times were decreased by 37.5% and 33.3%, respectively.

3.2.4 Compressive Strength

The compressive strength of Mix 1 increased over the period of 28 days, however, the rate of increase diminished over the time (Figure 3.14, overleaf). The compressive strength increased by 20% (from 33 MPa to 39.5 MPa (4.79 ksi to 5.73 ksi)) over the period between day three and

day seven after mixing, but it increased by only 16% (from 39.5 MPa to 45.7 MPa (5.73 ksi to 6.63 ksi)) for the period between day seven and day 28 after mixing. This is because the main part of hydration of major phases such as Alite, Belite, and Aluminate take place during the first few days and the hydration rate decreases over time.

For Mix 2, where PCM was directly added to the mix, the compressive strength was drastically decreased (Figure 3.14). The compressive strength of Mix 2 at the age of 28 days reached 36.1 MPa (4.93 ksi), a decrease of 21% compared to the control mix. This decrease was because of the interference of PCM with the hydration reaction. Also, the PCM that exists in the matrix could act as a retardant by coating cement particles and hampering the transport of water into those particles [26]. Since the utilized PCM had a lower density than any other material in the mix, it accumulated on the top of the mortar as a layer of wax and made the mixing process harder and more time consuming. Even after molding, there was a relatively thick layer of PCM stuck on the top of the mix. This shows that incorporation of PCM directly to the mortar not only decreases the compressive strength, but also causes practical, aesthetics, and safety problems when they are used as construction or pavement materials.

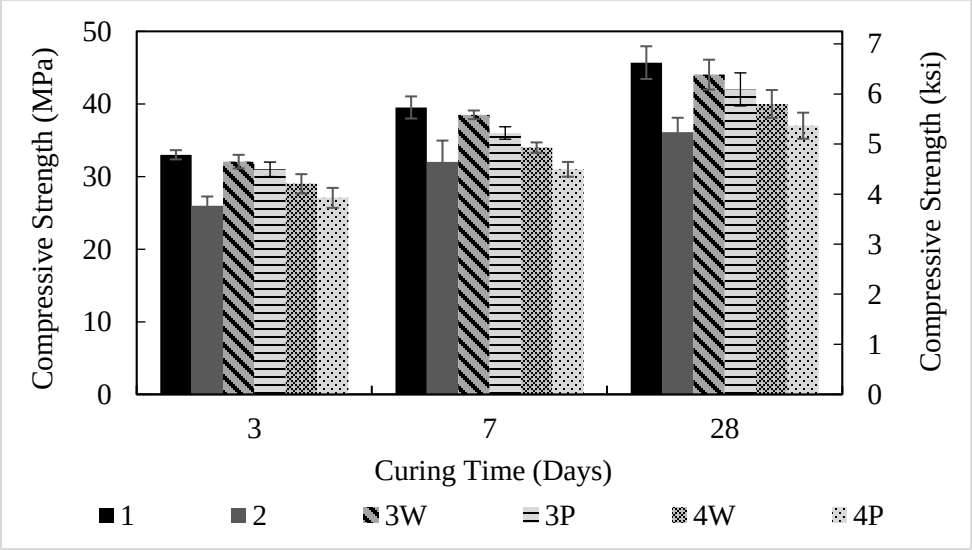

Figure 3.14. Compressive strength test for mixes with LWA as the carrier

For Mix 3W, with water-soaked LWA providing internal curing, the compressive strength was slightly lower than that of the control. Regarding the relatively high w/c that was used and the curing of the samples in the moisture room, all the samples had good curing condition and the internal curing was not a big advantage for Mix 3W. However, the presoaked water in LWA caused the mix to have a slightly higher w/c ratio and thus a slightly lower compressive strength. In addition to that, LWA is mechanically weaker than sand, which caused the samples that include LWA to have lower compressive strengths. However, regarding the error bars, this does not seem to be a meaningful decrease in compressive strength (Figure 3.14). Behnood *et al.* also reported that the compressive strength of concrete slightly decreases by increasing the w/c [96].

The compressive strength of Mix 3P was further decreased, attributed to the PCM that was stuck to the surface of LWA particles and/or the PCM that leaked out of LWA. The PCM can cover the surface of cement particles and diminish the hydration reaction. However, since the presoaked PCM was equal to the LWA absorption capacity, this did not drastically decrease the compressive strength (Figure 3.14).

Other studies show that the lower strength of LWA compared to sand and also the PCM covering the surface of sand particles and reducing the connection force between the sand and the bulk cement paste are the reasons for the diminished compressive strength of a mortar that incorporates LWA presoaked in PCM [26, 97]. Ling *et al.* argued that incorporating PCMs decreases the compressive strength of concrete, however, it remains within the range appropriate for most construction purposes [98]. For both Mix 4W and Mix 4P, there was a larger reduction in compressive strength. The presoaked water and PCM in these two mixes exceeded the LWA capacity. For Mix 4W, the w/c of the mortar was therefore further increased and for Mix 4P, the hydration reaction was further diminished by the PCM. Also, the existence of the PCM in the

mortar may cover the sand particles and reduce the connecting force between the binder and the aggregates (Figure 3.14).

For all of the mixes with RHA as the PCM carrier the compressive strength was drastically decreased (Figure 3.15). There are several parameters that may have diminished the compressive strength in these mixes, including:

- RHA is a weaker material compared to sand or LWA. Therefore, replacement of the aggregates with RHA yields a weaker mortar.
- A portion of the cement was replaced by RHA; therefore, the cement content was decreased and there was less creation of the rigid phase of C-S-H. If RHA is burned at a high temperature (above 800 °C (1472 °F)) and is ground to extremely fine powder in the range of the cement particle size (5 µm to 45 µm (196 µin to 1772 µin)), it shows pozzolanic behavior and enhances the compressive strength [67, 68, 99]. But the utilized RHA was burned at 650 °C (1202 °F), and was not ground into fine powder since it was meant to be used as the PCM carrier and grinding would lead to a reduced volume of pores in each particle.

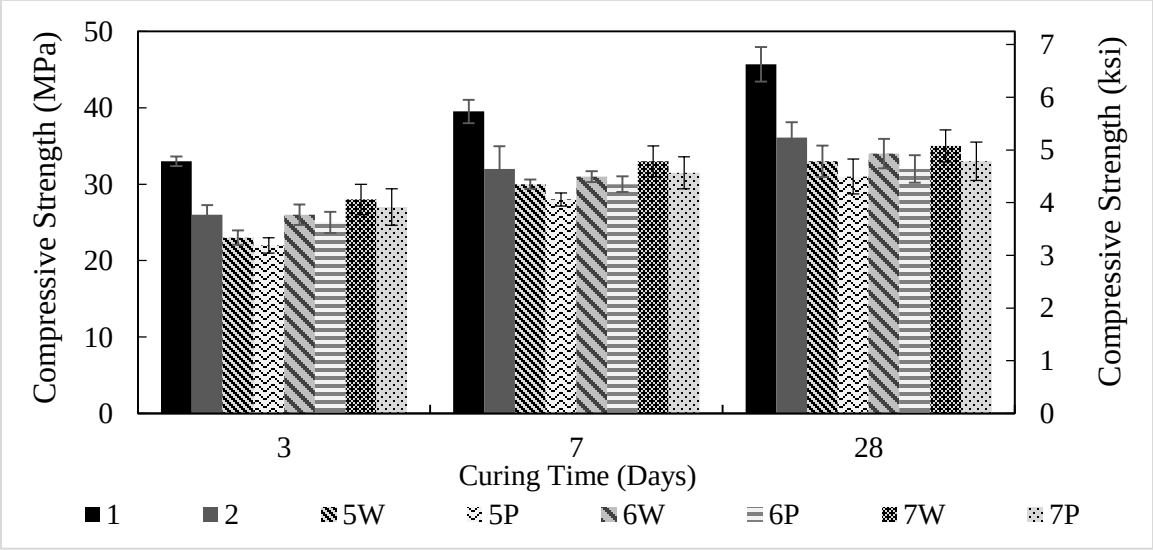

Figure 3.15. Compressive strength test for mixes with RHA as the carrier

- The RHA presoaked in water exceeded the absorption capacity of RHA and thus entered the bulk cement paste, resulting in an increase in water content of Mix 5W and Mix 6W.
- The RHA presoaked in PCM exceeded the absorption capacity of RHA and thus entered the bulk cement paste and interfered with the hydration reaction. It may also have covered the surface of sand particles and reduced the connective forces between them and the bulk cement paste (Mix 5P and 6P).

Comparing the results of Mix 2 with Mix 5P, 6P, and 7P shows that using a weak carrier for PCM, such as RHA, can decrease the compressive strength by as much as when the PCM is directly added to the mix (Figure 3.15). However, using RHA makes the mixing easier and faster and also prevents the PCM from accumulating on the top of mortar. Therefore, due to the compatibility of RHA with cementitious media, it may be considered a good candidate for being used as a PCM carrier, especially for applications in which high compressive strength is not required.

3.2.5 XRD and FTIR

XRD diffractograms of Mix 1 show a peak at 23°-2Θ indicative of calcite and/or hydrotalcite, a well-defined peak at 27°-2Θ indicative of aragonite, a hump centered around 28.5°-2Θ indicative of calcite and/or C-S-H, a wide hump centered around 46°-2Θ indicative of calcite, a hump at 50°-2Θ indicative of C-S-H, and a hump centered around 60°-2Θ indicative of calcite and/or hydrotalcite (Figure 3.16, overleaf). C-S-H does not have a completely crystalline structure, however the humps at 27°-2Θ and 50°-2Θ are attributed to its structure [100, 101]. XRD results elsewhere also show well-defined peaks at 23°-2Θ and 27°-2Θ for concrete [102].

To study the stability of the PCM structure, Zhang *et al.* conducted XRD tests on a composite PCM, based on n-octadecane and expanded graphite, undergoing cyclic melting and solidifying. The results showed that the XRD pattern of the composite PCM after 50 cycles of melting and

solidifying was almost as that of it before applying the cycles, indicating that the PCM exhibits good structural stability [103].

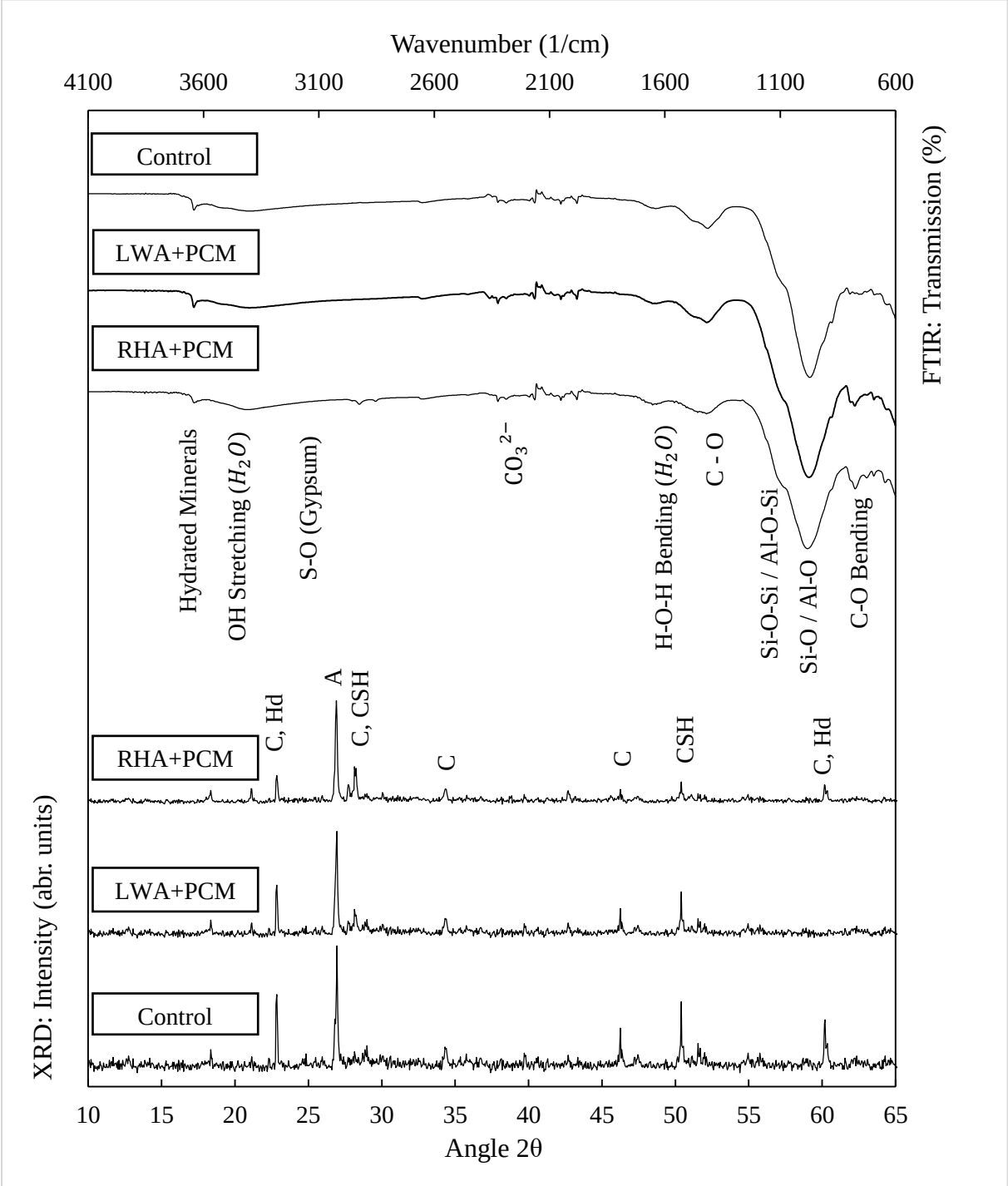

Figure 3.16. XRD diffractograms and FTIR spectra of Mix 1, Mix 4P, and Mix 5P. C = Calcite, A = Aragonite, Hd = Hydrotalcite, CSH = Calcium Silicate Hydrate (C-S-H), Al = alumina

The FTIR spectrum of this Mix 1 shows broad peaks around 3400 cm^{-1} indicating water, a broad peak centered around 1300 cm^{-1} that could indicate C-O bonds, a peak at 980 cm^{-1} indicating Si-O and/or Al-O stretching vibrations, and a weak peak around 760 cm^{-1} likely to indicate C-O bending vibrations. Similar results can be observed for the mixes with LWA or RHA presoaked in PCM, Mixes 4P and 5P respectively. The results of XRD and FTIR experiments show that the incorporation of the PCM in the media does not drastically change the crystal structure and chemical composition of the mortar, respectively (Figure 3.16). The FTIR results reported by Jeong *et al.* also show that incorporation of PCMs in a concrete that is made of other pozzolanic materials, such as silica fume, does not change the chemical properties of the composite [104]. These results imply that the reduced strength and heat evolution observed in mixtures containing the PCM are due to mechanical considerations, such as at the sand/cement interface, or chemical effects, such as reducing the overall reactivity of the system (and not the production of alternative phases).

3.2.6 Guarded Longitudinal Comparative Calorimetry

This test was conducted to see how incorporating different PCMs in mortar affects the mortar's thermal properties. This test was carried out only on the mixes in which LWA was used as the carrier. The presoaked PCM in LWA was as low as the absorption capacity of LWA, 17 wt.%, to avoid overestimating the effect of PCM by utilizing extra quantities in the mixtures. Therefore the test was solely done on Mix 3P, but with different presoaked PCMs, i.e., PCM6, PCM-10, and PCM28. Regarding the melting point of the utilized PCM, the cold plate was programmed with the two different temperature profiles described in Figure 3.5. However, to better illustrate the generated results, the tests were initially carried out on Mix 3W under both temperature profiles.

Changes in temperature at different points of the meter bar/sample/meter bar stack were recorded when Mix 3W underwent temperature Profile #1 and Profile #2, (Figure 3.17-a) and (Figure 3.17-b), respectively.

When the temperature approached 0 °C (32 °F), the slope of the temperature vs. time curve for the upper side of the sample (T_2) changed. There are two points where this change in the slope took place, the first one due to the solidifying and the second one due to the melting of water. This change in the slope is due to the latent heat of incorporated water when it undergoes solid/liquid phase transition. By definition, the latent heat of a material is the amount of heat energy that is needed to change the phase of that material without changing its temperature.

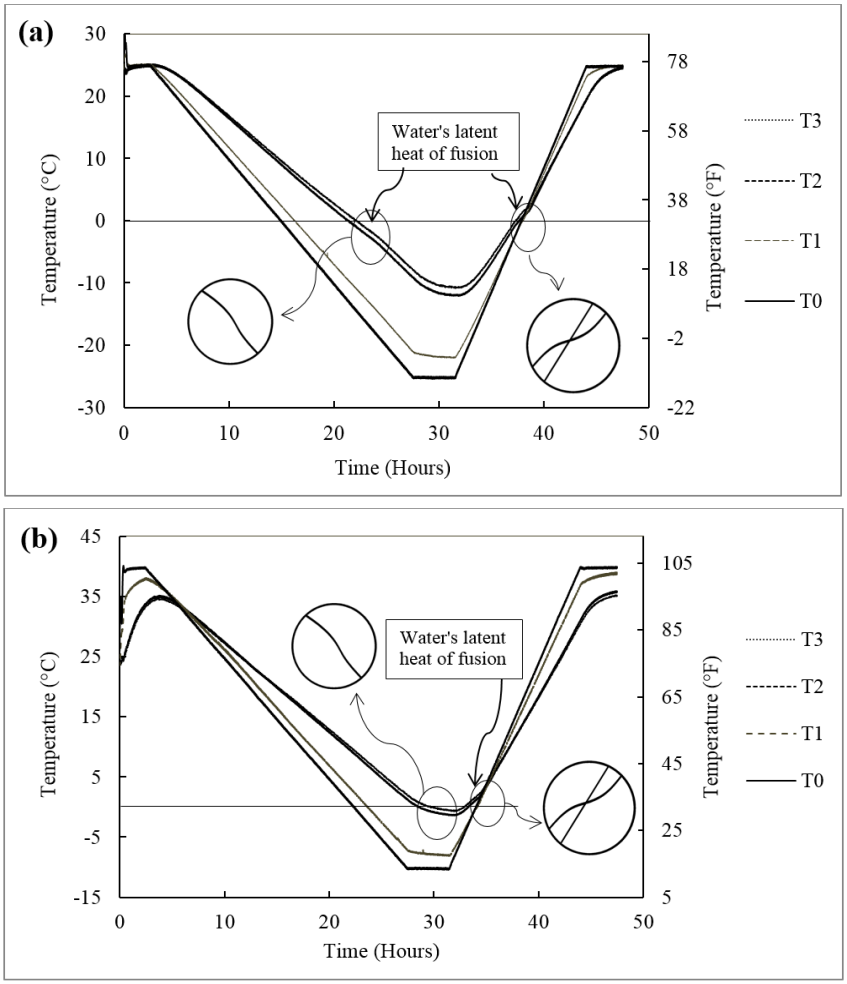

Figure 3.17. Temperature profile for the sample with LWA presoaked in water (Mix 3W). a) Under the temperature Profile #1. b) Under the temperature Profile #2

During thawing, applied heat converts the ice at a temperature of 0 °C (32 °F) to water at a temperature of 0 °C (32 °F). This phase transition delays the increase in the temperature of the sample during heating. A similar effect happens during cooling, when the transition from water to ice delays the decrease in the temperature of the sample. For Profile #2, the change in the slope is less because the entire sample does not reach 0 °C (32 °F) (Figure 3.17-b).

Graphs of heat flow vs. average temperature of Mix 3W under Profile #1 and Profile #2 are shown in (Figure 3.18-a) and (Figure 3.18-b), respectively.

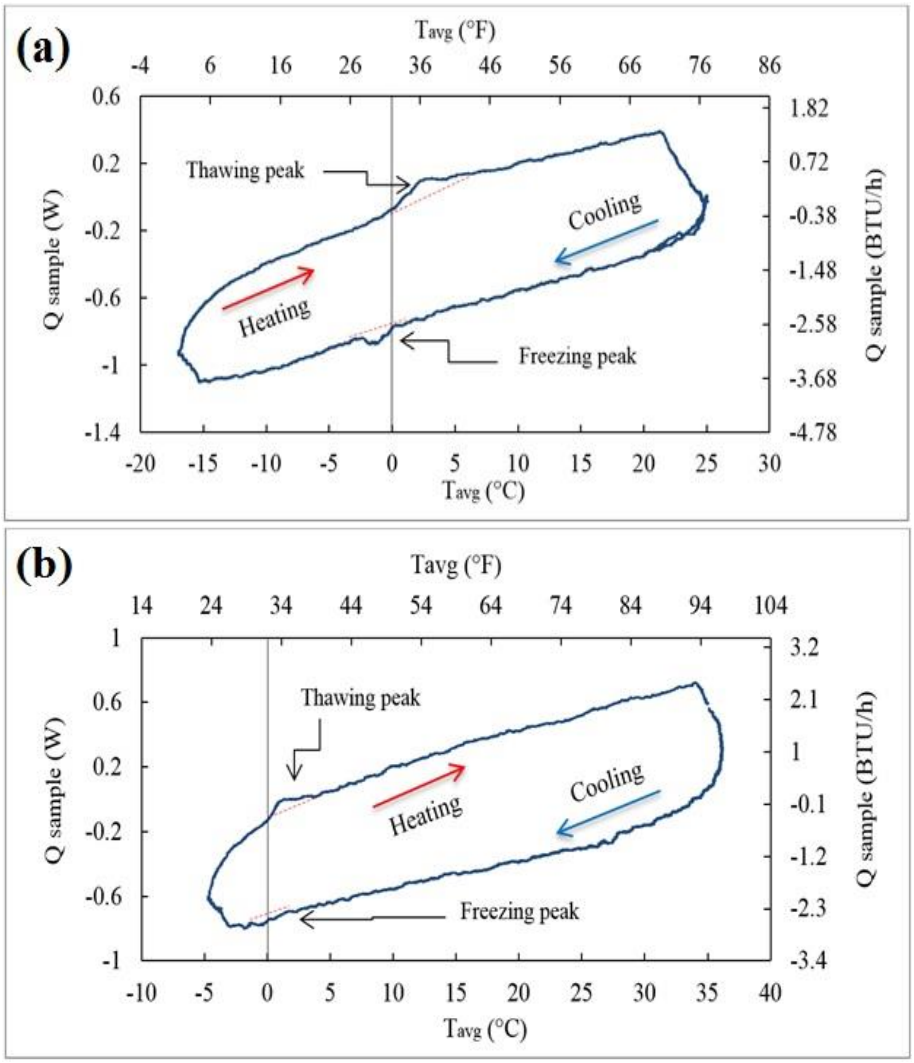

Figure 3.18. Heat flow vs. average temperature for sample with LWA presoaked in water (Mix 3W). a) Under the temperature Profile #1. b) Under the temperature Profile # 2

These graphs show how the latent heat of water changes the heat flow of the sample when it undergoes a cooling/heating cycle. During both heating and cooling, there is a peak in the heat flow around the temperature of 0 °C (32 °F) where the incorporated water melts and freezes, respectively. For Profile #2, the peaks are smaller because the entire samples does not get to 0 °C (32 °F) (Figure 3.18-b).

For Mix 3P, which contains LWA presoaked in PCM6, in addition to the latent heat of water, the latent heat of the incorporated PCM changes the temperature profile (Figure 3.19). During cooling, when the average temperature gets close to 6°C (42.8 °F), the PCM6 undergoes an exothermic solidification and decreases the slope of the changing in temperature. The reverse occurs during heating.

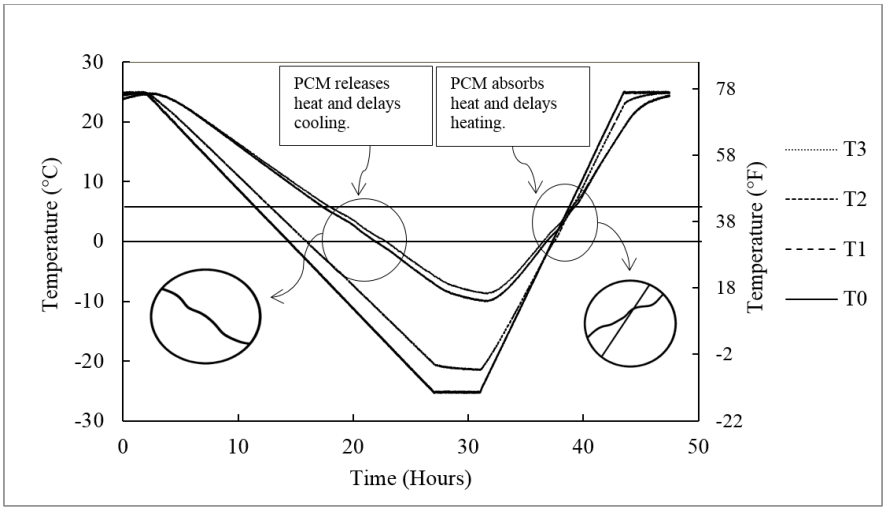

Figure 3.19. Temperature profile for the sample with LWA presoaked in PCM6 and under the Temperature Profile #1

The heat flow of this sample is shown as a function of average temperature (Figure 3.20, overleaf). There are two peaks that are the result of freezing and thawing of water, as well as two peaks that are due to the absorption and release of heat by the PCM6. During heating, when the average temperature of the sample gets closer to the melting point of PCM6, PCM absorbs the heat, and thus, the heat flow increases. During cooling, when the average temperature of the

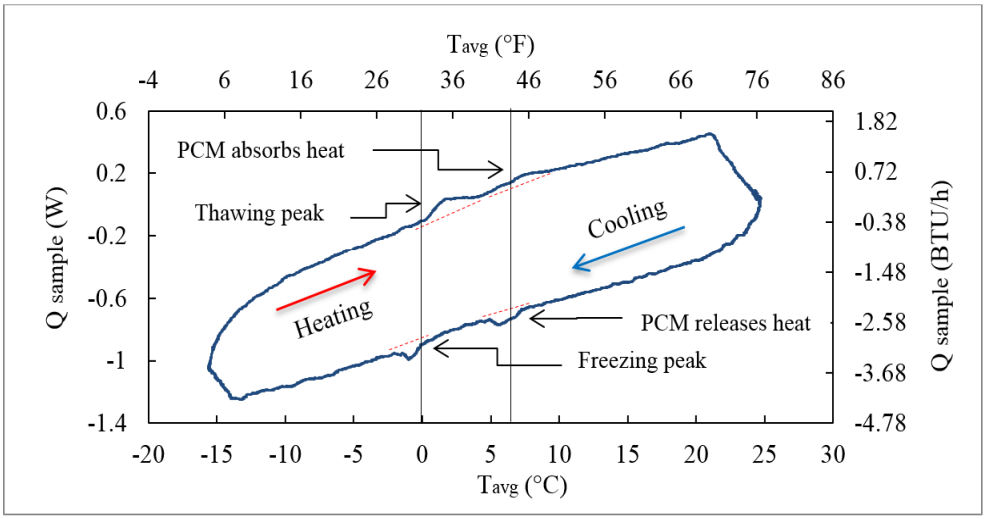

Figure 3.20. Heat flow vs. average temperature for sample with LWA presoaked in PCM6 under temperature Profile #1

sample is close to the melting point, PCM6 releases the heat energy which leads to increases in the absolute value of the heat flow through the sample.

The results for the samples with PCM-10 are shown in Figure 3.21. As the temperature of the upper side of the sample does not get to the melting point of the PCM, the change in the slope that is the result of phase transition of PCM cannot be seen, whereas the changes in slope because of the freezing and melting of the water can be seen.

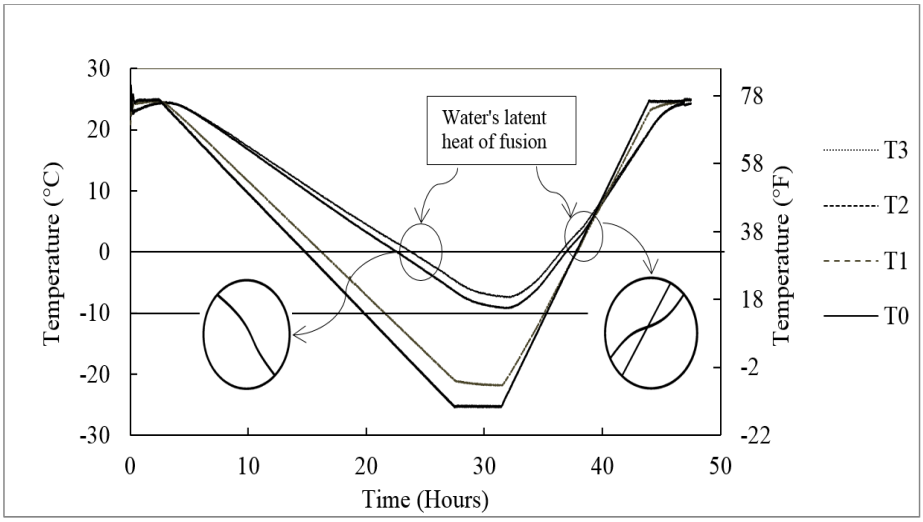

Figure 3.21. Temperature profile for the sample with LWA presoaked in PCM-10 and under the temperature Profile #1

In the heat flow graph (Figure 3.22), two peaks are due to the freezing and thawing of water, and two due to solidifying and melting of PCM-10. The peaks related to the phase transitions of PCM-10 are small, because the entire sample does not get to the melting point of the PCM-10.

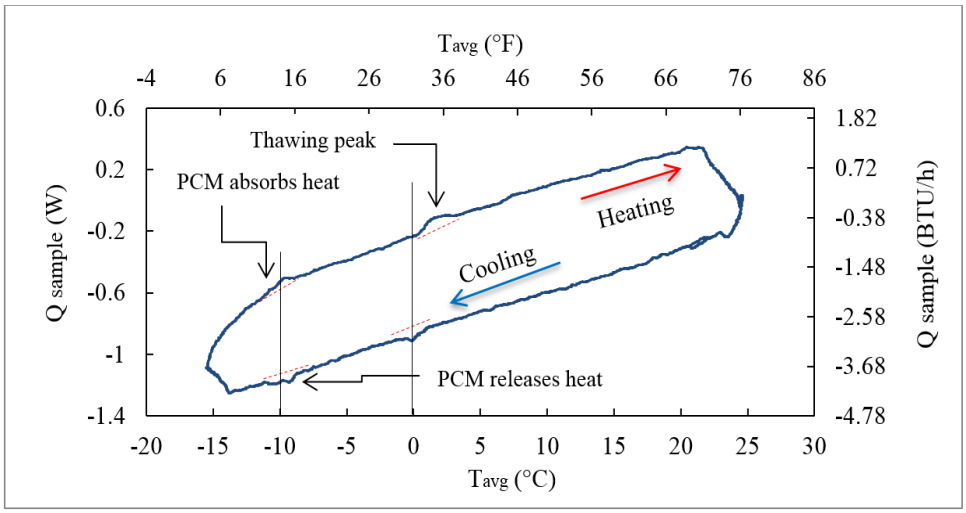

Figure 3.22. Heat flow vs. average temperature for sample with LWA presoaked in PCM-10 and under temperature Profile #1

The sample that included PCM28 was subjected to temperature Profile #2 (Figure 3.23). As the entire sample does not get to 0 °C (32 °F), the change in the slope of the temperature profile because of the freezing and thawing of water is negligible, whereas there are two changes in the slope that are the result of the phase transition of PCM28.

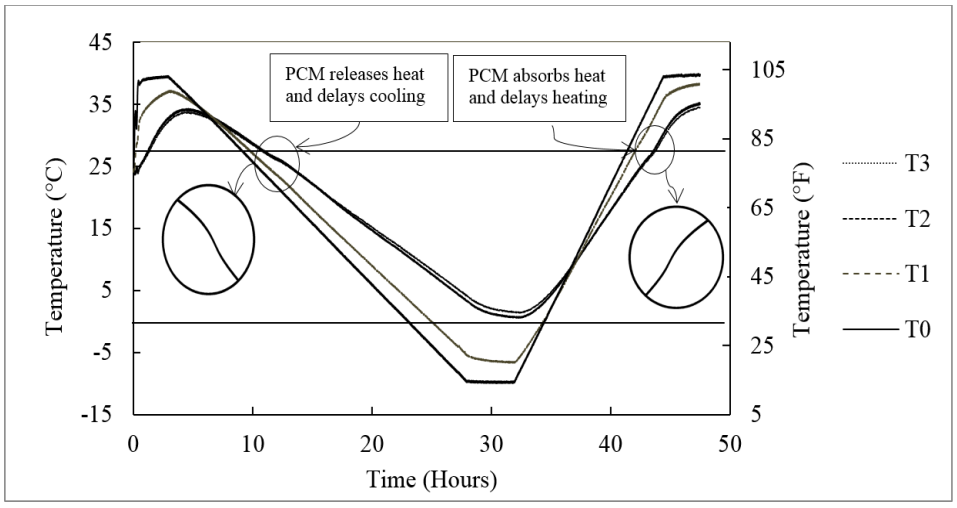

Figure 3.23. Temperature profile for the sample with LWA presoaked in PCM28 and under temperature Profile #2

For the heat flow vs. average temperature graph (Figure 3.24), there are two peaks because of freezing and thawing of water and two peaks due to the phase transition of PCM28. The peaks that are related to freezing and thawing of water are very small, because the upper side of the sample does not get to the melting point of water. The results presented in this section match with the results reported in another study where the existence of PCM in the mortar was shown to change the slope of the temperature profile when it got close to the melting temperature of the PCM [30]. These results show how the phase transition of the PCM incorporated in concrete can absorb and release heat energy and modify the temperature profile and heat flow rate of a sample. The latent heat of fusion of PCM and water increases the thermal inertia of the mixture and therefore affects the rate of temperature changes through the sample.

Since the latent heat of fusion of water is higher than that for the utilized PCMs[2], the peaks associated with the freezing and melting of water are larger. The results suggest that utilizing PCMs that have higher latent heats of fusion leads to larger slope changes in the temperature profile and bigger peaks in the heat flow graphs.

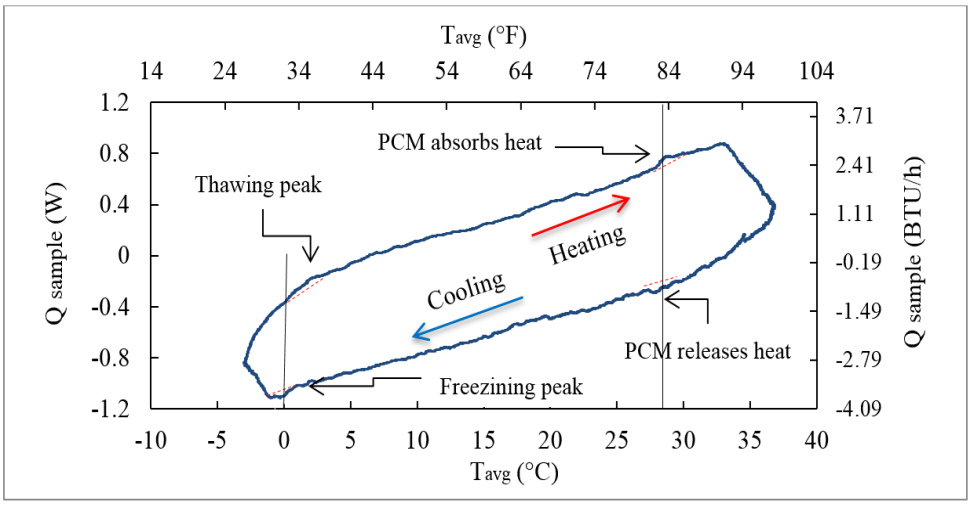

Figure 3.24. Heat flow vs. average temperature for sample with LWA presoaked in PCM28 and under temperature Profile #2

[2] Latent heat of fusion of water is 334 J/g (143.6 BTU/lb).

3.3 Summary of the chapter

Various experiments were discussed in this chapter to better understand the effect of incorporating PCMs on different chemical, physical, and mechanical properties of cementitious materials. The results suggest that the PCM should not be directly added to the mixtures, rather, it should be indirectly incorporated into the mix using a carrier. LWA and RHA were investigated as two potential carriers for the PCM. Considering the results of the experiments and their availability and compatibility with the cementitious media, LWA and RHA can be used as PCM carriers; however, they cannot perfectly hold PCM inside their structures. The calorimetry tests showed that the incorporation of PCMs can enhance the thermal inertia of cementitious media and thus suggested that they can be used to improve the thermal performance of buildings and pavements. However, the performance of PCM-impregnated structural and pavement elements needs to be studied when they are subjected to real temperature profiles. Although such investigations can be done by laboratory experiments, these experiments are usually costly, time consuming, and in some cases very hard to do. Therefore, computational simulations can be conducted instead of laboratory experiments. As described in the next chapter, a computational model of structural and pavement elements was developed, and the efficiency of PCMs to improve thermal performance was studied using real temperature profiles from different U.S. cities.

CHAPTER FOUR
COMPUTATIONAL SIMULATION

One of the goals of this study was to apply the temperature profiles of different cities to structural and pavement elements in order to investigate the ability of PCMs to modify the inside temperature of buildings and the core temperature of concrete pavements. The investigation time period for each of these studies was selected to be one week and two months, respectively. Instead of laboratory experiments, this investigation was done by computational simulation. The temperature profile of a location provided in the Typical Meteorological Year (TMY) databases contains 168 datapoints in a week and 1,440 datapoints in two months[3]; however, the experimental cold plate apparatus can be programmed with only eight set-points. Also, the use of an appropriate model can be both more rapid and more accurate than laboratory experiments.

[3] These durations are the selected durations for the simulations.

4.1 Outline

4.1.1 COMSOL Modeling

In the first section of this chapter, the physics and the corresponding mathematical equations are described. It is also shown how material properties and different physical phenomena were modeled in the COMSOL software, and how the simulations were conducted.

4.1.2 Validation of the Model

In the second section, the accuracy of the COMSOL model is validated by comparing its results with the results obtained from Guarded Longitudinal Comparative Calorimeter (GLCC) experiments (Section 3.2.6). This validation needed to be done before using the model to apply real[4] temperature profiles to simulated structural and pavement elements. To do this, two temperature profiles were applied to the samples in the GLCC and the results were compared to a similar model undergoing the same profiles in COMSOL. This test was done for three samples; the first contained LWA presoaked in water and the other two contained LWA presoaked in either PCM6 (with a melting point of 6 ºC (42.8 ºF)), or PCM28 (with melting point of 28 ºC (82.4 ºF)). Profile #1 was used for the samples incorporating water or PCM6; and Profile #2 was used for the sample incorporating PCM28 (please see Section 3.2.6).

The values that were assigned to the materials' parameters in the COMSOL model (physical properties, dimensions, etc.) matched the values that were used in the laboratory setup. Therefore, the results of the model should match with the results of the experiment. To have a quantitative

[4] The temperature profiles obtained from TMY databases are statistically derived from real data, and are generated by putting the hourly collected temperature of different months of different years together to establish the temperature profile for a year as a whole.

criterion, the Coefficient of Determination (R^2) was calculated for different cases. This number indicates how well the modeling results fit the experimental results [105]. The Coefficient of Determination can be calculated by:

$$R^2 = 1 - \frac{\sum(T_i - t_i)^2}{\sum(T_i - \bar{T})^2} \quad (12)$$

where for each temperature profile, T_i is the temperature at each time step obtained from laboratory experiments, $\bar{T}$ is the laboratory average temperature, and t_i is the temperature at each time step calculated by the COMSOL model. An R^2 of one would indicate that the COMSOL temperature profile perfectly fits the temperature profile obtained from the laboratory experiment, while an R^2 of zero would indicate that the two sets of temperature profiles do not fit at all.

4.1.3 Simulations

Finally, in the third section, various COMSOL models are generated and studied to better understand the application of PCMs in buildings and pavements. In the first model, a PCM-impregnated concrete wall is studied under real temperature profiles; in the second model, a brick-and-mortar wall equipped with a PCM-impregnated gypsum board is studied under sine function temperature profiles as well as real temperature profiles; finally, in the third model, a concrete pavement was studied under real temperature profiles.

4.1.3.1 PCM-impregnated concrete walls

A concrete wall with a thickness of 203 mm (8”) and with different percentages of PCM was studied. TMY data were used to simulate the real temperature changes of different cities as the input file for the COMSOL model. TMY is a collection of selected weather data for a specific location and for a specific period of time. The National Renewable Energy Laboratory’s latest

TMY collection (TMY3) was based on data for 1,020 locations in the U.S. between the years of 1991 and 2005 [106]. TMY2 provides the same set of data for fewer locations from 1961 to 1990 [107]. These two different TMY datasets were used to have a wide range of temperatures available for the simulations.

To illustrate how the incorporation of PCMs in walls modifies the inside temperature of buildings, the simulation was first conducted on a temperature profile sample with a short duration (one day). However, in order to have a more comprehensive study, the temperature profiles of twelve U.S. cities, with longer durations (one week), were simulated in order to compare the lengths of time during which the inside temperature stays in the comfort zone for conventional and PCM-impregnated concrete.

For all the structural models, the occupant comfort zone was defined as the range of 22.2 °C (72 °F) to 24.4 °C (76 °F) [108], and thus, the melting point of the simulated PCM was selected to be 23.3 °C (74 °F). The heat of fusion of the simulated PCM was set to be equal to that of PCM28, i.e. 150 J/g (64 BTU/lb) (please see Table 2.1).

4.1.3.2 Walls equipped with PCM-impregnated gypsum boards

For the second model, a brick-and-mortar wall with different thicknesses and equipped with a layer of gypsum board with a thickness of 25 mm (0.98”) and with different percentages of PCM was studied. The cross-sections of the four walls are shown in Figure 4.1, overleaf. They consist of two halves of bricks on the sides with a layer of mortar between them, and a layer of gypsum board. The gypsum board was placed in the inner surface of the wall. Including the thickness of the gypsum board, the total thicknesses of the models are 100 mm (3.94”), 150 mm (5.91”), 200 mm (7.87”), and 250 mm (9.84”), respectively.

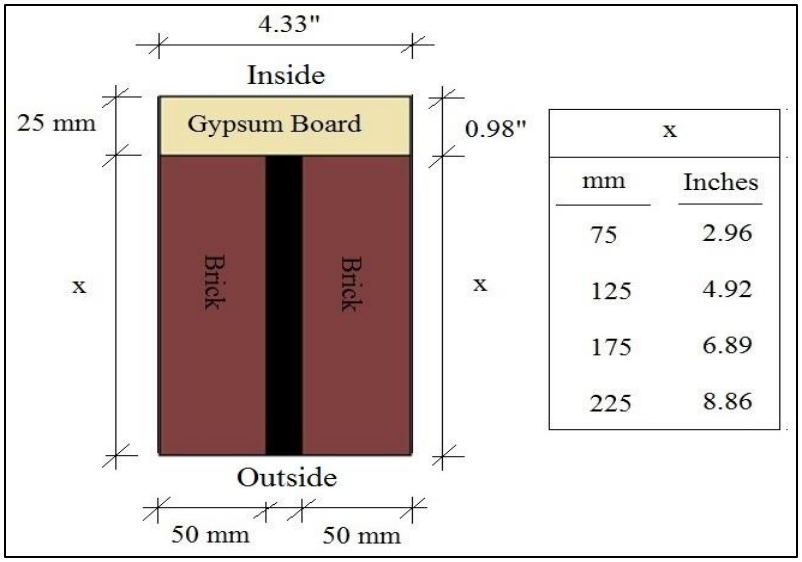

Figure 4.1. Cross-section of the walls equipped with PCM-impregnated gypsum board

Three sine temperature profiles with the amplitudes of 10 °C, 20 °C, and 30 °C (18 °F, 36 °F, and 54 °F, respectively), a reference temperature of 22 °C (71.6 °F), and a period of 24 h, were applied to the models. These temperature profiles were named T10, T20, and T30, respectively (Figure 4.2). Utilizing different amplitudes makes it possible to study the effect of the difference between the peak and the lowest temperature (the amplitude of the applied temperature) on the efficiency of PCMs. The melting point of the PCM was selected to be equal to the reference temperature. It should be mentioned that the reference temperature of 22 °C (71.6 °F) is an arbitrary number, and using another reference point does not change the results.

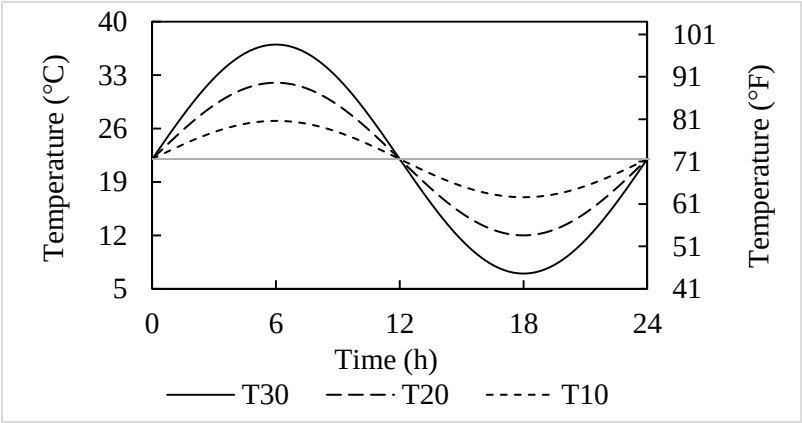

Figure 4.2. Sine temperature profiles

Four different criteria, including Time Lag (ϕ), Decrement Factor (f), duration of being in the comfort zone, and the energy required to keep the inside temperature in the comfort zone were used to evaluate the efficiency of PCMs to improve the thermal performance of buildings. By definition, time lag is the difference between the times that the peak temperature occurs inside and outside of the wall. Also, the decrement factor can be calculated by [109]

$$f = \frac{A_{x=0}}{A_{sa}} \tag{13}$$

where $A_{x=0}$ is the difference between the maximum temperature and minimum temperature of inside of the wall, and A_{sa} is this difference for the outside of the wall. Time Lag and Decrement Factor are illustrated in Figure 4.3.

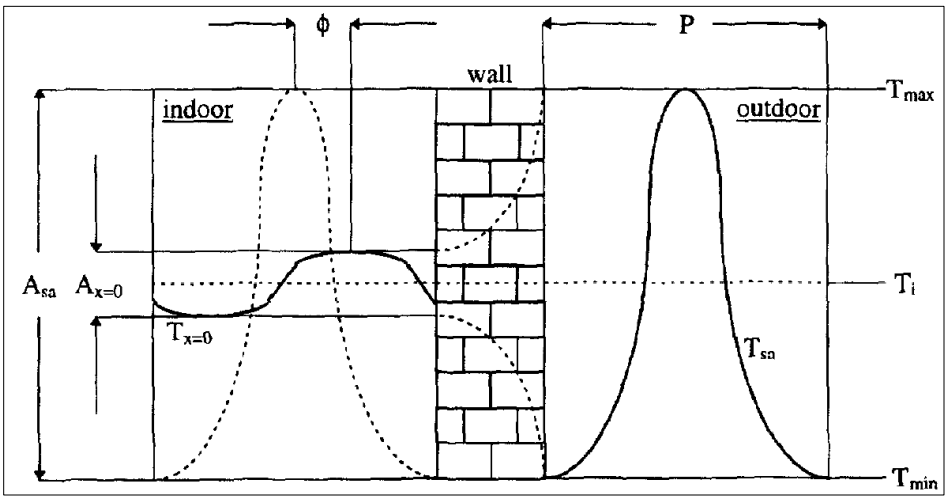

Figure 4.3. Time Lag and Decrement Factor in a wall [109]

The third criterion was the time duration that the inside temperature stays in the occupant comfort zone. For that, two comfort levels were introduced; for level 1, the comfort zone was the reference temperature ±1.5 °C (±2.7 °F), and for level 2, the comfort zone was the reference temperature ±3.0 °C (±5.4 °F). The melting temperature of the PCM was set equal to the reference

temperature and its heat of fusion was selected to be equal to 161 J/g (69 BTU/lb) that is equal to the heat of fusion of PCM28 (Table 2.1).

Finally, the fourth parameter was the energy required by a HVAC system to keep the room temperature in the comfort zone. The inside of the wall is in contact with the room air, therefore the heat energy can be transferred from the wall to the air by convection [110]:

$$\frac{dQ}{dt} = hA(T_R - T_s) \rightarrow Q = hA\int_{t_1}^{t_2}(T_R - T_s)dt \qquad (14)$$

where Q is the heat energy (J), h is the heat transfer coefficient (assumed to be 5 (W/m^2.K) for free air [110]). A is the area of the wall in contact with the air (m^2), T_R is the room temperature, and T_s is the temperature of the inside of the wall (K). The integral term in Equation 14 presents the area under the temperature-time curve. If the room temperature is in the occupant comfort zone, the HVAC system will not be engaged. But if the room temperature falls outside this zone, the HVAC system needs to use energy to adjust the temperature. Therefore the mentioned area is an index of the energy that is used by the HVAC system to bring the room temperature back to the comfort zone. This area was calculated by Simpson's trapezoidal integration method (Figure 4.4).

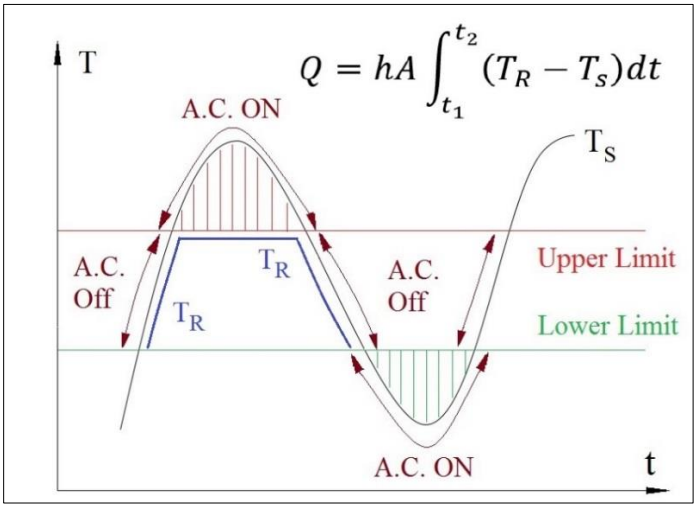

Figure 4.4. The area under the inside temperature graph that is outside the comfort range

In addition to the walls subjected to sine temperature functions, a wall with a total thickness of 250 mm (9.84”) was studied under real temperature profiles. A one-week profile for each of six cities was selected and applied to the model as thermal loads. Different PCM percentages were incorporated in the gypsum board. Since the time lag and the decrement factor are defined only for sine functions, only the two criteria of duration of being in the comfort zone and the energy required to keep the inside temperature in the comfort zone were used to evaluate the efficiency of the PCM. Similar to the case of PCM-incorporated concrete wall, the occupant comfort zone was defined as the range of 22.2 °C (72 °F) to 24.4 °C (76 °F), and thus, the melting point of the simulated PCM was selected to be 23.3 °C (74 °F). Also, the heat of fusion of the simulated PCM was set to be equal to that of PCM28.

A simplified cost analysis was also conducted for the walls equipped with PCM-incorporated gypsum boards under real temperature profiles. This cost analysis was based on the electricity rates reported in governmental catalogs provided for each state (Table 4.1).

Table 4.1. Electricity rates for different cities

City (State)	Residential Rates (cents/kWh)			Source
	On-peak hours	Off-peak hours	Ratio	
Portland (OR)	26.900	6.700	4.0	[111]
San Antonio (TX)	21.900	9.200	2.4	[112]
Miami (FL)	17.392	2.885	6.0	[113]
Concord (NH)	13.299	1.940	6.9	[114]
Minot (ND)	13.634	2.220	6.1	[115]
Elko (NV)	37.594	4.329	8.7	[116]

The electricity rates are divided into on-peak hours and off-peak hours for all cities. The ratio between these two tariffs is also presented in the table.

For each case, the cost of energy used by the HVAC system to keep the inside temperature in the comfort zone was calculated by multiplying the used energy obtained from Equation (14) to the electricity rates provided in Table 4.1. The on-peak hours and off-peak hours are allocated to different parts of a day in different states. Therefore, a MATLAB code was developed to multiply the energy used in each part of the day by the electricity rate specified for that part of the day for that case. The assumptions and considerations of the cost analysis were:

- The absolute total cost for each case was not calculated, rather, the percentage reduction in energy and cost was calculated. This means that since the actual area of the building would be required for calculating the total cost, the problem was solved for one square meter (or one square foot) of the described wall, and the percentage of change was calculated.

- In some of the states, the on-peak hours and off-peak hours are allocated to different parts of a day in different months of the year. However, for these states, the rates that are presented in Table 4.1 belongs to the months of the year that match with the months of the year that were used in the simulations.

- The simulation time periods of the cities do not match with the effective dates of the electricity rates. The rates are extracted from the catalogs that were mostly updated in 2016. However, the ratio between on-peak Hours and off-peak Hours rates is the parameter that is important in these calculations. It was assumed that these ratios have stayed constant over the years for all the cases.

- For each state, there is a monthly service fee in addition to the cost of the used electricity. This extra fee was not included in cost analysis and only the costs related to the power usage were considered.

- For some states, there is an extra charge for usage over a specific limit. This fee was not included in the calculations.

4.1.3.3 PCM-impregnated concrete pavement

For the third model, a concrete pavement with a thickness of 203 mm (8”) was studied under different temperature profiles, and the efficiency of incorporating PCM with a melting point close to the freezing temperature of water in order to decrease the number of freeze/thaw cycles experienced by the pavement was evaluated. It should be mentioned that freeze/thaw degradation is not a significant degradation mechanism in all locations because it only exists in certain environmental conditions – only locations that have sufficiently wet climates, as the concrete must be saturated with water for damage to occur, and that reach freezing temperatures regularly, are subject to significant freeze/thaw degradation [26].

In the United States, locations that meet these criteria are parts of the Northwest including California, parts of the Southeast, most of the Midwest and Mid-Atlantic, and the entire Northeast. In this study, it was assumed that there is enough moisture available in the environment for all the case studies and therefore the temperature of the pavement is the only parameter that affects the number of freeze/thaw cycles. Further, although it is well known that the freezing point of pore solution in concrete is lower than that of water and depends on the exact chemistry of the pore solution, for comparative purposes 0 °C (32 °F) was chosen as the freezing point [49].

4.2 COMSOL Multi-physics Modelling, Equations, and Boundary Conditions

A 2D heat transfer model was generated by using the COMSOL Multiphysics® software package to simulate the temperature changes in structural elements under real temperature profiles. The involved physics were heat transfer by conduction, convection, and radiation. The conduction heat transfer equation for a system without a heat source is described by [110]:

$$\frac{\partial}{\partial x}\left(\lambda\frac{\partial T}{\partial x}\right)+\frac{\partial}{\partial y}\left(\lambda\frac{\partial T}{\partial y}\right)=\rho C_p\frac{\partial T}{\partial t} \tag{15}$$

where λ is the thermal conductivity of the material (W/m·K), T is temperature (K), ρ is the density of the material (kg/m^3), and C_p is the specific heat of the material (J/kg·K). For constant thermal conductivities of the materials, the equation is reduced to:

$$\frac{\partial^2 T}{\partial x^2}+\frac{\partial^2 T}{\partial y^2}=\frac{\rho C_p}{\lambda}\frac{\partial T}{\partial t} \tag{16}$$

Initially, a model was generated to compare the results of the simulation with the results of a laboratory experiment. The setup involved a 50.8 mm × 50.8 mm (2” × 2”) mortar sample placed between two Pyroceram meter bars that, in turn, were encased in insulation. This comparison was done to validate the accuracy of the COMSOL model (Figure 4.5).

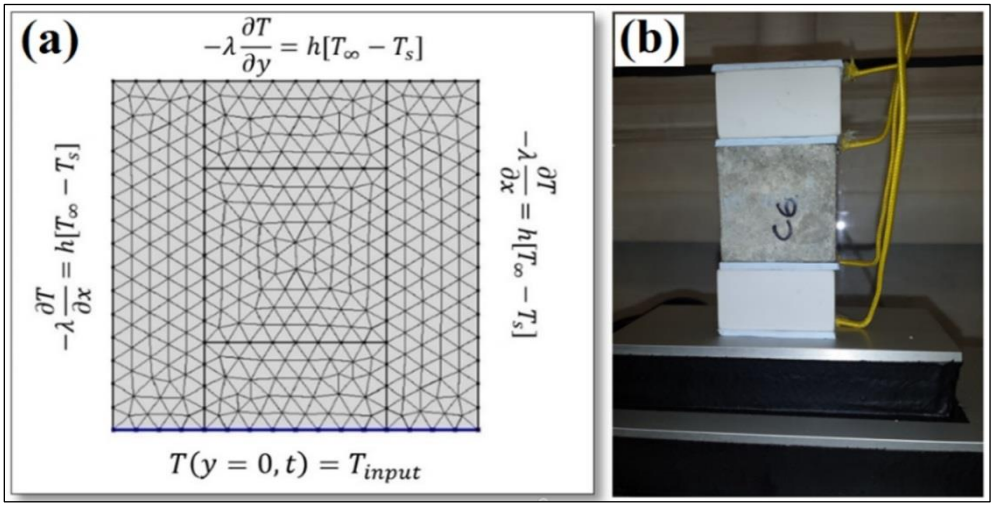

Figure 4.5. a) COMSOL heat transfer model geometry, mesh, and boundary conditions. b) Laboratory set up (Insulations are not shown in this picture)

Equation 16 is second order in the spatial coordinates in the x and y directions and first order in time; therefore, two boundary conditions in each direction and one initial condition need to be specified. The first boundary condition in the y-direction was the heat load that was applied to the bottom layer of the model:

$$T(y = 0, t) = T_{input} \tag{17}$$

The other three boundary conditions were based on the conservation of thermal energy at the sides of the model:

$$-\lambda \frac{\partial T}{\partial x} = h[T_\infty - T_s] \, , -\lambda \frac{\partial T}{\partial y} = h[T_\infty - T_s] \tag{18}$$

where λ is the thermal conductivity of the material (W/m·K), T is temperature (K), h is the heat transfer coefficient (assumed to be 5 W/m^2·K for free air [110]), T_∞ is the ambient temperature (assumed to be room temperature, i.e., 296.15 K), and T_s is the temperature of the material surface (K).

For the initial condition, the entire system was assumed to be at room temperature before the heat load was applied. Therefore:

$$T(x, y, t = 0) = T_R \tag{19}$$

where T_R is the room temperature and assumed to be 296.15 K. The surface radiation of the sides is described by [110]:

$$\lambda \frac{\partial T}{\partial x} = \varepsilon\sigma(T_\infty^4 - T_s^4)$$

$$\lambda \frac{\partial T}{\partial y} = \varepsilon\sigma(T_\infty^4 - T_s^4) \tag{20}$$

where ε is the surface emissivity and σ is the Stefan-Boltzmann constant. The properties of the materials are provided in Table 4.2. This was modeled as "Surface-to-Ambient Radiation" in the COMSOL software (Figure 4.6).

Table 4.2. COMSOL material properties inputs

Material	Density (kg/m^3)	Heat capacity at constant pressure (J/kg·K)	Thermal conductivity (W/m·K)	Latent heat of fusion (J/g)	Surface emissivity
Mortar	2200	880	1.4	-	0.94
Brick	1920	840	1.0	-	0.75
Gypsum	1380	1090	0.25	-	0.93
Water	997	4180	0.6	334	-
Ice	918	2052	2.1		-
Pyroceram	2600	790	Equation 6*	-	0.85
Insulation	24.8	1300	0.0285	-	0.95

* $\lambda_{PC} = -0.0061(T) + 4.2013 \quad (-50\,°C < T < 40\,°C)$

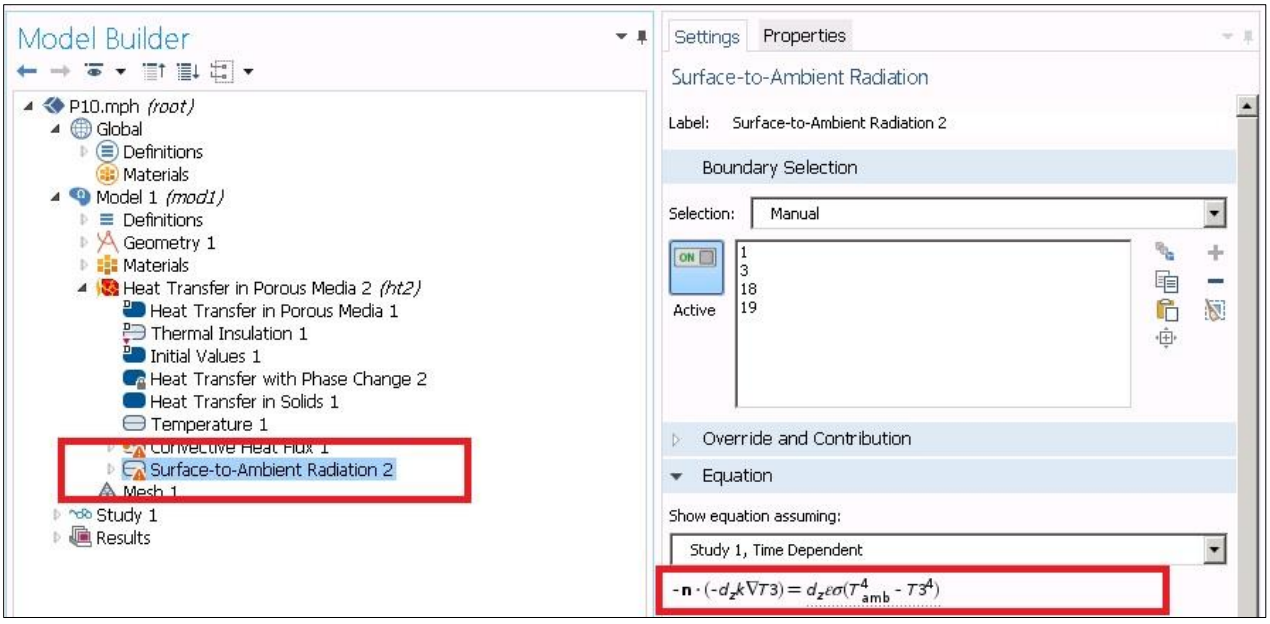

Figure 4.6. Modeling "Surface-to-Ambient Radiation" in COMSOL software

Equation 16 describes heat transfer in solid media, but for a model with a porous media, more equations are involved. Mortar that is a mix of sand, cement, and water was the main media under consideration. This media was modeled as "Heat Transfer in Porous Media" (Figure 4.7). The volume fraction of mortar was defined as θ_m, and thus the volume fraction of the porosity (the volume fraction filled with PCM) was equal to $(1-\theta_m)$. Therefore, the effective thermal conductivity of the media was defined as:

$$\lambda_{eff} = \lambda_m \theta_m + \lambda_{PCM}(1-\theta_m) \tag{21}$$

The subscript *m* stands for mortar.

Similarly:

$$(\rho C_p)_{eff} = \rho_m C_{p,m} \theta_m + \rho_{PCM} C_{p,PCM}(1-\theta_m) \tag{22}$$

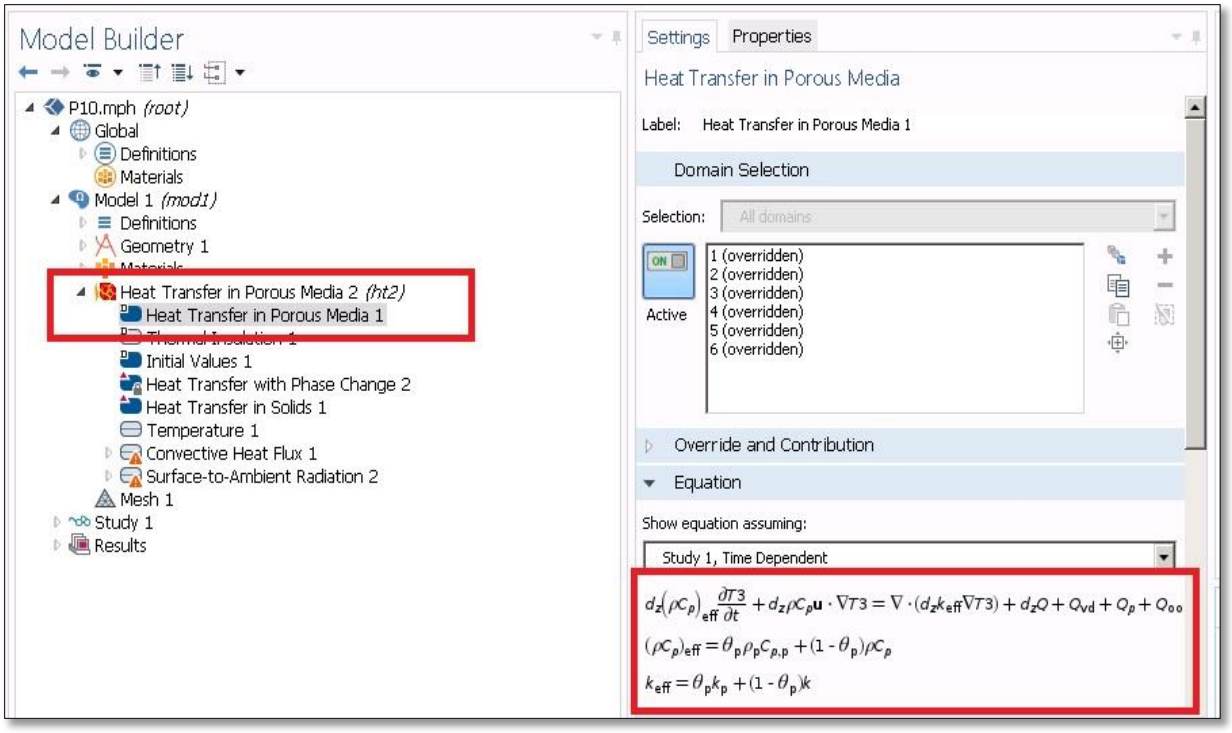

Figure 4.7. Modeling "Heat Transfer in Porous Media" in COMSOL software

The PCM was modeled as “Heat Transfer with Phase Change”, with β as the volume fraction of PCM at phase 1 (Figure 4.8). Therefore, the effective density of PCM was equal to:

$$\rho_{PCM} = \rho_{phase1}\beta + \rho_{phase2}(1-\beta) \tag{23}$$

Similarly:

$$\lambda_{PCM} = \lambda_{phase1}\beta + \lambda_{phase2}(1-\beta) \tag{24}$$

$$C_{p,PCM} = \frac{1}{\rho_{PCM}}(\rho_{phase1}C_{p,phase1}\beta + \rho_{phase2}C_{p,phase2}(1-\beta)) + L\frac{\partial \alpha_m}{\partial T} \tag{25}$$

where Cp is the specific heat (J/kg·K), L is the latent heat of fusion (J/kg), and α_m is:

$$\alpha_m = \frac{1}{2} \times \frac{\rho_{phase2}(1-\beta) - \rho_{phase1}\beta}{\rho_{phase2}(1-\beta) + \rho_{phase1}\beta} \tag{26}$$

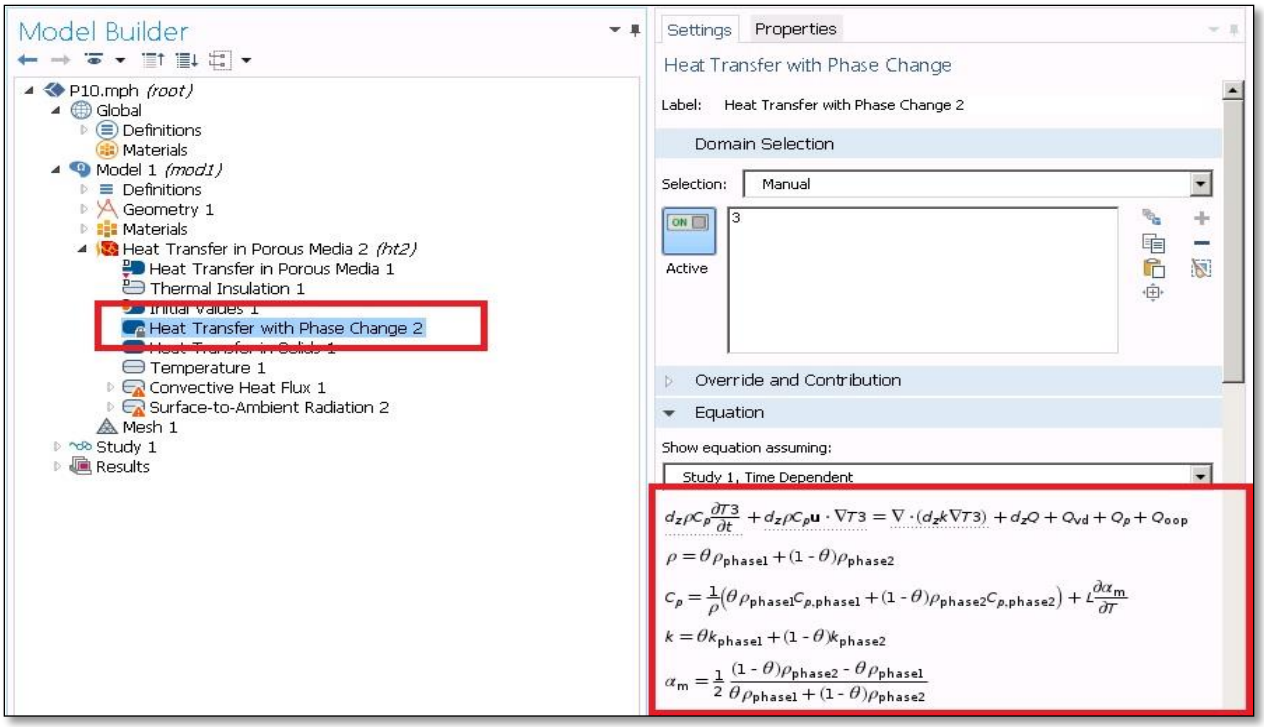

Figure 4.8. Modeling “Heat Transfer with Phase Change”

In Equation 26, α_m presents the mass percentage of PCM that is transferred from phase 1 to phase 2. Also, in Equation 25, the term $L\frac{\partial \alpha_m}{\partial T}$ presents the effect of the latent heat of fusion on the specific heat of PCM as a function of the mass percentage of PCM that is transferred from phase 1 to phase 2. This term will be equal to zero when the temperature is not close to the PCM's melting point; however, when the temperature gets closer to the PCM's melting point, the phase of PCM starts to change, and because of its latent heat of fusion, the PCM starts to either absorb or release heat energy. This phenomenon instantaneously changes the specific heat of the PCM (Figure 2.10). The temperature transition interval between Phase 1 and Phase 2 of the PCM was selected to be 3 °C (5.4 °F). This number was selected based on the results of Differential Scanning Calorimetry tests (Section 2.4.1). Modeling the temperature changes was a time dependent problem that was carried on as a "Time Dependent Study." The time intervals and the relative tolerance were selected to be 1 second and 0.01, respectively; however, they were modified depending on the problem. For the cases with high percentages of PCM, both of them were reduced to a smaller number in order to obtain accurate results and smooth graphs.

4.3 Verifying the validity of the COMSOL model

By applying the temperature profiles as thermal loads to the base of the sample stack, the temperature at the tops of the specimens changed gradually when the average temperature of the specimen was not close to the phase transition temperatures of water or PCM. When the average temperature approached the phase transition temperature, the slope of the temperature profile changed as a result of the latent heat of fusion of water or PCM. The COMSOL model was supposed to accurately calculate the gradual temperature changes in the specimen, and also correctly calculate the effect of the latent heat of fusion of the incorporated water and PCMs during the phase changes.

For the sample incorporating LWA presoaked in water, the calculated gradual changes of temperature for both the declining temperature (at a rate of 2 °C/h (3.6 °F/h)) and the increasing temperature (at a rate of 4 °C/h (7.2 °F/h)) are in agreement with the results of the laboratory setup (Figure 4.9-a, overleaf). The COMSOL model also accurately simulates the effects of the phase change of water when sample temperatures approach the freezing point. The same conclusions can be reached for the samples incorporating LWA presoaked in PCM6 or PCM28, Figure 4.9-b and Figure 4.9-c, respectively. R^2 for the samples incorporating LWA presoaked in water, PCM6, and PCM28 were equal to 0.97, 0.97, and 0.96, respectively. This shows that the computational model can accurately calculate changes in temperature both due to the gradual temperature changes and the phase transition of water and PCM.

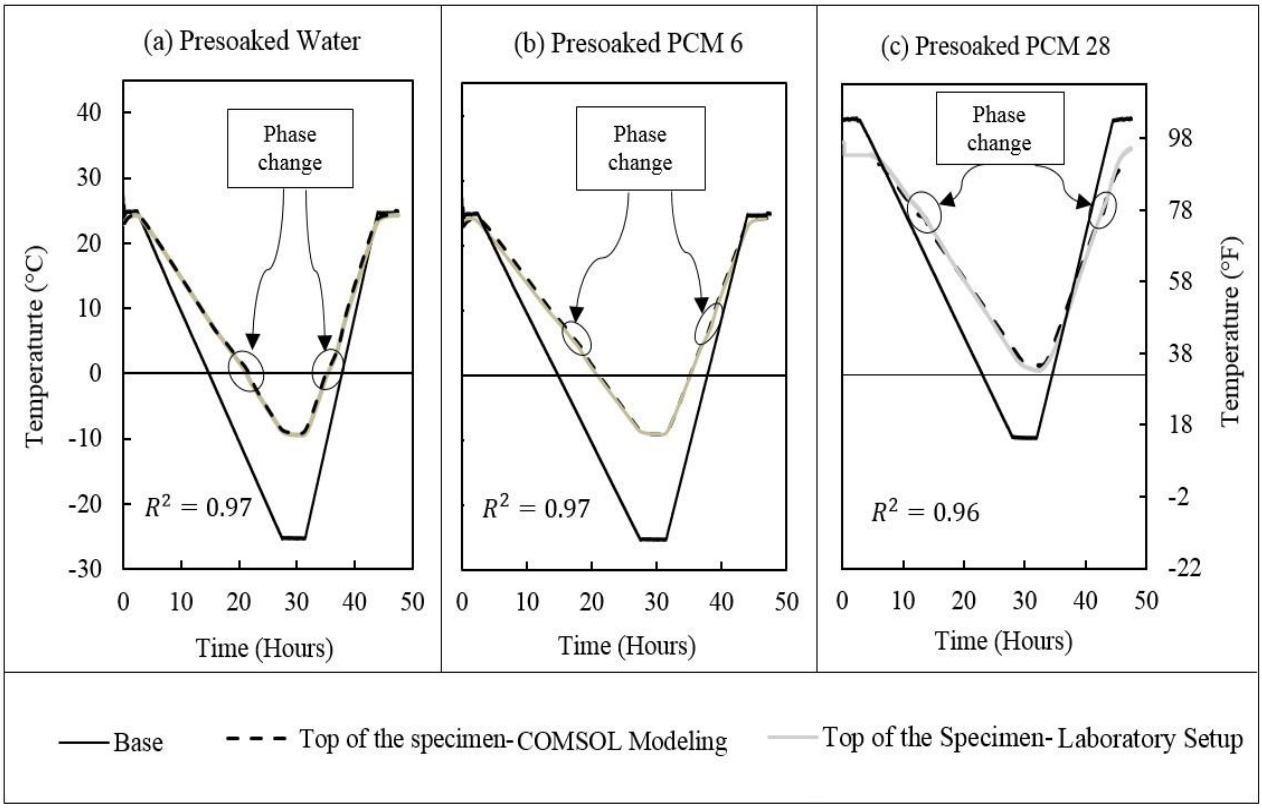

Figure 4.9. Comparison between results of the laboratory experiments and results of the COMSOL models

4.4 Results and Discussion

4.4.1 PCM-impregnated concrete walls

The temperature profile of the first day of July 1992 for Worcester, Massachusetts was applied to a concrete specimen containing 0 vol.%, 10 vol.%, or 30 vol.% of PCM (Figure 4.10). The results of the simulation demonstrate how including PCM in the concrete increases the thermal inertia of the media and thus makes the changes in the inside temperature smoother. Further, the duration for which the inside temperature stays within the occupant comfort range increases from 10 h for the sample without PCM to 13 h 30 min for the sample with 10 vol.% PCM (a 35% increase) and to 16 h 30 min for the sample with 30% by volume of PCM (a 65% increase). This happens because when the outside temperature rises, the latent heat of fusion of PCM absorbs the applied heat load and prevents drastic temperature changes on the inside of the specimen; and during the night when the outside temperature drops, the PCM releases the absorbed heat and keeps the inside warmer.

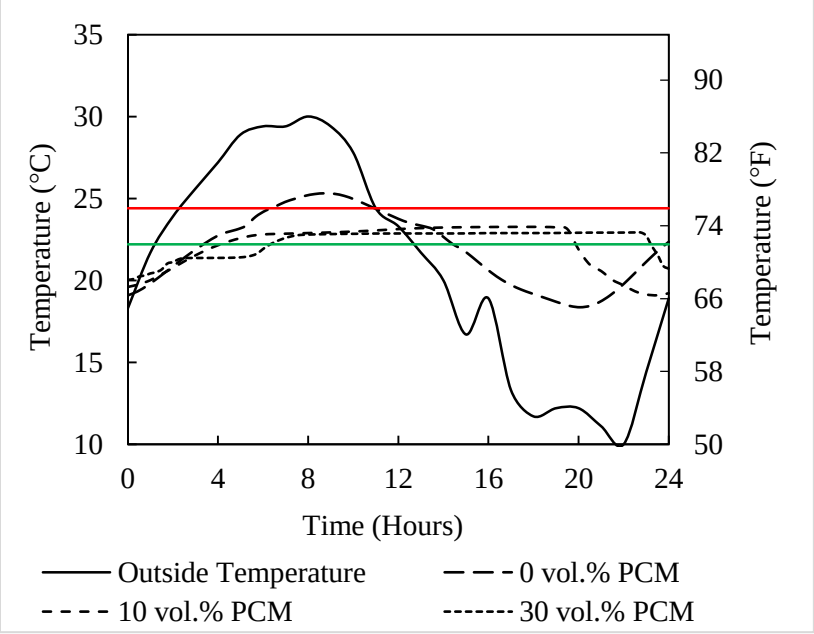

Figure 4.10. First day of July 1992 – Worcester (MA)

In order to have a more comprehensive study, temperature profiles with one week duration for 12 U.S. cities were studied. Depending on the maximum and minimum temperatures, the 12 cities were divided into three categories: cold, moderate, and hot (Table 4.3). These cities were selected from various parts of the U.S. to investigate the efficiency of PCMs in different locations. The 'hot' category included Austin, Texas; Delta, Utah; Casa Grande, Arizona; and Reno, Nevada, with maximum temperatures of 35 °C (95 °F), 35 °C (95 °F), 41 °C (105.8 °F), and 33.3 °C (91.9 °F), respectively.

Table 4.3. Temperature properties of the selected cities

Category	City (State)	Period of Time (week of)	Temperature °C (°F)		
			Minimum	Average	Maximum
Hot Climate	Austin (TX)	First / Jun. 2003	15.6 (60.1)	25.7 (78.3)	35 (95)
	Delta (UT)	Second / Jul. 2000	13.5 (56.3)	24.4 (75.9)	35 (95)
	Casa Granda (AZ)	Third / Jun. 2001	17.3 (63.1)	30.8 (87.4)	41 (105.8)
	Reno (NV)	Fourth / Aug. 1987	9.4 (48.9)	22.2 (72)	33.3 (91.9)
Moderate Climate	Boston (MA)	Fourth / Jun. 2002	15.6 (60.1)	24 (75.2)	33 (91.4)
	Grand Forks (NV)	Third / Jun. 1998	11 (51.8)	18.1 (64.6)	28 (82.4)
	San Diego (CA)	First / Sep. 1990	18.9 (66)	22.6 (72.7)	28 (82.4)
	New York (NY)	First / Sep. 1979	20.6 (69.1)	24.8 (76.6)	28.9 (84)
Cold Climate	Miles City (MT)	First / Jun. 2002	6.7 (44.1)	17.2 (63)	27.8 (82)
	Chicago (IL)	Second / May 2003	9 (48.2)	15 (59)	29 (84.2)
	Worcester (MA)	First / Jun. 1990	6.3 (43.3)	16.4 (61.5)	27.8 (82)
	Hulton (ME)	Fourth / Jul. 2004	5.9 (42.6)	17.9 (64.2)	29.8 (82)

For the first four days of the Austin simulation, the maximum temperature was above 32.2 °C (90 °F), which is significantly above the upper limit of the comfort zone and also the melting point of the PCM. Therefore the PCM cannot keep the inside temperature in the occupant comfort zone (Figure 4.11-a, overleaf). But for the last three days of the simulation, the oscillation of temperature is close to the comfort zone, and therefore the PCM can effectively increase the length of time for which the inside temperature is in the comfort zone. In the case that 30 vol.% of PCM is used, the inside temperature of the last three days stays in the comfort zone.

The same conclusion can be reached for the other three cases that are in this category (Figure 4.11-b to Figure 4.11-d). Increasing the percentage of PCM from 10% to 30% increases the duration of time during which the inside temperature is in the comfort zone. When the variation in temperature for a single day is about 16.7 °C (30 °F), 30% PCM can effectively keep the inside temperature in the comfort zone. When the temperature difference is more than 20 °C (36 °F), the PCM cannot completely keep the temperature in the comfort zone, but instead delays the time at which the temperature becomes uncomfortable.

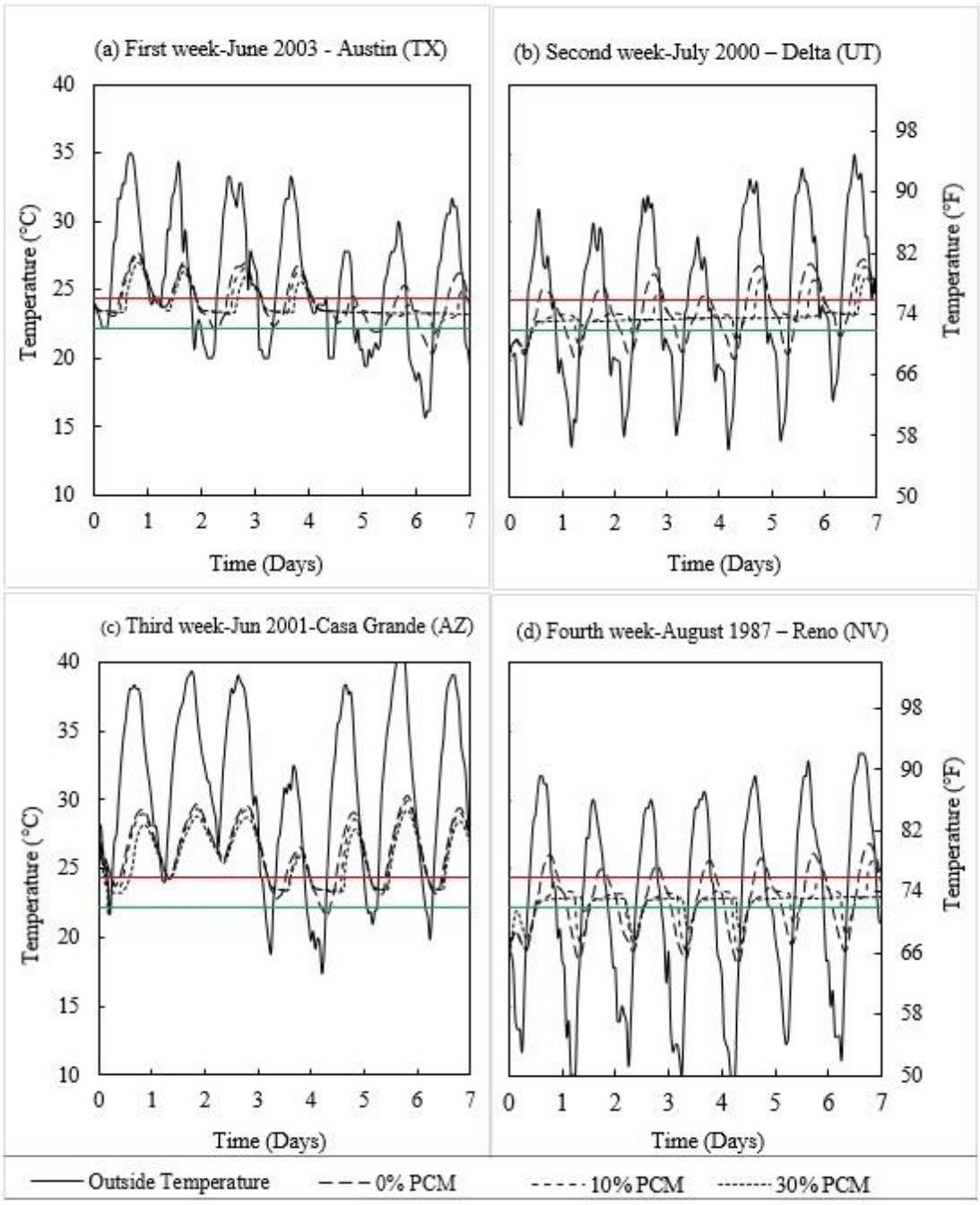

Figure 4.11. Hot climate category – changes in temperature for one week duration

The ‘moderate’ temperature category includes Boston, Massachusetts; Grand Forks, Nevada; San Diego, California; and New York City, New York. The average temperatures of these locations are in the comfort zone. In Boston, the maximum temperature for the first day is 27.8 °C (82 °F), which is relatively close to the comfort zone (Figure 4.12-a, overleaf). Therefore, not all the incorporated PCM will turn to liquid, and thus not enough heat energy will be stored in the PCM. When the minimum temperature of the following night falls to 15.6 °C (60.1 °F), the PCM cannot provide the required heat energy to keep the inside temperature in the comfort zone. But for the third day, the maximum temperature during the day is 30 °C (86 °F), therefore the PCM stores enough heat energy to make it possible to keep the inside temperature in the comfort zone for the following night. The same general behavior is observed for Grand Forks (Figure 4.12-b) and San Diego (Figure 8-c). The temperature oscillation of New York is very close to the comfort zone and the minimum temperature during the nights is only 1.1 °C (2 °F) less than the lower limit of the comfort zone. Therefore the PCM, especially when 30% is used, can keep the inside temperature in the comfort zone almost for the entire week (Figure 4.12-d).

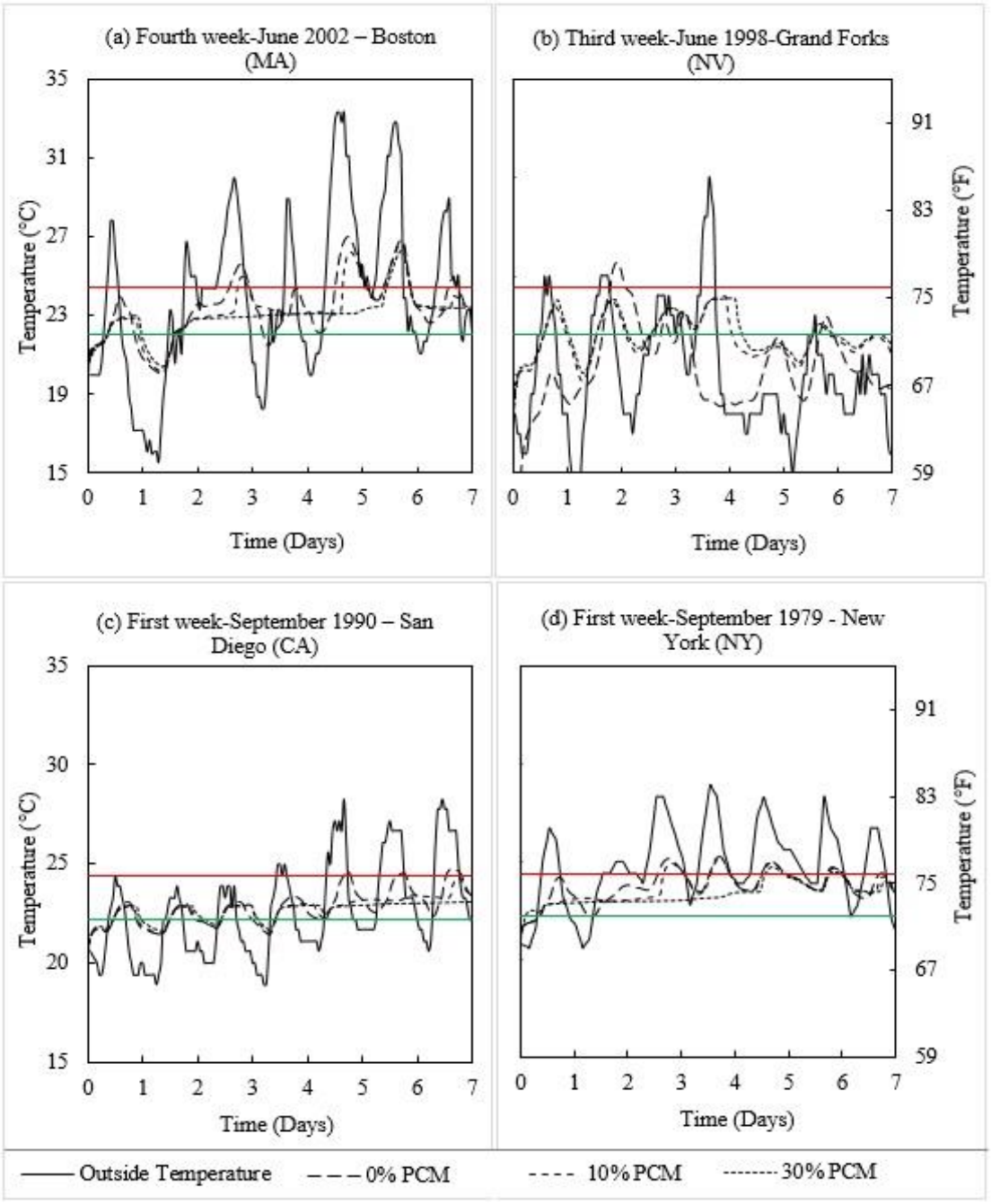

Figure 4.12. Moderate climate category – changes in temperature for one week duration

The ‘cold’ climate category includes Miles City, Montana; Chicago, Illinois; Worcester, Massachusetts; and Hulton, Maine. The minimum temperature of these cities is about 5.6 °C (42.1 °F). For the first three days of the Miles City temperature profile, the outside temperature is below the comfort zone during the nights and barely goes above the upper limit of comfort zone during the days (Figure 4.13-a, overleaf). Therefore no heat energy is stored in the PCM, and the inside temperature does not stay in the occupant comfort zone, even for the case that 30% PCM is used. But for the last three days of the week, as the temperature oscillates evenly above and below the comfort zone, PCM can effectively keep the inside temperature in the comfort zone. This shows that in addition to the percentage of the incorporated PCM, the temperature change range plays an important role in the effectiveness of the PCM. The same results can be reached for the other cities in this category (Figure 4.13-b to Figure 4.13-d).

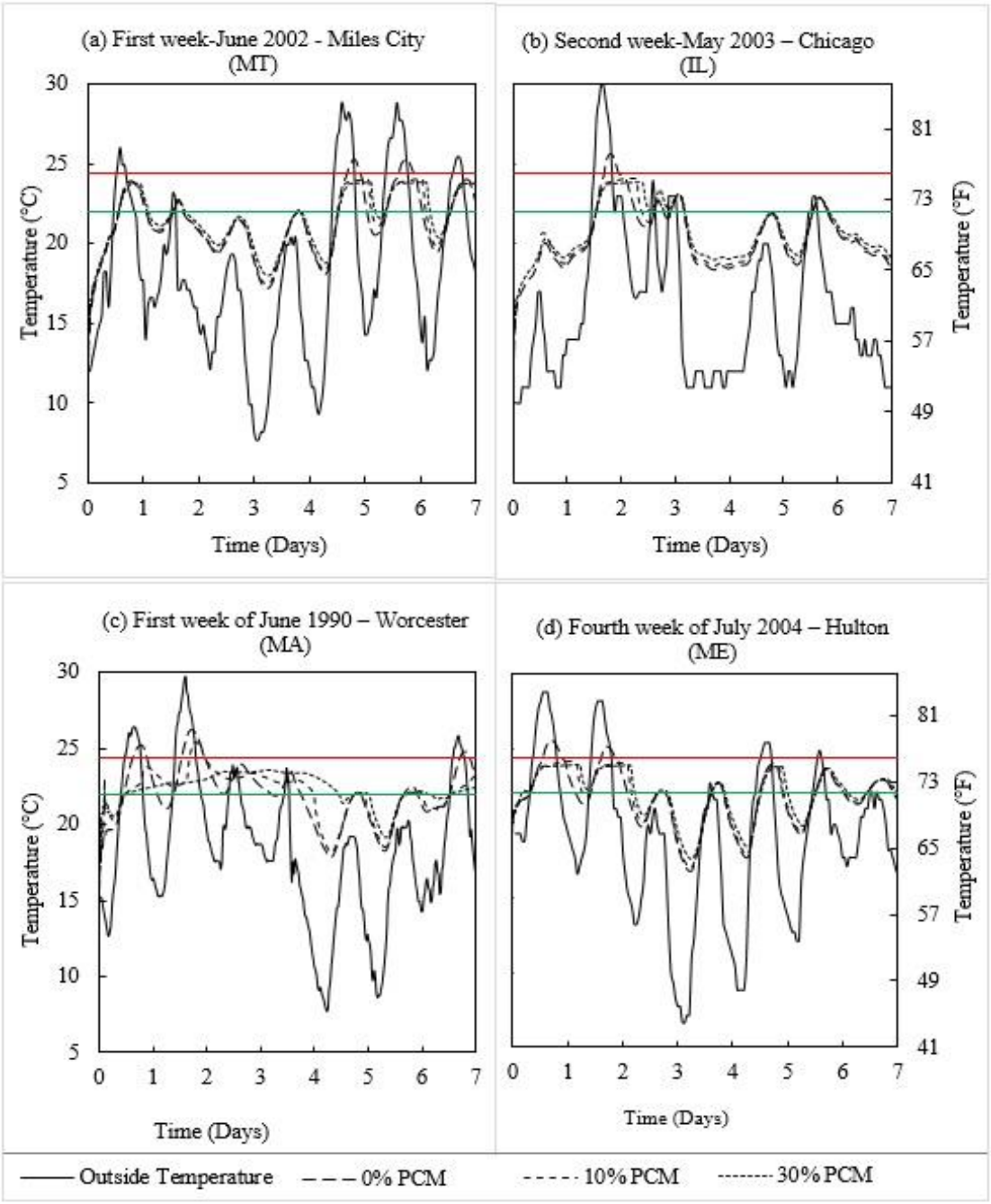

Figure 4.13. Cold climate category – changes in temperature for one week duration

The data generated from the computational model were used to calculate the percentage increase in the occupant comfort duration for different locations (Table 4.4). For each case, the number of hours that the inside temperature stays in the comfort zone is calculated for samples containing 0%, 10%, and 30% by volume PCM. For specimens containing 10% PCM, Delta saw the greatest increase, with the duration of being in the occupant comfort zone increased by 53.7%. For San Diego this increase was less than 22%. This shows that the efficiency of PCM to increase the occupant comfort is dependent on the profile temperature. The same conclusion can be reached for the cases that 30% PCM was used. In Chicago, the increase in being in the comfort zone was up to 78%. In San Diego this number was as low as 25%, which is even less than in some of the other cases where 10% PCM was used. Comparing the cases of San Diego and New York shows that even for the cases with the same comfort duration without utilizing PCM, the

Table 4.4. Increase in the occupant comfort duration

Category	City (State)	Duration of being in the comfort zone for one week (Hours)				
		0% PCM	10 vol.% PCM		30 vol.% PCM	
		Duration	Duration	Increase %	Duration	Increase %
Hot Climate	Austin (TX)	92	118	28.3	130	41.3
	Delta (UT)	82	126	53.7	140	70.7
	Casa Granda (AZ)	38	50	31.6	62	63.2
	Reno (NV)	77	114	48.1	130	68.8
Moderate Climate	Grand Forks (ND)	47	66	40.4	70	48.9
	Boston (MA)	98	120	22.4	134	36.7
	San Diego (CA)	105	128	21.9	132	25.7
	New York (NY)	105	130	23.8	156	48.6
Cold Climate	Miles City (MT)	44	64	45.5	72	63.6
	Chicago (IL)	28	40	42.9	50	78.6
	Worcester (MA)	72	96	33.3	114	58.3
	Hulton (ME)	70	94	34.3	102	45.7
Average of percentage increase ± Standard deviation			35.5% ± 7.6%		51.2% ± 11.3%	

efficiency of PCM is dependent on the applied temperature profile and PCM percentage.

To investigate the effect of ambient temperature differences on the efficiency of PCM incorporation, the percentage increase in the duration of being in the comfort zone was graphed as a function of temperature difference between day and night for one single day (Figure 4.14). When the temperature difference in a day is as low as 5 °C (9 °F), the comfort duration can be almost doubled if 30 vol.% PCM is used. For the same temperature difference, the comfort duration can be increased by more than 50% when 10 vol.% PCM is used. These numbers are respectively about 90 % and 40% when the temperature difference is 9 °C (16.2 °F) for 30% and 10% PCM. But when the temperature difference in a day is as high as 20 °C (36 °F), the efficiency for both cases will be dropped to about 15%. This shows the PCM efficiency is highly dependent on the temperature difference between day and night.

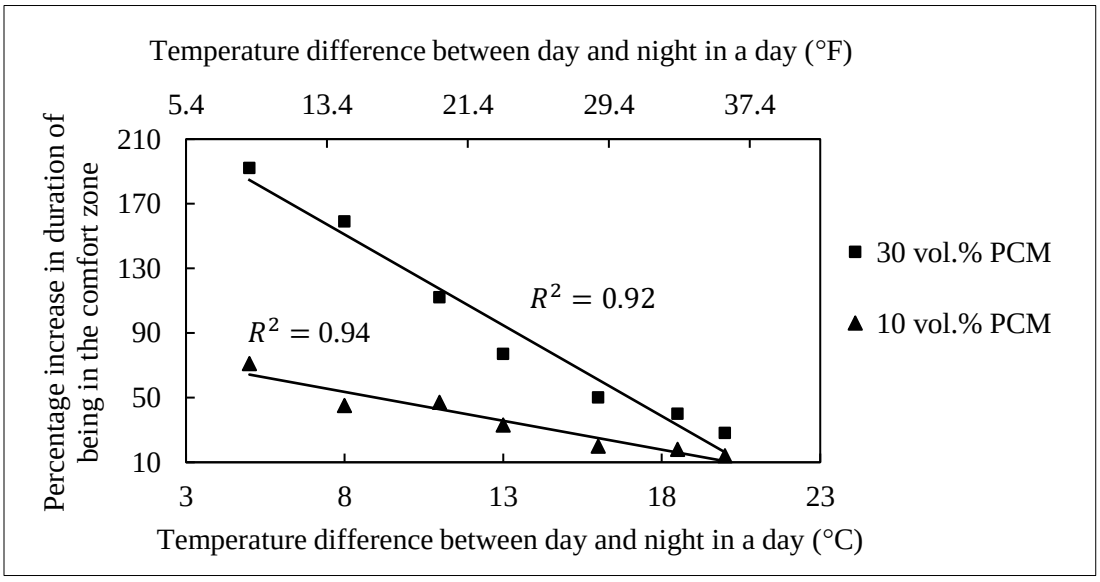

Figure 4.14. Efficiency of PCM as a function of temperature difference

These results match with the results of a study on a passive house duplex located in the U.S. state of Oregon where utlizing PCM in a building was reported to be able to reduce the annual overheated hours, the total hours in a year that the inside temperature is above the occupant comfort

level of 26 °C (78.8 °F), by 50% [47]. Another laboratory test showed that using PCM panels in a building can reduce interior peak temperatures by 4.43 °F (2.46 °C) during the summertime [40].

4.4.2 Walls equipped with PCM-incorporated gypsum boards

4.4.2.1 Sine Function Temperature Profiles

The results of the wall with different thicknesses and no PCM in their gypsum boards, under temperature profiles T10, T20, and T30, shows that as expected, with increase in the wall thickness, the peak temperature decreases and the time lag increases (Figure 4.15).

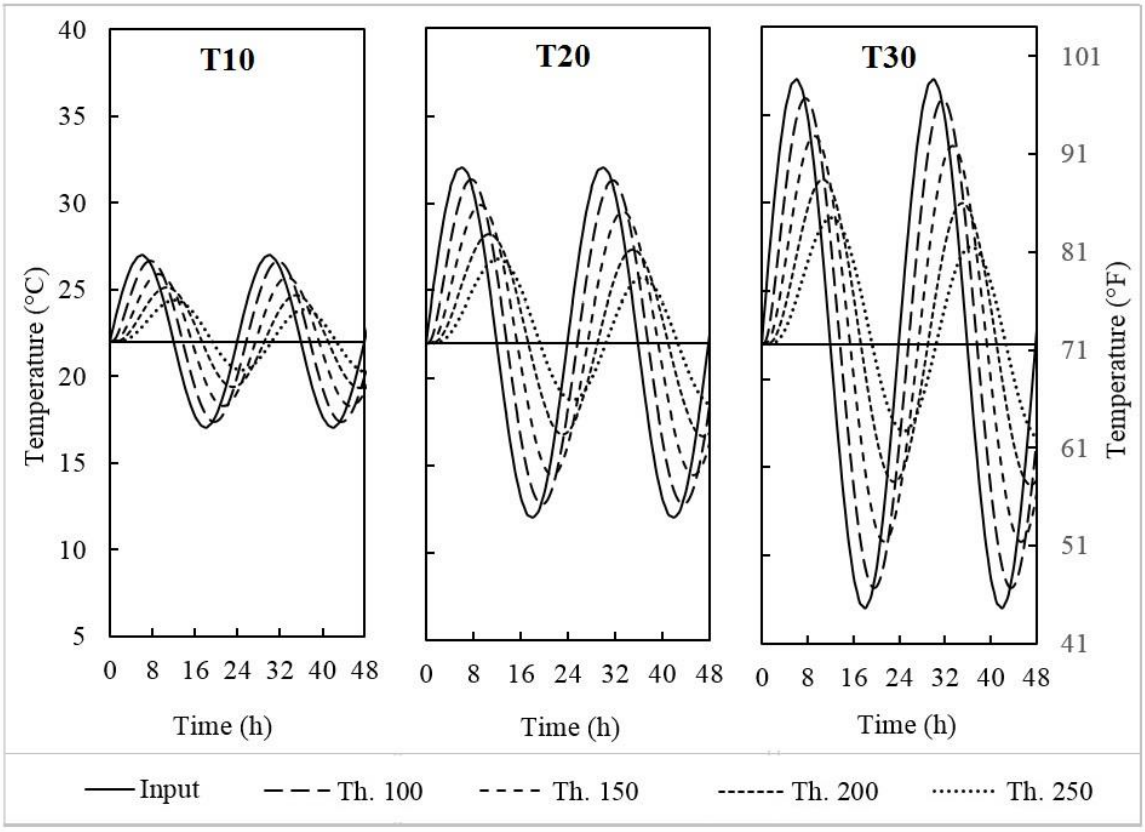

Figure 4.15. Temperature changes in walls with the thicknesses of 100 mm (3.94”), 150 mm (5.91”), 200 mm (7.87”), and 250 mm (9.84”) and with 0 vol.% of PCM under sine function temperature profiles with different amplitudes

However, the increase in the time lag is the same for all the temperature profiles (Figure 4.16). This means that for a wall with a specific thickness, the time lag is independent from the amplitude of the input sine temperature profile[5]. Also, by increasing the wall thickness, the increment factor decreases for all the temperature profiles. This drop is bigger for the sine function with bigger amplitude. These results suggest that by increasing the wall thickness the inside temperature can be controlled, however, there are structural, architectural, and economical restrictions on the maximum thickness of the walls.

The same temperature profiles were applied to the 250 mm (9.84") wall with different percentages of PCM incorporated in its gypsum board. When the temperature rises, the PCM absorbs the applied heat energy and turns to liquid, and thus reduces the peak temperature. When the applied

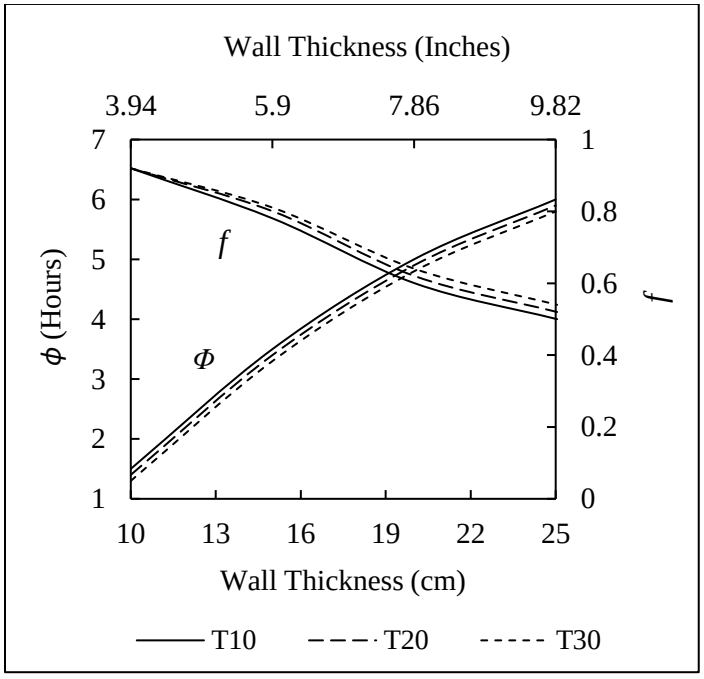

Figure 4.16. Time Lag and Decrement Factors for walls with different thicknesses and with 0 vol.% of PCM and under sine temperature profiles with different amplitudes

[5] The amplitude of the sine function input temperature will appear as a constant in the solution of the heat transfer differential equation, and the arguments of the exponential and sine functions in the solution will not be a function of this amplitude.

temperature drops below the melting temperature, the PCM releases the heat energy that was absorbed initially and thus increases the minimum temperature. This suggests that PCMs can be used as passive heat storage units in the walls that make the inside temperature changes profile to have smaller peaks. This effect increases by incorporating more PCM; however, PCM has a limited latent heat of fusion and therefore it cannot completely eliminate changes in temperature (Figure 4.17).

The results of the effects of different percentages of PCM on the Time Lag and Decrement Factor shows that by increasing the PCM percentage, the time lag increases. This increase is bigger when the applied temperature has a smaller amplitude. This is because of limited latent heat of fusion of the PCM. The decrement factor decreases by increasing the PCM percentage. When 50 vol.% of

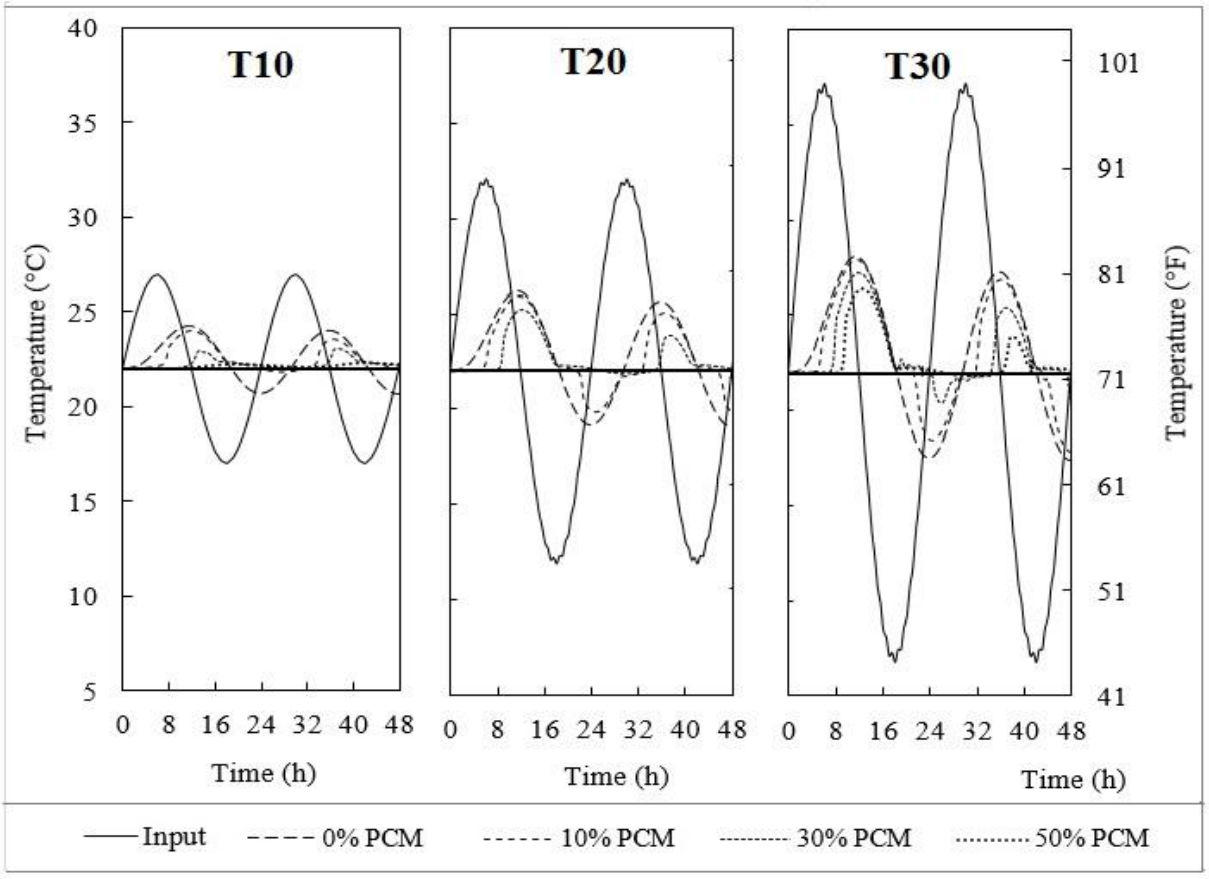

Figure 4.17. Temperature changes in 250 mm (9.84") wall with 0 vol.%, 10 vol.%, 30 vol.%, and 50 vol.% of PCM in the gypsum board under sine temperature profiles with different amplitudes

the gypsum board volume is replaced with PCM and for the temperature profile with the magnitude of 10 °C (18 °F) is applied, this factor can be as low as 8% which means more than 90% of the peak temperature is damped (Figure 4.18). Comparing Figure 4.17 and Figure 4.18 shows that using PCMs is more efficient in reducing the amplitude of the temperature than increasing the thickness of the wall. The effects of the latent heat capacity of PCM on the time lag and the decrement factor was studied by Asanand Sancaktar, who reported that there is an exponential relationship between time lag and heat capacity and inverse exponential relationship between decrement factor and heat capacity [109].

The increase of time spent in the comfort zone for the 250 mm (9.84") wall, with different percentages of PCM incorporated in its gypsum board under different temperatures profiles is presented in Table 4.5, overleaf. For T10 and for the first comfort level[6], by using 30 vol.% PCM, the inside temperature stays in the comfort zone for the entire time, therefore increasing the PCM percentage does not increase the comfort duration.

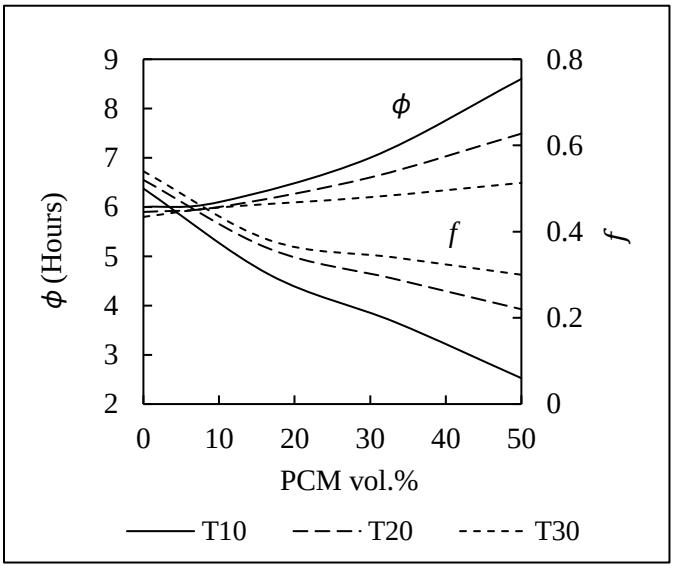

Figure 4.18. Time Lag and Decrement Factors for 250 mm (9.84") wall with different PCM percentages in its gypsum board and under sine temperature profiles with different amplitudes

[6] The comfort levels are described in Section 4.1.3.2.

Table 4.5. The effect of PCM on the comfort duration and the area out of the comfort zone for sine function temperature profiles

Input	PCM vol.%	Percentage increase in the comfort time duration		Percentage decrease in the area out of the comfort zone*	
		22 ± 1.5 °C 71.6 ± 2.7 °F	22 ± 3.0 °C 71.6 ± 5.4 °F	22 ± 1.5 °C 71.6 ± 2.7 °F	22 ± 3.0 °C 71.6 ± 5.4 °F
T10	10	29	0	82	100
	30	41	0	100	100
	50	41	0	100	100
T20	10	69	18	43	63
	30	181	29	88	95
	50	202	33	98	100
T30	10	75	26	26	35
	30	208	97	73	84
	50	323	118	92	93

* It is described in Section 4.1.3.2

For the level 2, without using PCM, the entire graph falls inside the comfort zone, therefore using PCM does not increase the comfort duration. For all of the input temperatures, the ability of PCM to increase the comfort duration is higher for the first level of comfort, because when the temperature tolerance is larger, even without PCM a relatively large portion of the inside temperature stays within the comfort zone. This suggests that PCM are more applicable when a narrower range of comfort zone is desired (Table 4.5).

These results suggest that utilizing PCM-incorporated gypsum boards can be effective in improving the thermal performance of the buildings. The other advantages of these boards are being flexible for the alteration and refurbishment of a conventional building. However, problems such as long-term thermal behavior of PCM-impregnated wallboards, durability, fire rating and heat transfer enhancement, architectural considerations, etc., still need to be addressed [117].

4.4.2.2 Real Temperature Profiles

To evaluate the efficiency of PCM-incorporated gypsum board at increasing the comfort duration under real temperature inputs, the real temperatures of six cities were applied to the model. The cities include Portland, Oregon; San Antonio, Texas; Miami, Florida; Concord, New Hampshire; Minot, North Dakota; and Elko, Nevada. These cities are located in different parts of the US, and their temperature parameters, such as peak temperature, the lowest temperature, and the difference between day and night temperatures, are completely different. Therefore, by studying theses climates, it would be possible to evaluate the efficiency of PCMs for different climates. For each city, one week was selected. Using a longer period of time yields more comprehensive and reliable results; however, the goal here is to demonstrate how PCM works in different climates and how the optimum percentage of PCM in different cases can be calculated.

The results show that by increasing the PCM percentage, the duration of being in the comfort zone increases for all the cities but this increase is not the same for all the cases (Table 4.6, overleaf). For the case of Concord, this duration was increased by up to 40% when 50% of the gypsum board volume was replaced by PCM; however, with the same amount of PCM for the case of San Antonio, this increase was as low as 4%.

This is because for the case of Concord, the highest and lowest temperatures were close to the comfort zone, i.e. the difference between the temperatures of day and night was low; therefore, the PCM was able to absorb a considerable amount of the applied heat energy during the days and release it during the nights. In contrast to the case of Concord, the temperature difference between day and night was very high for the case of San Antonio. The latent heat of fusion of PCM is limited, therefore, it was not able to absorb all the applied heat and thus, the duration of

Table 4.6. The effect of PCM on the comfort duration and the area out of the comfort zone for walls equipped with PCM-impregnated gypsum boards under real temperature profiles

City (State)	Period of Time (week of)	PCM vol.%	Percentage of increase in the comfort time duration	Percentage of reduction in the area out of comfort zone	Energy Efficiency Factor
Portland (OR)	First Mar. 2002	10	7	24	2.4
		30	16	25	0.8
		50	29	35	0.7
San Antonio (TX)	Second Aug. 1990	10	1	5	0.5
		30	2	7	0.2
		50	4	10	0.2
Miami (FL)	Third May 2000	10	2	6	0.6
		30	3	8	0.3
		50	5	12	0.2
Concord (NH)	Third Aug. 2004	10	8	12	1.2
		30	32	31	1.0
		50	38	45	0.9
Minot (ND)	Second Jun. 1980	10	8	17	1.7
		30	23	39	1.3
		50	29	43	0.9
Elko (NV)	Second Jun. 2001	10	8	12	2.5
		30	14	28	0.9
		50	20	36	0.7

being in the comfort zone was not efficiently increased. This shows that the efficiency of PCM is completely dependent on the outside temperature profile.

Considering the utilized PCM percentages and the percentage increase in being in the comfort zone shows that there is not a linear relationship between these two parameters. For the case of Minot, when the amount of utilized PCM was increased by three times (from 10 vol.% to 30 vol.%), the effectiveness of the PCM was also increased by about three times (from 8% to 23%). However, when the amount of utilized PCM was quintupled (from 10 vol.% to 50 vol.%),

the effectiveness of the PCM was increased by less than four times. The results suggest that by increasing the PCM percentage, its efficiency decreases.

The same pattern was observed for the decrease in the area out of the comfort zone (Table 4.6). This area is important because it is an index of the required energy by the HVAC system to keep the inside temperature in the comfort zone. For all the cases, the percentage of the area out of the comfort zone was decreased when the amount of utilized PCM was increased. Again for the case of Concord, this area was decreased by 45% when 50 vol.% of PCM was used; however, this number was as low as 10% for the case of San Antonio.

These results match with the results presented by Pieppo *et al.* [118] and Feldman *et al.* [119] where the energy saving in buildings by utilizing PCM walls with approximately the same percentages of the PCM was reported to be between 5% to 20% and about 22%, respectively, depending on the climate and temperature profile of the location. Hittle reported that by incorporating PCMs in floor tiles, the annual heating costs of a building can be greatly reduced [120]

Athienitis *et al.* also reported that the utilization of PCM-impregnated gypsum wallboard was shown to reduce maximum room temperatures by about 4 °C (7.2 ^{o}F) during the day and can significantly reduce the heating load at night [39]. The results of an outdoor test room experiment indicated that the peak temperature in PCM-impregnated wallboards can be as much as 10 °C (18 ^{o}F) lower than the peak temperature in the control test room during sunny days [121]. Another research showed that up to 90% of a daily cooling load could be stored each night in a system in which a 30 mm (1.18") thick packed bed of granular PCM has been used [43]. However, the reults of this study suggets that the effciency of PCMs was overestimated in that research. Considering the results shown in the area out of comfort zone column and the values in the PCM percentage column shows

that there is not a linear relationship between the amount of utilized PCM and the decrease in the area out of the comfort zone. As an example, for the case of Miami, this decrease in the area out of the comfort zone was only doubled (from 6% to 12%) when the amount of utilized PCM was increased by five times (from 10 vol.% to 50 vol.%), respectively. Therefore, an Energy Efficiency Factor (EEF) was introduced to find the energy-wise optimum percentage of PCM for each case. This factor was calculated by dividing the value of the percentage decrease in the area out of comfort zone by the value of the PCM percentage (Table 4.6).

The results show that for all the cases, by increasing the amount of utilized PCM, the EEF was decreased. This means that by doubling the amount of PCM, for instance, the effectiveness of PCM to decrease the energy required by HVAC system will not be doubled. For the case of Portland, the PCM efficiency was dropped from 2.4 to 0.8 and 0.7 when the PCM percentage was increased from 10 vol.% to 30 vol.% and 50 vol.%, respectively. For San Antonio, this factor was the same when 30 vol.% and 50 vol.% of PCM were used. In between the all, Concord by 25% had the lowest and Elko by 72% had the highest drop in PCM-efficiency when the PCM content was increased from 10 vol.% to 50 vol.%.

Cost analysis was also conducted to evaluate the efficiency of PCM-equipped gypsum boards to reduce the electricity costs regarding to air-conditioning in buildings. If the electricity rates were the same for all the parts of a day, the percentage of reduction in costs for each case was exactly the same as percentage of reduction in the energy required by the HVAC system to keep the inside temperature in the comfort zone for that case; because the total cost was equal to the energy consumed by the HVAC system multiplied in a constant number (the electricity rate). However, the electricity rates for the on-peak hours and off-peak hours are not the same.

The results show that by increasing the PCM percentage, the electricity costs of the HVAC system were reduced for all the cases (Table 4.7). In the case of Minot, the air-conditioning cost was reduced by one quarter when 50 vol.% of the gypsum boards was replaced by PCM. For the same case, 10% of the costs were reduced by incorporating 10 vol.% of PCM. However, this reduction in costs was as low as 7% and 3% for both Miami and San Antonio when 50 vol.% and 10 vol.% of PCM were used, respectively.

Similar to energy, a Cost Efficiency Factor (CEF) was used to find the economic-wise optimum percentage of PCM for each case. This factor was calculated by dividing the value of the percentage decrease in the costs by the value of the PCM percentage. The results show that

Table 4.7. Costs analysis for walls equipped with PCM-impregnated gypsum boards under real temperature profiles

City (State)	Ratio	PCM vol.%	Percentage of reduction in costs	Cost Efficiency Factor
Portland (OR)	4.0	10	15	1.5
		30	17	0.6
		50	21	0.4
San Antonio (TX)	2.4	10	3	0.3
		30	4	0.2
		50	7	0.1
Miami (FL)	6.0	10	3	0.4
		30	5	0.2
		50	7	0.1
Concord (NH)	6.9	10	6	0.6
		30	14	0.5
		50	20	0.4
Minot (ND)	6.1	10	10	0.9
		30	21	0.7
		50	25	0.5
Elko (NV)	8.7	10	5	0.5
		30	12	0.4
		50	16	0.3

similar to EEF, CEF was also decreased when the PCM percentage was increased, i.e., CEF was the efficiency of PCM to reduce the costs of air-conditioning was maximum when only 10 vol.% of PCM was used. Comparing the results of Table 4.6 with Table 4.7 shows that CEF is always smaller than EEF. This means that the efficiency of PCM to reduce the energy used by the HVAC system is smaller than the efficiency of that to reduce the cost of air-conditioning. The electricity rates are lower during off-peak Hours; therefore, although a considerable amount of energy was used by the HVAC system during these hours, the costs of that were not considerable compared to the costs during the on-peak hours.

The results of this section show that utilizing PCM-impregnated gypsum boards in new buildings could be a reliable and effective strategy to achieve the thermal performance desired by governmental plans and building codes. On the other hand, following this strategy in existing buildings represents a huge opportunity for accomplishing governmental plans. Existing buildings were mostly built before the recognition and implementation of thermal efficiency in buildings codes. For instant, more than half of California's 13 million residential units and over 40% of the commercial buildings were built before 1978, when the first building energy efficiency standards were implemented [8]. Thus, most of these buildings do not meet the current energy code requirements. Therefore, adding a layer of PCM-impregnated gypsum board, or replacing conventional wall layers with these boards, could have a significant contribution to achieving the desired level of thermal performance of the buildings.

4.4.3 Concrete Pavements

In addition to increasing occupant comfort in buildings, PCMs can be used to increase the service life of concrete pavements by decreasing the number of freeze/thaw cycles that they

experience [26]. To evaluate the effectiveness of PCMs at decreasing the number of freeze/thaw cycles experienced by concrete pavements, the temperature profiles of two sequential months in six different cities were applied to models that contained different percentages of a PCM. As described earlier, only in locations that have sufficiently wet climates and that regularly reach freezing temperatures are subject to significant freeze/thaw degradation. Therefore the cities of Blacksburg, Virginia; Lancaster, Pennsylvania, Montpelier, Vermont; New York City, New York; Oxford, Connecticut; and Portland, Maine, which all are located in the northeast part of the U.S., were selected.

For each city, the two harshest sequential months of year, in which the temperature drops to the freezing point most often, were used. (TMY puts the temperature of the sequential months that belong to different years next to each other to create the data for one entire year. For example, in the case of Blacksburg city, January 1996 is followed by February 1999). The models contained 0 vol.%, 10 vol.%, or 30 vol.% PCM. The melting point of the utilized PCM was selected to be equal to 2 °C (35.6 °F), which is slightly above the freezing temperature of water. Finally, the temperature at the depth of 101 mm (4") was considered as the parameter to count for the number of freezing cycles (Table 4.8, overleaf).

When 10 vol.% PCM by volume was used, the reduction in the number of freeze/thaw cycles varied between 11.5% to 18.5%, and on average, about one sixth of the freeze/thaw cycles were eliminated. When 30 vol.% PCM was used, the reduction percentage varied between 29.4% and 41.7% depending on the temperature profile of the city, and on average, about one third of the cycles was mitigated.

Table 4.8. Percentage reduction in the number of freeze/thaw cycles experienced by the pavement

City (State)	Two months period of time	Number of freeze/thaw cycles				
		0% PCM	10 vol.% PCM		30 vol.% PCM	
		Number	Number	Reduction %	Number	Reduction %
Blacksburg (VA)	Jan. 1996 Feb. 1999	18	15	16.7	11	38.9
Lancaster (PA)	Jan. 2002 Feb. 2002	26	23	11.5	16	38.5
Montpelier (VT)	Mar. 1995 Apr. 1991	24	20	16.7	14	41.7
New York (NY)	Jan. 1976 Feb. 1988	17	14	17.6	12	29.4
Oxford (CT)	Feb. 2000 Mar. 2005	27	22	18.5	18	33.3
Portland (ME)	Apr. 1998 Jun. 2001	31	27	15.1	19	38.4
Average of percentage reduction ± Standard Deviation			15.2% ± 2.4%		35.6% ± 4.2%	

The results match with the results presented in another study where it was shown that the presence of a PCM in the concrete pavement efficiently decreases the annual number of freeze/thaw cycles experienced by the pavement [49]. This percentage decrease was as high as 100% for Tampa, Florida, and as low as 19% for Cheyenne, Wyoming. However, the average percentage decrease for 12 cities from different parts of the U.S. was reported to be about 29%.

In another study, CONCTEMP program, developed at National Institute of Standards and Technology (NIST), was used to investigate the effectiveness of incorporating different percentages of PCMs in concrete to increase the service life of bridge decks [26]. It was shown

that this efficiency was dependent on the location of the bridge deck. For states such as Utah, Wyoming, Montana, and Colorado, located in the central part of the U.S., incorporating a PCM did not increase the service life, since freeze/thaw damage was not the limiting parameter for the service life of bridge decks. However, incorporation of 50 kg/m^3 (3.12 lb/ft^3) of PCM was effective in increasing the service life of bridge decks by at least one year in states such as Georgia, Alabama, Mississippi, Tennessee, and Louisiana, located in the south-east part of the U.S; as well as Oregon and Washington, located in the north-west part of the U.S. These results show that using PCMs in concrete pavements can effectively reduce the number of freeze/thaw cycles experienced by the pavement; however, its efficiency is dependent on the input temperature profile and the weather conditions.

4.5 Summary of the chapter

Studying the efficiency of PCMs to improve the thermal performance of buildings and pavements under real temperature profiles by laboratory experiments was found to be very time consuming, expensive, and in some cases impractical. Therefore, a series of computational models were generated to carry out this investigation. The accuracies of the models were validated by comparing their results with the results of the Guarded Longitudinal Comparative Calorimetry experiment. The real temperature profiles of different cities and with different durations, extracted from TMY database, were applied to the models as thermal loads. All the building and pavement models had the same core, however they were customized with respect to their application.

The results showed that incorporation of PCMs directly into the concrete walls increases the duration of the inside temperature to stay within the comfort zone. Also, utilizing PCM-impregnated gypsum boards decreases the peak temperature and delays the occurrence, increases the comfort duration, and decreases the energy and cost required by the HVAC system to keep the inside temperature within the comfort zone. However, it was shown that the efficiency of PCM decreases when the amount of utilized PCM increases, both energy-wise and cost-wise. Finally, incorporation of PCMs in concrete pavements was found efficient to reduce the number of freeze/thaw cycles experienced by the pavement.

CHAPTER FIVE
CONCLUSION AND FUTURE WORK

5.1 Conclusion

Improving the thermal performance of buildings and defining different strategies to achieve Zero-Net-Energy (ZNE) buildings has been the topic of many governmental plans. Utilizing PCM-incorporated gypsum boards was shown to be a promising strategy to achieve the aforesaid objectives. These boards not only can be used in new buildings, but also can be added to existing buildings to improve their thermal performance. Utilizing these boards delays the occurrence and decreases the magnitude of the inside peak temperature, increases the duration of being in the occupant comfort zone, and meaningfully decreases the cost and energy required by the HVAC system to keep the inside temperature in this range. Since a large portion of the total energy consumption in the world is allocated to heating and cooling buildings, the decrease in the required energy for buildings' air-conditioning not only decreases the required energy and costs, but also reduces the emission of harmful gases such as CO_2 to the environment. On the other hand, incorporating PCMs in concrete pavements were shown to increases pavement service life, and thus, reduce the required maintenances' costs.

Moreover, as part of strategy for incorporating PCM in concrete walls and pavements, the problems associated with utilizing Lightweight Aggregate (LWA) as a PCM carrier were studies in depth through laboratory experiments. Also, the applicability of Rice Husk Ash (RHA), a common material never before used to encapsulate PCM, as a PCM carrier agent was investigated. The results show that both LWA and RHA can absorb and contain liquids in their porous structure; and regarding their compatibility with the cementitious media, they can be used as PCM carriers. However, it was shown that the carriers release a portion of PCM into the bulk cement paste, but the chemical composition of the media does not change drastically.

5.2 Future Work

To continue this study, the following works are suggested:

- Generate a more comprehensive computational model, which can take into account the effects of solar radiation and air humidity, and increase the simulation period to one entire year for different models to obtain more realistic results.
- Conduct more studies to find the optimum melting temperature of the utilized PCMs for different applications. In addition, a comprehensive cost analysis should be conducted to compare the efficiency and life cycle costs of PCMs to alternative methods.
- Perform more investigations in order to address the problems associated with LWA and RHA as PCM carrier agents.
- Introduce novel PCM carrier agents, and compare their efficiency with the aforesaid carrier agents.

CHAPTER SIX

REFERENCES

1. Chwieduk, D., *Towards sustainable-energy buildings.* Applied Energy, 2003. **76**(1–3): p. 211-217.
2. Papadopoulos, A.M., T.G. Theodosiou, and K.D. Karatzas, *Feasibility of energy saving renovation measures in urban buildings: The impact of energy prices and the acceptable pay back time criterion.* Energy and Buildings, 2002. **34**(5): p. 455-466.
3. https://www.eia.gov. 2009.
4. http://www.rockwool.com. 2012.
5. http://www.eia.gov. 2015.
6. Kong, X., et al., *Numerical study on the thermal performance of building wall and roof incorporating phase change material panel for passive cooling application.* Energy and Buildings, 2014.
7. Laustsen, J., *Energy efficiency requirements in building codes, energy efficiency policies for new buildings.* International Energy Agency (IEA), 2008.
8. Commission, C.E., *Achieving energy savings in California buildings: Saving energy in existing buildings and achieving a zero-net-energy future*. 2011, Draft Staff Report CEC-400-2011-007-SD. July. http://www. energy. ca. gov/2011publications/CEC-400-2011-007/CEC-400-2011-007-SD. pdf.
9. *Energy Efficiency- Building Strategy, Update 2014. Washington State Department of Commerce, State Energy Office, Olympia, WA.*
10. Ürge-Vorsatz, D., et al., *Heating and cooling energy trends and drivers in buildings.* Renewable and Sustainable Energy Reviews, 2015. **41**: p. 85-98.
11. http://www.controltheproject.com/energy/. 2010.
12. Pérez-Lombard, L., J. Ortiz, and C. Pout, *A review on buildings energy consumption information.* Energy and buildings, 2008. **40**(3): p. 394-398.

13. Akbari, H. and S. Konopacki, *Calculating energy-saving potentials of heat-island reduction strategies.* Energy Policy, 2005. **33**(6): p. 721-756.

14. Erlandsson, M., P. Levin, and L. Myhre, *Energy and environmental consequences of an additional wall insulation of a dwelling.* Building and environment, 1997. **32**(2): p. 129-136.

15. Steiger, R., *Lightweight insulating concrete for floors and roof decks.* Journal of the American Concrete Institute, 1967: p. 433-469.

16. Feng, Y., *Thermal design standards for energy efficiency of residential buildings in hot summer/cold winter zones.* Energy and Buildings, 2004. **36**(12): p. 1309-1312.

17. Nicol, J.F. and M.A. Humphreys, *Adaptive thermal comfort and sustainable thermal standards for buildings.* Energy and buildings, 2002. **34**(6): p. 563-572.

18. Omer, A.M., *Energy, environment and sustainable development.* Renewable and sustainable energy reviews, 2008. **12**(9): p. 2265-2300.

19. *Federal Highway Administration, Moving ahead for progress in the 21st century act (MAP-21) - A summary of highway Provisions. O.o.P.a.G. Affairs (Ed.), 2012.*

20. *The Department of the Treasury with the Council of Economic Advisers, An economic analysis of infrastructure development, in D.o.t. Treasury (Ed.). 2010: Washington DC. p. 25.*

21. *American Society of Civil Engineers, 2013 Report Card for America's Infrastructure. 2013, ASCE.*

22. Cao, J. and D. Chung, *Damage evolution during freeze–thaw cycling of cement mortar, studied by electrical resistivity measurement.* Cement and Concrete Research, 2002. **32**(10): p. 1657-1661.

23. Qian, S.Z., et al., *Life cycle analysis of pavement overlays made with Engineered Cementitious Composites.* Cement and Concrete Composites, 2013. **35**(1): p. 78-88.

24. Walker, S., D. Bloem, and W. Mullen. *Effects of temperature changes on concrete as influenced by aggregates*. in *ACI Journal Proceedings*. 1952. ACI.

25. Bentz, D.P., *A computer model to predict the surface temperature and time-of-wetness of concrete pavements and bridge decks*. 2000: US Department of Commerce, Technology Administration, National Institute of Standards and Technology.

26. Sakulich, A.R. and D.P. Bentz, *Increasing the service life of bridge decks by incorporating phase-change materials to reduce freeze-thaw cycles.* Journal of Materials in Civil Engineering, 2011. **24**(8): p. 1034-1042.

27. Baetens, R., B.P. Jelle, and A. Gustavsen, *Phase change materials for building applications: a state-of-the-art review.* Energy and Buildings, 2010. **42**(9): p. 1361-1368.

28. Raoux, S. and M. Wuttig, *Phase change materials: science and applications*. 2009: Springer.

29. Zalba, B., et al., *Review on thermal energy storage with phase change: materials, heat transfer analysis and applications.* Applied Thermal Engineering, 2003. **23**(3): p. 251-283.

30. Sharma, A., et al., *Review on thermal energy storage with phase change materials and applications.* Renewable and Sustainable energy reviews, 2009. **13**(2): p. 318-345.

31. Hale, D., M. Hoover, and M. ONeill, *Phase change materials handbook.* 1971.

32. Abhat, A., et al., *Development of a modular heat exchanger with an integrated latent heat storage.* Report no. BMFT FBT, 1981: p. 81-050.

33. Lane, G., et al., *Macro-encapsulation of PCM.* Report No. oro/5117-8, Dow Chemical Company, Midland, Michigan, 1978. **152**.

34. George, A., *Hand book of thermal design; Phase change thermal storage materials.* 1989: McGraw Hill Book Co.

35. Pasupathy, A., R. Velraj, and R. Seeniraj, *Phase change material-based building architecture for thermal management in residential and commercial establishments.* Renewable and Sustainable Energy Reviews, 2008. **12**(1): p. 39-64.

36. Hunger, M., et al., *The behavior of self-compacting concrete containing micro-encapsulated Phase Change Materials.* Cement and Concrete Composites, 2009. **31**(10): p. 731-743.

37. Kuznik, F., J. Virgone, and J. Noel, *Optimization of a phase change material wallboard for building use.* Applied Thermal Engineering, 2008. **28**(11): p. 1291-1298.

38. Sharma, A., et al., *Review on thermal energy storage with phase change materials and applications.* Renewable and Sustainable Energy Reviews, 2009. **13**(2): p. 318-345.

39. Athienitis, A.K., et al., *Investigation of the thermal performance of a passive solar test-room with wall latent heat storage.* Building and Environment, 1997. **32**(5): p. 405-410.

40. Kong, X., et al., *Experimental research on the use of phase change materials in perforated brick rooms for cooling storage.* Energy and Buildings, 2013. **62**: p. 597-604.

41. Khudhair, A.M. and M.M. Farid, *A review on energy conservation in building applications with thermal storage by latent heat using phase change materials.* Energy conversion and management, 2004. **45**(2): p. 263-275.

42. Kuznik, F. and J. Virgone, *Experimental assessment of a phase change material for wall building use.* Applied energy, 2009. **86**(10): p. 2038-2046.

43. Nagano, K., et al., *Study of a floor supply air conditioning system using granular phase change material to augment building mass thermal storage—heat response in small scale experiments.* Energy and Buildings, 2006. **38**(5): p. 436-446.

44. Eddhahak-Ouni, A., et al., *Experimental and multi-scale analysis of the thermal properties of Portland cement concretes embedded with microencapsulated Phase Change Materials (PCMs).* Applied Thermal Engineering, 2014. **64**(1): p. 32-39.

45. Dutil, Y., et al., *A review on phase-change materials: mathematical modeling and simulations.* Renewable and Sustainable Energy Reviews, 2011. **15**(1): p. 112-130.

46. Tan, F., et al., *Experimental and computational study of constrained melting of phase change materials (PCM) inside a spherical capsule.* International Journal of Heat and Mass Transfer, 2009. **52**(15): p. 3464-3472.

47. Sage-Lauck, J. and D. Sailor, *Evaluation of phase change materials for improving thermal comfort in a super-insulated residential building.* Energy and Buildings, 2014. **79**: p. 32-40.

48. Farid, M. and X. Chen, *Domestic electrical space heating with heat storage.* Proceedings of the Institution of Mechanical Engineers, Part A: Journal of Power and Energy, 1999. **213**(2): p. 83-92.

49. Bentz, D.P. and R. Turpin, *Potential applications of phase change materials in concrete technology.* Cement and Concrete Composites, 2007. **29**(7): p. 527-532.

50. Huang, Y.-H., T.M. Adams, and J.A. Pincheira, *Analysis of life-cycle maintenance strategies for concrete bridge decks.* Journal of Bridge Engineering, 2004. **9**(3): p. 250-258.

51. Armstrong, A., et al. *An Integrated Approach for Designing and Building Sustainable Roads*. in *Green Streets, Highways, and Development 2013@ sAdvancing the Practice*. 2013. ASCE.

52. Eddhahak, A., et al., *Effect of phase change materials on the hydration reaction and kinetic of PCM-mortars.* Journal of Thermal Analysis and Calorimetry: p. 1-9.

53. Tyagi, V., et al., *Thermodynamics and performance evaluation of encapsulated PCM-based energy storage systems for heating application in building.* Journal of Thermal Analysis and Calorimetry, 2014. **115**(1): p. 915-924.

54. Miyamoto, S. and M. Takeuchi. *Snow-melting and de-icing system on road using natural thermal energy sources*. in *New Challenges for Winter Road Service XIth International Winter Road Congress. World Road Association-PIRAC, Sapporo, Japan*. 2002.

55. Sakulich, A. and D. Bentz, *Incorporation of phase change materials in cementitious systems via fine lightweight aggregate.* Construction and Building Materials, 2012. **35**: p. 483-490.

56. Merzouki, T., et al., *Contribution to the modeling of hydration and chemical shrinkage of slag-blended cement at early age.* Construction and Building Materials, 2013. **44**(0): p. 368-380.

57. Pang, X., et al., *An innovative test apparatus for oil well cement: In-situ measurement of chemical shrinkage and tensile strength.* Construction and Building Materials, 2015. **74**(0): p. 93-101.

58. de Sensale, G.R., A.B. Ribeiro, and A. Gonçalves, *Effects of RHA on autogenous shrinkage of Portland cement pastes.* Cement and concrete composites, 2008. **30**(10): p. 892-897.

59. Onojah, A.D., et al, R*ice husk ash refractory: the temperature dependent crystalline phase aspects.* IJRRAS, 2013. **15**(2): p. 246-248.

60. Yu, Q., et al., *The reaction between rice husk ash and Ca (OH) 2 solution and the nature of its product.* Cement and concrete research, 1999. **29**(1): p. 37-43.

61. Van Tuan, N., et al., *Hydration and microstructure of ultra high performance concrete incorporating rice husk ash.* Cement and Concrete Research, 2011. **41**(11): p. 1104-1111.

62. Wettlaufer, J., *Impurity effects in the premelting of ice.* Physical Review Letters, 1999. **82**(12): p. 2516.

63. Zhou, D., C.-Y. Zhao, and Y. Tian, *Review on thermal energy storage with phase change materials (PCMs) in building applications.* Applied energy, 2012. **92**: p. 593-605.

64. Castro, J., et al., *Absorption and desorption properties of fine lightweight aggregate for application to internally cured concrete mixtures.* Cement and Concrete Composites, 2011. **33**(10): p. 1001-1008.

65. Bentz, D.P., P. Lura, and J.W. Roberts, *Mixture proportioning for internal curing.* Concrete International, 2005. **27**(2): p. 35-40.

66. Mehta, P.K. *Properties of blended cements made from rice husk ash*. in *ACI Journal Proceedings*. 1977. ACI.

67. Zhang, M., R. Lastra, and V. Malhotra, *Rice-husk ash paste and concrete: some aspects of hydration and the microstructure of the interfacial zone between the aggregate and paste.* Cement and Concrete Research, 1996. **26**(6): p. 963-977.

68. Zhang, M.-H. and V.M. Malhotra, *High-performance concrete incorporating rice husk ash as a supplementary cementing material.* ACI Materials Journal, 1996. **93**(6).

69. Bentz, D.P. and O.M. Jensen, *Mitigation strategies for autogenous shrinkage cracking.* Cement and Concrete Composites, 2004. **26**(6): p. 677-685.

70. Holt, E., *Contribution of mixture design to chemical and autogenous shrinkage of concrete at early ages.* Cement and Concrete Research, 2005. **35**(3): p. 464-472.

71. Bentur, A., S.-i. Igarashi, and K. Kovler, *Prevention of autogenous shrinkage in high-strength concrete by internal curing using wet lightweight aggregates.* Cement and concrete research, 2001. **31**(11): p. 1587-1591.

72. Cusson, D. and T. Hoogeveen, *Internal curing of high-performance concrete with pre-soaked fine lightweight aggregate for prevention of autogenous shrinkage cracking.* Cement and Concrete Research, 2008. **38**(6): p. 757-765.

73. Bentz, D. and K. Snyder, *Protected paste volume in concrete: extension to internal curing using saturated lightweight fine aggregate.* Cement and concrete research, 1999. **29**(11): p. 1863-1867.

74. Bentz, D.P. and W.J. Weiss, *Internal curing: a 2010 state-of-the-art review*. 2011: US Department of Commerce, National Institute of Standards and Technology.

75. Trtik, P., et al., *Release of internal curing water from lightweight aggregates in cement paste investigated by neutron and X-ray tomography.* Nuclear Instruments and Methods in Physics Research Section A: Accelerators, Spectrometers, Detectors and Associated Equipment, 2011. **651**(1): p. 244-249.

76. Taylor, H.F., *Cement chemistry*. 1997: Thomas Telford.

77. National Institute of Standards and Technology, *Thermal properties of pyroceram code 9606, in Private Communication from the NIST.*

78. Salmon, D., R. Brandt, and R. Tye, *Pyroceram 9606, A Certified Ceramic Reference Material For High-Temperature Thermal Transport Properties: Part 2—Certification Measurements.* International Journal of Thermophysics, 2010. **31**(2): p. 355-373.

79. Farnam, Y., et al., *Measuring freeze and thaw damage in mortars containing deicing salt using a low-temperature longitudinal guarded comparative calorimeter and acoustic emission.* Adv. Civ. Eng. Mater, 2014. **3**(1): p. 23.

80. Zhutovsky, S., K. Kovler, and A. Bentur, *Efficiency of lightweight aggregates for internal curing of high strength concrete to eliminate autogenous shrinkage.* Materials and Structures, 2002. **35**(2): p. 97-101.

81. Tazawa, E.-i. and S. Miyazawa, *Influence of cement and admixture on autogenous shrinkage of cement paste.* Cement and Concrete Research, 1995. **25**(2): p. 281-287.

82. Lura, P., *Autogenous deformation and internal curing of concrete*. 2003: TU Delft, Delft University of Technology.

83. Kovler, K., et al., *Internal curing of concrete–State-of-the-art report of RILEM Technical Committee 196-ICC.* RILEM Report, 2007. **41**.

84. Wittmann, F.H., *Physikalische Messungen an Zementstein*. 1968, Mikrokopie.

85. Bentz, D.P. and P.E. Stutzman, *Internal curing and microstructure of high-performance mortars.* ACI SP-256, Internal Curing of High Performance Concretes: Laboratory and Field Experiences, 2008: p. 81-90.

86. Geiker, M.R., D.P. Bentz, and O.M. Jensen, *Mitigating autogenous shrinkage by internal curing.* ACI SPECIAL PUBLICATIONS, 2004: p. 143-154.

87. Persson, B., *Experimental studies on shrinkage of high-performance concrete.* Cement and Concrete Research, 1998. **28**(7): p. 1023-1036.

88. Hansen, W., *Drying shrinkage mechanisms in Portland cement paste.* Journal of the American Ceramic society, 1987. **70**(5): p. 323-328.

89. Hobbs, D. *Influence of aggregate restraint on the shrinkage of concrete*. in *ACI Journal Proceedings*. 1974. ACI.

90. QIAN, X.-q., et al., *Influence of superplasticiser on early shrinkage and total shrinkage of concrete [J]*. Concrete, 2004. **5**: p. 004.

91. Bentz, D.P., M.A. Peltz, and J. Winpigler, *Early-age properties of cement-based materials. II: Influence of water-to-cement ratio.* Journal of materials in civil engineering, 2009. **21**(9): p. 512-517.

92. Pane, I. and W. Hansen, *Investigation of blended cement hydration by isothermal calorimetry and thermal analysis.* Cement and Concrete Research, 2005. **35**(6): p. 1155-1164.

93. Uchikawa, H., D. Sawaki, and S. Hanehara, *Influence of kind and added timing of organic admixture on the composition, structure and property of fresh cement paste.* Cement and Concrete Research, 1995. **25**(2): p. 353-364.

94. Lv, S., et al., *Preparation and characterization of poly-carboxymethyl-β-cyclodextrin superplasticizer.* Cement and Concrete Research, 2012. **42**(10): p. 1356-1361.

95. Kim, G., et al., *Hydration heat and autogenous shrinkage of high-strength mass concrete containing phase change material.* Journal of Asian Architecture and Building Engineering, 2010. **9**(2): p. 455-462.

96. Behnood, A. and H. Ziari, *Effects of silica fume addition and water to cement ratio on the properties of high-strength concrete after exposure to high temperatures.* Cement and Concrete Composites, 2008. **30**(2): p. 106-112.

97. Meshgin, P. and Y. Xi, *Effect of Phase-Change Materials on Properties of Concrete.* ACI Materials Journal, 2012. **109**(1).

98. Ling, T.-C. and C.-S. Poon, *Use of phase change materials for thermal energy storage in concrete: an overview.* Construction and Building Materials, 2013. **46**: p. 55-62.

99. Hanafi, S., et al., *Surface properties of silicas produced by thermal treatment of rice-husk ash.* Thermochimica Acta, 1980. **37**(2): p. 137-143.

100. Hunnicutt, W.A., *Characterization of calcium-silicate-hydrate and calcium-alumino-silicate-hydrate*. 2013, University of Illinois at Urbana-Champaign.

101. Hartmann, A., M. Khakhutov, and J.-C. Buhl, *Hydrothermal synthesis of CSH-phases (tobermorite) under influence of Ca-formate.* Materials Research Bulletin, 2014. **51**: p. 389-396.

102. Wang, K., D.E. Nelsen, and W.A. Nixon, *Damaging effects of deicing chemicals on concrete materials.* Cement and Concrete Composites, 2006. **28**(2): p. 173-188.

103. Zhang, Z., et al., *Thermal energy storage cement mortar containing n-octadecane/expanded graphite composite phase change material.* Renewable energy, 2013. **50**: p. 670-675.

104. Jeong, S.-G., et al., *Preparation and evaluation of thermal enhanced silica fume by incorporating organic PCM, for application to concrete.* Energy and Buildings, 2013. **62**: p. 190-195.

105. Dirk P. Kroese, J.C.C.C., *Statistical Modeling and Computation*. 2013: Springer.

106. http://rredc.nrel.gov/solar/old_data/nsrdb/1991-2005/tmy3/.

107. http://rredc.nrel.gov/solar/old_data/nsrdb/1961-1990/tmy2/.

108. *ASHRAE Standard 55-2004. Thermal Environmental Conditions for Human Occupancy*.

109. Asan, H. and Y. Sancaktar, *Effects of wall's thermophysical properties on time lag and decrement factor.* energy and buildings, 1998. **28**(2): p. 159-166.

110. Incropera, F., *Introduction to Heat Transfer*. Fifth ed. 2005: John Wiley & Sons.

111. Oregon Summary of Electricity Rates - https://www.pacificpower.net/ - *2016.*

112. Texas Summary of Electricity Rates - http://www.cleantechnica.com/ - *2011.*

113. Florida Summary of Electricity Rates - https://www.duke-energy.com/ - *2016.*

114. New Hampshire Summary of Electricity Rates - https://www.eversource.com/ - *2016.*

115. North Dakota Summary of Electricity Rates - https://www.xcelenergy.com - *2016.*

116. Nevada Summary of Electricity Rates - https://www.nvenergy.com/ - *2016.*

117. Zhang, Y., et al., *Application of latent heat thermal energy storage in buildings: state-of-the-art and outlook.* Building and environment, 2007. **42**(6): p. 2197-2209.

118. Peippo, K., P. Kauranen, and P. Lund, *A multicomponent PCM wall optimized for passive solar heating.* Energy and buildings, 1991. **17**(4): p. 259-270.

119. Feldman, D., et al., *Obtaining an energy storing building material by direct incorporation of an organic phase change material in gypsum wallboard.* Solar energy materials, 1991. **22**(2-3): p. 231-242.

120. Hittle, D.C., P*hase change materials in floor tiles for thermal energy storage*, in *Other Information: PBD: 1 Oct 2002*. 2002. p. Medium: ED; Size: 42 pages.

121. Kissock, J.K., et al., *Testing and simulation of phase change wallboard for thermal storage in buildings.* Solar Engineering, 1998: p. 45-52.